UNICA

UNIVERSITÀ
DEGLI STUDI
DI CAGLIARI

Ph.D. DEGREE IN
NEUROSCIENCE

Cycle XXXVIII

TITLE OF THE Ph.D. THESIS

Taste physiological mechanisms and their health implications, analyzed by genetic, epigenetic, and artificial intelligence analyses

Scientific Disciplinary Sector(s)

BIOS-06/A-Physiology

Ph.D. Student:	Lala Chaimae Naciri
Supervisor	Iole Tomassini Barbarossa
Co-Supervisor	Melania Melis

Final exam. Academic Year 2024/2025
Thesis defence session: February 2026

Academic Acknowledgements

I am deeply grateful to **Professor Iole Tomassini Barbarossa** for her exceptional mentorship, unwavering support, and inspiring guidance throughout my PhD journey. Under her supervision, I have grown not only scientifically but also personally, learning rigorous research methods and, above all, invaluable life lessons in patience, resilience, and strength. Her wisdom, dedication, and humanity have left a lasting impact on me, and she will always remain a role model to look up to. I sincerely thank her for her trust, her encouragement during challenging moments, and her ability to see potential even when I doubted myself.

I also wish to express my heartfelt thanks to **Professor Melania Melis** for her constant guidance, constructive feedback, and generous assistance over the years. Her scientific insight, clarity of thought, and readiness to help at every stage have been immensely valuable. Her encouragement and expertise helped me overcome many research challenges, while her kindness and dedication made my academic journey both enriching and rewarding. I will always treasure her example of professionalism, passion, and intellectual curiosity. I would like to thank **Mariano Mastinu** for his kind support and valuable advice.

My warmest thanks go to **Dr. Diego Ulisse Pizzagalli** and **Dr. Raffaella Fiamma Cabini** for their kind and welcoming support at the University of Italian Switzerland. Their generosity, thoughtful advice, and collegial spirit greatly enriched my research experience, making it both productive and enjoyable.

Finally, I extend my sincere gratitude to all the collaborators at the Department of Biomedical Science – Section of Physiology. Their cooperation, assistance, and shared expertise have been essential to the completion of this work. I deeply appreciate the collaborative and supportive environment they helped create, which made this experience truly meaningful.

Personal Acknowledgements

I want to express my deepest and most heartfelt gratitude to my husband, **Ilyas**. His unconditional love, patience, and constant support have been the foundation of this entire journey. His understanding, encouragement, and unwavering belief in me gave me the strength to persevere through every challenge. His sacrifices, kindness, and quiet strength made this achievement possible in ways that words can hardly capture. In many ways, this work is as much his as it is mine.

I am profoundly grateful to my father, **Sidi Zoubair**, whose wisdom, strength, and unshakable belief in my potential have been a constant source of inspiration and courage throughout my life.

My deepest thanks also go to my mother, **Asmae**, for her endless love, patience, and unwavering care. Her nurturing spirit, resilience, and steadfast faith in me have been guiding lights, especially during the most demanding moments of this journey.

I extend my heartfelt appreciation to my sisters, **Imane** and **Nouhaila**, for their love, laughter, and continuous encouragement. Their presence has been a constant source of joy, balance, and motivation.

I am also deeply grateful to **my husband's family** for their kindness, support, and encouragement during difficult times.

Lastly, I warmly thank my friends for their companionship, understanding, and encouragement, which have brought lightness and happiness throughout these years. Their friendship has been a beautiful reminder of the power of connection, kindness, and shared strength.

Abstract

Taste perception is a complex trait influenced by genetic, epigenetic, physiological, and pathological factors, with significant implications for nutrition, health, and disease. Our studies integrated molecular biology, psychophysics, and advanced machine learning methods to explore inter-individual variability in taste function. We demonstrated that supervised learning algorithms, such as CatBoost and Random Forest, can automatically identify TAS2R38 genotypes and accurately analyze taste and oral sensitivity in healthy individuals and patients with chemosensory loss, highlighting the differential contribution of gustatory, olfactory, and trigeminal components. In parallel, convolutional neural networks enabled the reliable and automatic detection of fungiform papillae, overcoming the limitations of the manual method. On the molecular level, we demonstrated that methylation of the Gustin gene influences salivary protein levels and fungiform papillae density, while methylation of the TAS2R38 gene is associated with COVID-19 severity, highlighting the role of epigenetic regulation in taste physiology and the immune system. In addition, we investigated taste impairments in Parkinson's disease (PD) and their association with α-synuclein (SNCA) gene polymorphisms. Taste deficits in PD were modality-specific, particularly affecting saltiness and astringency, and were modulated by specific SNCA genotypes. Supervised learning models classified PD versus healthy controls and stratified disease severity, identifying key sensory and genetic predictors. Taken together, these findings demonstrate how the integration of computational approaches, genetic/epigenetic profiling, and psychophysical data can advance the understanding of human taste function, offering innovative perspectives for personalized nutrition, clinical diagnostics, and therapeutic applications.

Table of Contents

Chapter 1
Introduction

Human senses serve as the link between the environment and consciousness, interacting with external stimuli and conveying information to the brain. Among all the senses, the sense of taste has the most influence on food choices and eating behavior, which in turn impacts the individual's nutritional status and health [1, 2]. Taste enables organisms to distinguish nutrient-rich food from noxious substances. This ability allows one to avoid the intake of toxic substances or spoiled foods, which are perceived as bitter and sour, respectively. and favours the intake of sweet compounds such as glucose, which represents a source of energy [3]. Recognizing the difference between toxic and nutrient-containing food was an evolutionary essential when humans had to choose from a variety of natural sources in the environment. Furthermore, the taste evaluation of the food in the mouth leads to its final acceptance before its ingestion [1].

1. Anatomy and Physiology of the Human Gustatory System

Taste can recognize five sensory qualities: sweet, sour, salty, bitter, and umami. Each of these represents different nutritional or physiological requirements or indicates potential dietary risk, therefore the primary taste categories reflect complementary strategies to obtain essential nutrients and avoid harmful compounds [4, 5]. Sweet, umami, and salty are linked to specific classes of nutrients, and they are perceived as good and pleasant at low and moderate concentrations; however, they are avoided at high concentrations [6]. Sweet taste usually indicates the detection of soluble carbohydrates that serve as an energy source. The taste of umami is associated with the taste of L-glutamate and some other L-amino acids; it reflects the protein content of a food [3] and is triggered by monosodium glutamate (MSG), disodium inosinate (IMP), or disodium guanylate (GMP) [7]. Umami is often described as "savoury" or "meaty", although many foods contain these compounds in addition to meat. The salty flavour indicates the presence of sodium (Na+) and other salts, such as lithium or potassium [8], which are essential for maintaining homeostasis in the body [9, 10]. In contrast, bitter and sour are associated with potentially harmful compounds. In fact, the perception of bitter taste is linked with various compounds, including alkaloids (e.g., caffeine, strychnine, quinine, and glycosides). It is considered an innate aversion, thought to protect against poisons or substances that are toxic or inhibit digestion. Similarly, sour taste detects acids (H^+ ions), helping avoid excess intake that could disrupt the body's acid–base balance. While acceptable at low concentrations, sour taste triggers rejection at higher levels and can indicate unripe fruits or spoiled foods [3, 9, 11]. Several studies include free fatty acids among basic tastes, demonstrating taste's important role in fat detection [12-15]. Though dietary lipids are mainly triglycerides, free long-chain fatty acids released during oral processing appear responsible for fat taste perception [16, 17]. Dietary fats were thought to have no inherent taste but be perceived through texture (viscosity, lubricity, moistness) and odor properties. However, even when these properties are masked, humans can still distinguish between fatty acid and control solutions. Beyond providing energy, fats are required to synthesize various biological compounds involved in neural function, epithelial integrity, blood clotting, and immune function. Moreover, free fatty acid detection thresholds vary based on chain length and saturation [18]. Human taste begins when taste receptors in taste cells interact with gustatory stimuli. Taste buds are clusters of 50-100 polarized neuroepithelial cells [19, 20] forming compact, columnar pseudostratified "islands" within the oral cavity's stratified epithelium [3].The human gustatory system contains approximately 5000 taste buds in the oral cavity, mostly on the tongue's superior surface. Isolated taste buds also occur on the palate, throat, and epiglottis [21]. On the tongue, taste buds are grouped in specialized structures called gustatory papillae of the lingual epithelium. Three morphological papillae types exist: fungiform (mushroom-shaped) on the anterior two-thirds, concentrated toward the tip; foliate (leaf-shaped) on the lateral sides; and circumvallate on the posterior two-thirds (Figure 1). In addition, there are also another type, which are filiform papillae that cover the entire superior surface but lack taste buds (non-gustatory). Each taste bud has a single apical pore where microvilli of taste receptor cells (TRCs) come into contact with tastants present within the oral cavity.

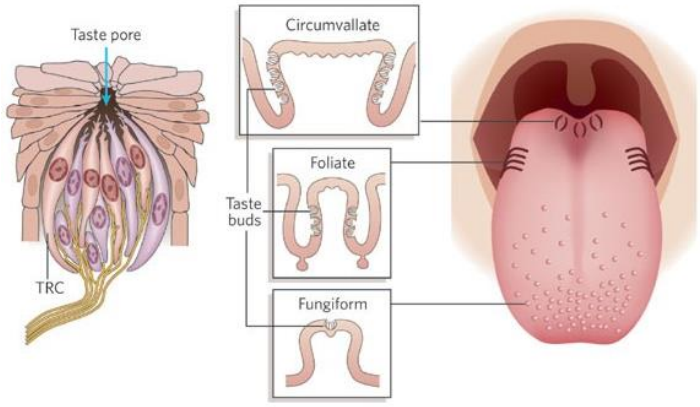

Figure 1. Tongue gustatory papillae and taste buds. Circumvallate papillae are located at the tongue's posterior region and house thousands of taste buds. Foliate papillae are present at the posterior lateral edge of the tongue and contain a dozen to hundreds of taste buds. Fungiform papillae hold one to several taste buds and are situated in the anterior two-thirds of the tongue. Taste receptor cells (TRC) extend microvilli to the apical surface of the taste bud, where they form the 'taste pore', the site of interaction with tastants [20].

Each taste bud contains four cell types. Type I cells (also called dark cells) represent the most abundant and are characterized by extended cytoplasmic lamellae that envelop other cells. Because they seem to play a role in synaptic transmission and limiting the spread of transmitters, they are described as “glial-like” [3]. More specifically, Type I cells express various enzymes and transporters that are involved in the uptake of neurotransmitters from the extracellular environment. Among them, GLAST, a glutamate transporter, suggests their involvement in glutamate uptake[22], while NTPDase2, a plasma membrane-bound nucleotidase responsible for hydrolyzing extracellular ATP [23], has also been identified. In addition, these cells appear to modulate the ionic environment [24, 25] by expressing ROMK, a K channel that may be implicated in potassium homeostasis within the taste bud [25]. When prolonged trains of action potentials occur as a consequence of strong taste stimulation, Type I cells may act to remove K+ (depicted as the blue cell in Figure 2) that would otherwise accumulate in the limited interstitial spaces of the taste bud and reduce the excitability of Type II and Type III cells. Lastly, type I cells may exhibit ionic currents implicated in salt taste transduction [23]. Type II cells have a spindle-like shape and contain a large, round, transparent nucleus. They are also referred to as “receptor” cells [19] due to the presence, in their plasma membrane, of receptors for bitter, sweet, and umami. These cells are regarded as the primary receptors in the taste bud [6, 19, 26-28]. In fact, they express G protein–coupled receptors (GPCRs) with seven transmembrane domains, each specialized for a single taste quality [29]. Moreover, Type II cells expresss voltage-gated Na+ and K+ channels, which are essential for generating action potentials, and they are capable of releasing ATP (depicted as the yellow cell in Figure 2). In summary, Type II cells are specifically tuned to detect sweet, bitter, or umami stimuli [30]; however, they do not appear to be directly sensitive to sour or salty tastes [3]. Each of these cells expresses only one receptor type, which is localized in apical microvilli that interact with the oral cavity.Type III cells are distinguished by their slender morphology and share several presynaptic, neuron-like features, as they establish synapses with afferent sensory fibers (green cell in Figure 2) [19, 31]. These cells express the enzymatic machinery required for the synthesis of at least two neurotransmitters and contain voltage-gated Ca2+ channels, which are typically associated with neurotransmitter release [19, 32]. The activity of these channels gives rise to depolarization-dependent Ca2+ transients. Like receptor cells, Type III cells are excitable and express a set of voltage-gated Na+ and K+ channels that allow them to generate action potentials [33-36]. In addition to these neuronal features, they respond directly to sour stimuli and to carbonation, and are considered to mediate the signaling of these specific sensations [30, 37-39]. Unlike receptor cells, however, presynaptic cells are not narrowly tuned to a single taste modality; instead, they respond more broadly to sweet, salty, sour, bitter, and umami compounds [30]. As for Type IV cells, they correspond to basal cells, which are nonpolarized and generally considered as undifferentiated or immature taste cells (progenitors) [40]. These basal cells are small and rounded, located at the base of the taste bud, and are believed to function as stem cells from which other cell types arise during the natural turnover of taste bud cells [31].

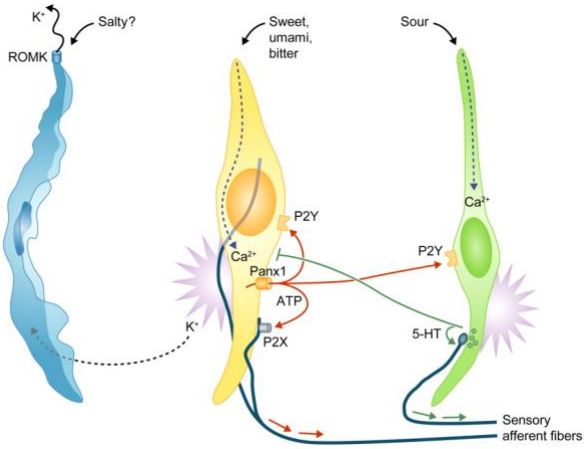

Figure 2. Schematic representation of the three major classes of taste cells and their communication patterns. Types I (blue), type II (yellow), and type III (green) taste cells [3].

The transduction mechanisms in the gustatory system rely on multiple pathways and differ in several aspects from those of the other sensory modalities [11, 31, 41]. Also, the six basic tastes are distinguishable in different pathways. Salty and sour taste sensations are detected by ion channels, whereas sweet, bitter, and umami are detected by G protein–coupled receptors (GPCRs) with seven transmembrane domains. More specifically, these taste qualities are recognized by the two receptor families *TAS1R* and *TAS2R* [42], which are localized in the apical microvilli of Type II cells [26, 28, 29, 43-45].Within the human *TAS1R* family, only three genes exist: *TAS1R1*, *TAS1R2*, and *TAS1R3*. Sweet taste is detected by receptor cells expressing the heterodimer *TAS1R2/TAS1R3*, while a different class of receptor cells expresses the heterodimer GPCR, *TAS1R1/TAS1R3*, which responds to umami stimuli, particularly to l-glutamate in combination with compounds generated during protein hydrolysis in foods [43, 44]. In contrast, the bitter taste is detected by the *TAS2R* family of GPCRs [46]. Humans possess 25 apparently functional *TAS2R* genes, encoding receptors responsible for bitter detection [46-48]. These receptors vary in their specificity: some respond to only a few (2–4) bitter compounds, whereas others are activated by a wide range of ligands [49]. Importantly, bitter-sensitive taste cells can discriminate among different bitter molecules [50]. This pattern of *TAS2Rs* expression, along with polymorphisms across the gene family, is thought to allow humans and animals to detect the vast range of potentially toxic bitter compounds found in nature [38]. In addition, two GPCRs, GPR40 and GPR120 (also known as free fatty acid receptors 1 and 4), have been implicated in fat perception. Nevertheless, the *CD36* scavenger receptor is currently considered the most likely candidate: it induces intracellular Ca2+ elevation when stimulated by fatty acids [51]. *CD36* is localized in taste bud cells of the circumvallate papillae, although how the transporter couples to Ca^{2+} signaling is not yet known. Despite the diversity of taste receptors, their signaling relies on similar effectors. The binding of a tastant to its receptor triggers second messenger cascades that lead to taste cell depolarization. In the case of sweet, umami, and bitter transduction, the G-protein subunit α-gustducin (Gα-gustducin) participates in the signaling process (Figure 3A) [26, 29, 52-55], and the subunit Gγ13 contributes specifically to bitter taste transduction [56]. The pathway begins with GPCR activation [9]. Considering sweet taste, GPCR activation depolarizes the cell through the intracellular messenger cyclic adenosine monophosphate (cAMP), which leads to transmitter release, though the underlying mechanism is still unclear [57-59]. IP_3 receptors, located in the endoplasmic reticulum, release Ca^{2+} from intracellular stores. Other key intracellular messengers include phospholipase Cβ2 (PLCβ2) and inositol 1,4,5-trisphosphate (IP3) [28, 60-63]. IP3 receptors in the endoplasmic reticulum release Ca2+ from intracellular stores, and the increased intracellular Ca^{2+} activates transient receptor potential cation channel- subfamily M member 5 (TRPM5), which is a cation-permeable channel that allows the entry of sodium ions (Na^+), finally leading to cell depolarization [9, 58-61].

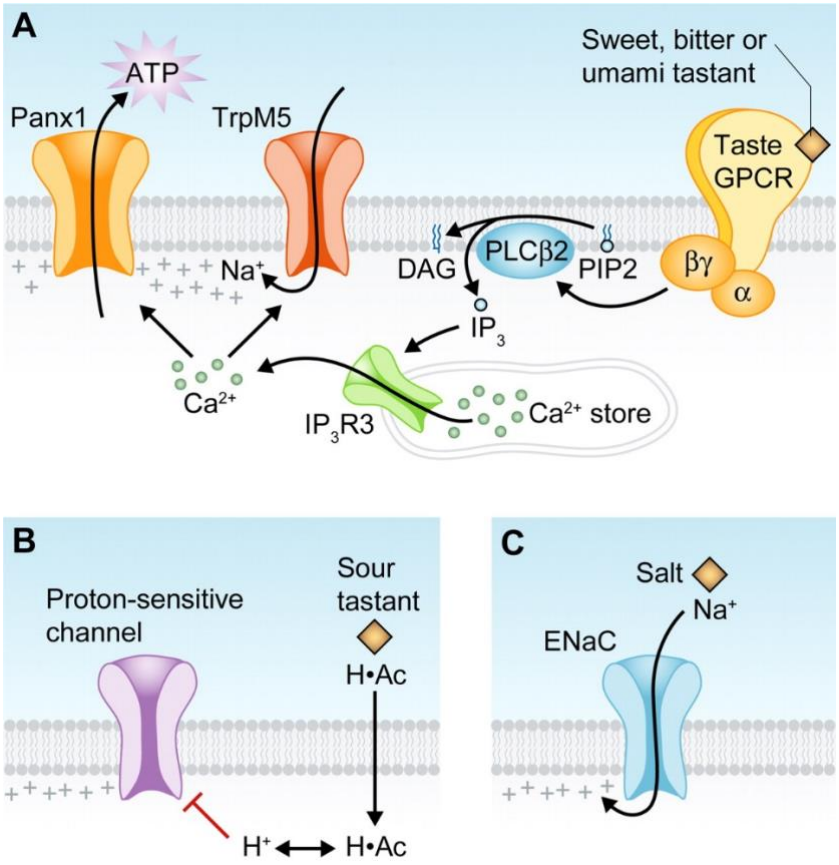

Figure 3. Mechanisms by which five taste qualities are transduced in taste cells for sweet, bitter and umami in receptor (Type II) cells (A); for sour in presynaptic (Type III) cells (B), for salty in Type I cells (C) [3].

The depolarization produced by Na+ and Ca2+ entry leads to the opening of pannexin (Panx) channels in the membrane of taste cells, releasing ATP. The precise role of ATP is not yet fully understood. However, ATP secreted by receptor cells activates purinergic receptors located on the sensory nerve fibers innervating the taste buds, thus transmitting a signal to the brain [3]. At the same time, Type II cells release ATP through paracrine mechanisms that excite adjacent presynaptic cells (Type III), stimulating them to secrete serotonin and/or norepinephrine [21, 64] and eliciting afferent nerve output [11, 31]. The transduction of salty and sour tastes occurs in the microvilli of taste cells as well as along the basolateral membranes [64]. Sour stimuli (acids) are detected by a specific subpopulation of cells, including presynaptic cells [30]. The prevailing hypothesis suggests that sour receptors rely on non-selective cation channels formed by PKD2L1 and PKD1L3 [37, 65, 66]. This channel is sensitive to extracellular pH instead of cytoplasmic pH, which is known to be the direct stimulus for sour taste (Figure 3B) [34, 63]. In addition, there is evidence that weak organic acids, such as acetic acid, which remain partially undissociated at physiological pH, can directly diffuse across the plasma membrane of Type III cells, acidify the cytoplasm, and therefore generate an electrical response. According to this mechanism, intracellular protons inhibit or block a proton-sensitive K+ channel that normally acts to hyperpolarize the cell. A combination of direct intake of hydrogen ions (which depolarizes the cell) and inhibition of the hyperpolarizing current triggers action potentials in the taste cell and promotes neurotransmitter release. Nevertheless, the complete transduction pathways underlying sour taste perception are still not fully clarified [3]. The detection of Na+ salts is mediated by their direct entry through apical ion channels. These channels, known as amiloride-sensitive epithelial sodium channels (ENaC) (Figure 3C) [9, 67-69], allow Na+ influx, which depolarizes the taste cells. ENaC is also permeable to H+ ions, implying that sour stimuli may additionally involve proton entry via these channels. Moreover, salty and sour sensations can partially interfere with each other at the peripheral level, depending on their concentrations in saliva [70]. Variations in the perception of different sodium salts may also depend on the different permeability of their associated anions across tight

junctions, and the consequent ability to influence other ion channels located in the basal lateral membranes of taste cells. In most cases, transduction mechanisms determine the depolarization of the taste cell membrane (receptor potential). This depolarization determines an increase in the concentration of Ca2+ for opening voltage-dependent channels or for mobilizing Ca2+ from intracellular stores. The elevation of Ca2+ then induces the exocytosis of chemical mediators, and the consequent transmission of the signal (make synapses) to the primary gustatory afferent fibers.

Three cranial nerves transmit sensory input from taste buds to the brain. The anterior two-thirds of the tongue and the palate are innervated by the facial nerve (cranial nerve VII). The taste buds of the fungiform and foliate papillae are innervated by the chorda tympani, which is a branch of the facial nerve [71-74]. By contrast, the posterior third is innervated by the lingual branch of the glossopharyngeal nerve (cranial nerve IX). The area around the throat, including the glottis, epiglottis, and pharynx, receives branches of the vagus nerve (cranial nerve X). Overall, each fiber has the capacity to respond to all gustatory qualities, though with different degrees of intensity. The first synaptic relay of the gustatory pathway occurs at the terminals of the sensory afferent fibers and the individual synaptic cells [75]. The central axons of these primary sensory neurons, located in the respective cranial nerve ganglia, project to rostral and lateral regions of the nucleus of the solitary tract in the medulla, also referred to as the gustatory nucleus of the solitary tract complex (Figure 4). From this gustatory nucleus, neurons extend to the ventral posterior medial nucleus (VPM) of the thalamus. This thalamic nucleus then projects to various cortical regions, such as the anterior insula and frontal operculum (gustatory cortex) in the ipsilateral cerebral cortex. The gustatory cortex is the structure that mediates the conscious discrimination of taste stimuli [75-77]. Lesions of the insula lead to ageusia, which is the complete inability to perceive any tastants [78]. Moreover, reciprocal connections link the nucleus of the solitary tract, via the pons, to both the hypothalamus and the amygdala. These pathways are believed to regulate appetite, satiety, and other homeostatic responses related to eating. Projections from the gustatory cortex also extend forward to the dysgranular caudolateral region of the orbitofrontal cortex, where they join with inputs from visual and olfactory areas. At this site, the integration of visual, olfactory, and gustatory inputs enables the perception of flavor, defined as the combination of taste, smell, and somatosensory sensations (such as texture and pain) [77, 79, 80]. In fact, flavor plays a crucial role in food recognition, guiding the assessment of whether a food is edible and whether it provides hedonic pleasure and enjoyment. Beyond the basic taste qualities, other sensory perceptions have been identified. One of these is pungency, perceived as an irritating sensation of heat and/or pain, elicited by compounds such as capsaicin from chili peppers, zingerone from ginger, and allyl isothiocyanate from horseradish. These substances appear to activate transient receptor potential (TRPs) ion channels, which are expressed in nociceptors within the oral cavity and transmitted through the trigeminal nerve [81-84]. Another example is astringency, a common sensation produced by consuming foods rich in polyphenols. It is characterized by a drying, roughening, and puckering effect on oral surfaces [85], and is typically associated with foods such as green tea, coffee, cocoa, berries, and red wine. The most widely accepted explanation for astringency is based on the interaction between polyphenols and salivary proteins, leading to hydrogen bonding or hydrophobic interactions, which ultimately result in insoluble precipitates [86-89].

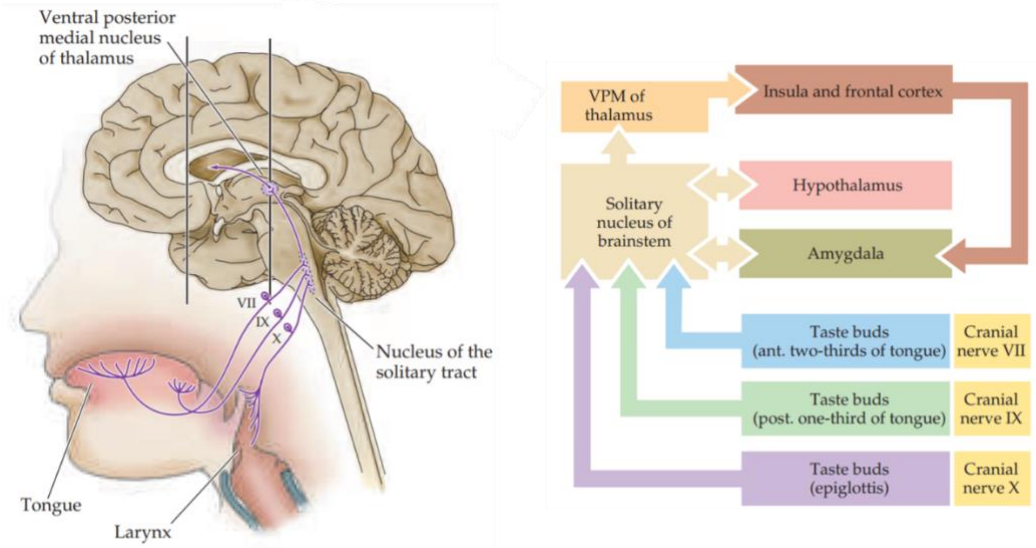

Figure 4. Organization of the human taste system. Left: drawing on the left shows the relationship between receptors in the oral cavity and upper alimentary canal, and the nucleus of the solitary tract in the medulla. The section on the right shows the VPM nucleus of the thalamus and its connection with gustatory areas of the cerebral cortex. Right: diagram of the basic pathways for processing taste information [82].

In general, oral perception is defined as the combination of the multisensory interactions of taste, smell, and the trigeminal system that we perceive when tasting food. While gustatory, olfactory, and trigeminal systems are anatomically separated with different functions, this does not necessarily mean that they cannot interact on a cognitive level. As a consequence, people frequently report a loss of their sense of taste when their nose is blocked, which is only one common example illustrating that the senses of taste and smell are frequently confused. Individual differences in oral sensitivity are significant, and they can substantially impact dietary preferences and nutritional status. In addition, numerous diseases and medical interventions can have an impact on oral sensitivity. This may have significant effects on the quality of life.

2. Individual differences and influencing factors in taste perception

Taste sensitivity shows a significant variability in humans, a strong influence on both food choice and satiety [90]. In this regard, the physiologic role of taste variability may be linked to evolutionary adaptation to particular environments, allowing recognition of substances that are either harmful or essential for bodily function [91]. For example**,** bitter taste exerts a dual role in human nutrition, functioning both as a warning signal and as an attractant. A wide range of bitter-tasting compounds is produced by plants as a means of defense against predation [92]. Given that intense bitterness is often associated with toxic substances, the human ability to perceive bitterness at low concentrations represents an important evolutionary mechanism to restrict or avoid the intake of potentially harmful plant foods [90]. On the other hand, several classes of bitter polyphenols, such as tannins, catechins, and anthocyanins (from grapes, tea, coffee, dark-colored fruit, citrus, and chocolate), together with glucosinolates from cruciferous vegetables [93], confer positive health benefits due to their anti-bacterial and antioxidant properties [94]. The perception of bitter thiourea compounds, phenylthiocarbamide (PTC) and 6-n-propylthiouracil (PROP), constitutes a widely studied human trait [95]. These thiourea compounds include the thiocyanate moiety (N-C=S), which gives them the bitter taste [96, 97] (Figure 5). Interestingly, the N-C=S group is likewise present in glucosinolates and goitrin, naturally occurring substances commonly identified in cruciferous vegetables such as broccoli, cabbage, cauliflower, and Brussels sprouts (Brassica oleracea), as well as in other Brassica plants [98]. Goitrin displays potent anti-thyroid activity and may be toxic if ingested in large quantities by populations vulnerable to thyroid deficiency [99]. At the same time, these vegetables also provide remarkable anti-cancer effects [98]. Depending on regional dietary patterns, excessive consumption of these vegetables can result in either positive or negative health outcomes [100]. One possible explanation for the persistence of this trait in humans is that it acted as an evolutionary adjustment to local eating environments [101]. Accordingly, stronger rejection of Brassica plants would

have conferred survival advantages on individuals who were more sensitive to their bitterness [102]. Individual variability in sensitivity to the bitter taste of PTC was first identified by Fox more than eight decades ago [96]. According to threshold methods, PROP-sensitive and non-sensitive individuals are classified as tasters and non-tasters, respectively**.** The frequency of non-tasters differs among populations, ranging from as little as 7% to more than 40% [103]. Specifically, in the Caucasian population, the estimated proportion of non-tasters is about 30% [104-108]. Bartoshuk [108, 109] was the first to introduce the term *"supertaster"* to distinguish individuals who experience PROP as extremely bitter from those who perceive it as moderately bitter. Although numerous studies support the categorization of individuals into three phenotypic groups (non-tasters, medium-tasters, and super-tasters) [110-118], other evidence indicates that PROP tasting may actually represent a more continuous phenotype [111, 115, 119]. The ability to taste PROP is greatly linked to haplotypes of the *TAS2R38* gene, defined by three single-nucleotide polymorphisms that result in three amino acid substitutions (Pro49Ala, Ala262Val, and Val296Ile) [114, 120] (Figure 5). Two common haplotypes are found: PAV, the dominant (sensitive) variant, and AVI, the recessive (insensitive) one. Non-tasters are homozygous for AVI, while it was originally assumed that super-tasters were homozygous for PAV and medium-tasters were heterozygous for PAV. Yet, studies have shown a considerable genotypic overlap between medium and super-taster groups [110, 114, 120], with many super-tasters carrying the PAV/AVI diplotype. Furthermore, some findings suggest that having two PAV alleles, compared with one, does not provide any additional advantage for perceiving stronger PROP bitterness, at least within the suprathreshold range [115].Consequently, TAS2R38 genotypes alone do not fully account for the oro-sensory distinctions between medium and super-tasters. In fact, *TAS2R38* predicts most (55–85%) but not all of the phenotypic variation in PROP threshold, suggesting that epigenetic mechanisms may contribute to the expression of this trait [48, 90, 107, 115]. Supporting this idea, evidence for modifying genes has emerged from studies using diverse approaches, including family segregation, family-based linkage, and genome-wide association analyses [121-123]. Nonetheless, research has consistently shown that super-tasters possess a higher density of fungiform papillae on the anterior tongue compared to other groups [109, 124-126]. These anatomical differences may partly explain why super-tasters exhibit stronger oral responsiveness to a range of oral sensations that extend beyond the bitter taste receptor.

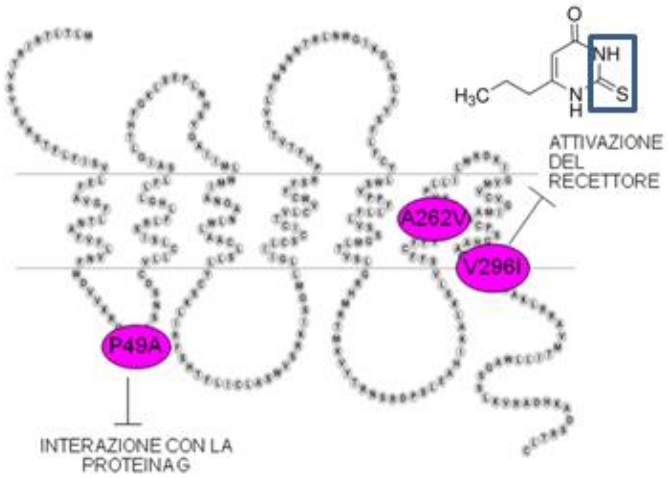

Figure 5. Schematic representation of the *TAS2R38* receptor and the three polymorphisms associated with different levels of sensibility. Chemical structure of 6-n-propylthiouracil (PROP). The isothiocyanate chemical group is highlighted in blue.

More recently, attention has turned to the role of the *Gustin* (CA6) gene, which encodes a trophic factor involved in taste bud development, in relation to PROP phenotype [127]. It has been demonstrated that the *rs2274333* (A/G) polymorphism of the *Gustin* gene led to a modification of gustin's primary structure, crucial for zinc binding and the full functionality of the protein [127]. The AA genotype (linked to a fully functional protein) was more frequent among super-tasters, whereas the GG genotype (linked to protein disruption) was more common in non-tasters. Taken together, these findings suggest that variation in

Gustin contributes to differences in papillae density and oral chemosensory function across PROP taster groups.

Contemporary research in human nutrition has revealed that PROP bitterness may act as a general marker for oral sensations and food preferences. This assumption arises from evidence showing that individuals who perceive PROP/PTC as strongly bitter are also more responsive than non-tasters to multiple oral stimuli, including other bitter compounds [108, 113, 128-132], sweet substances [133], chemical irritants [114, 134], and fats [111, 112]. Among these associations, the link between PROP bitterness intensity and the perception or acceptance of fats is particularly noteworthy, given the nutritional importance of dietary lipids. Indeed, several studies have demonstrated that PROP non-tasters exhibit a reduced ability to discriminate fat content in foods, with greater acceptance of dietary fats [111, 119, 135, 136], and consume more daily servings of discretionary fats compared with tasters [135]. On this basis, an inverse relationship between PROP status and body mass index (BMI) has been hypothesized and is supported by multiple investigations [110, 137-139].

The *CD36* protein, whose expression is controlled by the *CD36* gene and its allelic variation, plays a crucial role in fat perception. The substitution of A with G in the rs1761667 SNP has been shown to reduce protein expression [140], and it is associated with a diminished oral sensitivity to fatty acids [15, 141, 142]. Interestingly, ethnic-specific effects have also been observed: in one study, East Asians with the AA genotype exhibited reduced fatty acid perception, while this effect was absent in Caucasians [143]. The same SNP substitution (A→G) has also been linked to variations in fat preference [144]. In addition, some authors have proposed that PROP-related sensory differences may be connected to olfactory function [125, 145], suggesting that PROP tasting could influence food perception via aromas or flavors [111, 146]. Conversely, other studies have reported no significant associations between PROP taster status and these variables [125, 147-150]. Such discrepancies imply that further factors contribute to feeding behavior, food perception, and food preference across PROP taster groups. For example, the chemical-physical composition of saliva may play a role in individual taste differences [96, 105]. Salivary proteins, in particular, are known to influence sweet [151], salty [152], and umami [153] taste, as well as preferences for fat and salt [154] and acceptance of bitterness [155]. Variations in the salivary proteome have also been linked to human responses to bitter stimuli such as calcium nitrate, urea, or quinine [156, 157].

Our laboratory has focused on the role of salivary proteins in sensitivity to PROP, the prototypical bitter taste stimulus [158-160], demonstrating that PROP super-tasters possess higher basal levels of two basic proline-rich proteins (bPRPs: Ps-1 and II-2), and that PROP stimulation further increases the concentration of these proteins only in super-taster subjects. Moreover**,** supplementation with amino acids from the sequence of these proteins (i.e., L-Arg and L-Lys) enhances sensitivity not only to PROP but also to other taste qualities [159-162]. According to the proposed mechanism, these proteins or amino acids may exert a permissive role in taste perception, depending on their salivary concentration. Specifically, they are thought to act as “carriers” of tastants by increasing their solubility in saliva and thereby increasing their availability to taste receptor sites [160]. Salivary proteins also appear to play a role in eliciting the sensation of astringency [163-166]. These proteins are primarily identified as acidic proline-rich proteins (aPRPs), histatins (Hist), cystatins (S-Cyst), and statherin (Stath). In addition, other proteins such as mucins, glycosylated proteins, and bPRPs contribute to this phenomenon, as they are mainly adsorbed onto oral surfaces and are fundamental for maintaining oral lubricity while protecting the salivary pellicle against damage and microbial attack [167, 168]. When polyphenols interact with these proteins, large aggregates are formed, eventually compromising the protective lubricating layers. As a result, these combined effects generate the astringency sensation [169, 170], which, in evolutionary terms, may have functioned as a warning signal against toxicity due to excessive consumption of plant materials. Despite this knowledge, the time course of astringency perception and subsequent oral recovery remains poorly understood. It is established that astringency after oral stimulation can last from 100 to 300 seconds, or even longer, before subsiding [85, 171-173]. Yet, complementary studies investigating the salivary protein response over time are still limited [174]. The intensity of astringent sensation, its qualitative attributes (such as drying, roughing, or puckering), and its temporal dynamics depend on both the type and concentration of the stimulus used [85, 175, 176]. Furthermore, different compounds used in astringency research, including various polyphenols (e.g., grape seed tannins, catechins), metal salts, and organic acids, have been shown

to produce distinct profiles of astringency perception [177, 178]. This variety indicates that multiple mechanisms may underlie the astringency response. Nevertheless, our current understanding of how astringent sensations are generated remains incomplete.

3. Methods for the measurement of taste sensitivity

In humans, taste function has been extensively investigated using various kinds of approaches. Psychophysical approaches have provided important insights into individual variations of gustatory sensitivity. Generally, screening procedures are divided into two main categories: threshold assessments**,** which evaluate an individual's ability to detect or discriminate minimal concentrations of a stimulus, and suprathreshold assessments**,** which rely on rating scales to evaluate perceived taste intensity at higher concentrations. Threshold-based evaluations are considered reliable and have been used for decades in sensory research [90]. Among the techniques that assess responsiveness at suprathreshold levels, those based on the classification of PROP (6-n-propylthiouracil) taster status are the most widely employed for distinguishing individuals according to their sensitivity to bitter compounds [117, 179]. Suprathreshold procedures typically involve rating scales that quantify perceived PROP bitterness across the psychophysical spectrum. This approach enables the differentiation of individuals as super-tasters**,** medium-tasters**,** or non-tasters [90, 109, 117, 127, 179, 180]. Suprathreshold evaluations are performed by having participants rate the perceived intensity of PROP after stimulation with multiple samples, a single solution, or PROP-impregnated filter papers [109, 117, 179, 181]. The pioneering work of Bartoshuk and colleagues [109] introduced a screening protocol in which five concentrations of PROP and five of sodium chloride (NaCl) were presented; participants were categorized based on how intensely they rated PROP relative to NaCl. Those perceiving PROP as stronger than NaCl were labeled super-tasters, those giving comparable ratings were medium-tasters, and those rating NaCl higher than PROP were classified as non-tasters.

However, some researchers have questioned the reliability of NaCl as an independent comparison stimulus [182, 183]. Evidence indicates that at elevated NaCl concentrations (>0.35 M), ratings for NaCl may correlate with PROP taster status and diverge in super-tasters [183]. Despite this, the use of NaCl as a reference standard has been widely adopted and validated across numerous laboratories worldwide [109, 110, 119, 124, 127, 137, 139, 159, 163, 181, 184-200]. The two principal psychophysical scales employed in PROP evaluations are the Labeled Magnitude Scale (LMS) [201] and the General Labeled Magnitude Scale (gLMS) [202]. Both scales allow participants to rate PROP intensity relative to their "strongest imaginable oral sensation" (LMS) or the "strongest imaginable sensation of any kind," encompassing the most intense experiences of pain, sound, or light (gLMS). Participants typically receive training before using these scales. To accommodate the need for brief, field-applicable screening methods**,** Tepper and colleagues [117, 179] developed simplified procedures derived from Bartoshuk's original method [109]. These include the 3-solution**,**1-solution, and paper disk methods. The latter two rely on empirically determined cutoff values for PROP taster classification. Such techniques have been successfully used in numerous studies [110, 124, 127, 137, 139, 159, 163, 181, 184, 185, 187-200]. Importantly, PROP classifications obtained using these methods exhibit strong correlations with *TAS2R38* genotypes [110, 160, 185, 203-205], as well as with physiological differences such as variations in prefrontal cortex activity [206] and in the activation of peripheral taste mechanisms [207, 208]. Other psychophysical paradigms have been developed to evaluate taste function across the five basic modalities: sweet, salty, sour, bitter, and umami [209, 210]. Among these, the Taste Strip Test (TST), inspired by ideas from Kobal [211] and later refined by Mueller and colleagues [209], represents a significant methodological advancement. The TST employs spoon-shaped filter papers impregnated with specific tastants, allowing for selective application to particular regions of the tongue. This design not only facilitates controlled testing but also ensures a longer shelf life compared to liquid solutions. The Taste Strip Test has been widely adopted and validated in several studies [210, 212-219], demonstrating its reliability in assessing differences between tongue sides and in evaluating gustatory function before and after interventions. However, the original study by Mueller et al. [210], presented some methodological limitations, most notably the absence of a forced-choice testing paradigm, a feature later integrated by subsequent researchers to improve test accuracy and consistency. To overcome these limitations, subsequent large-scale studies established normative values for the Taste Strip Test, confirming its reliability and clinical usefulness across age and sex groups. In addition to the TST, other threshold and

suprathreshold tests are used to explore individual sensitivity to particular tastants. For instance, sucrose detection thresholds are typically measured using a three-alternative forced-choice (3-AFC) procedure. The detection threshold corresponds to the lowest concentration correctly identified on three consecutive trials. On the other hand, suprathreshold sucrose tests are conducted with increasing concentrations, and subjects must rate the perceived sweetness intensity using a general labeled magnitude scale (gLMS). Similarly, oral sensitivity to fatty acids, such as oleic acid, has been explored through modifications of the staircase method implemented in a 3-AFC procedure. In this paradigm, stimuli are delivered using three filter paper disks impregnated, one with a mixture of the fatty acid and the other two with mineral oil. This approach enabled the examination of oro sensory perception of fatty acids and its association with genetic variants (e.g., CD36) or other taste phenotypes such as PROP sensitivity [220].

In addition to psychophysical assessment, morphological analyses have been employed to investigate anatomical correlates of taste perception. Among these, the evaluation of fungiform papillae (FP) on the anterior tongue has attracted considerable attention as a structural marker of oral sensory responsiveness. The density of fungiform papillae (FPD) has been proposed as an indicator of gustatory capacity, since these papillae contain taste buds innervated by the chorda tympani and are surrounded by trigeminal endings involved in somatosensory and chemesthetic perception [221-223]. Individuals with higher papilla density often exhibit greater taste sensitivity, supporting the link between structural and functional aspects of taste. Identification of FP typically relies on visual inspection of the anterior portion of the tongue, where these structures are most densely distributed. Their recognition is based on specific morphological features: FP appear as small, circular or slightly oval elevated structures that differ in size, shape, and colour from the surrounding filiform papillae. In research practice, digital images of the tongue surface are commonly acquired to quantify FPD, often after dyeing procedures that enhance contrast between FP and the background mucosa. The Denver Papillae Protocol [224] represents the most widely adopted methodological reference, providing dichotomous criteria for papilla identification according to their elevation, circularity, and diameter relative to adjacent structures. Despite the apparent simplicity of visual identification, several methodological variables can influence FP count reliability, including image resolution, lighting conditions, dyeing agents, and the precise definition of the counting area on the tongue surface [225, 226]. For this reason, operator training and inter-rater validation are considered essential steps to ensure consistency across studies. Automated image analysis techniques have recently been developed to improve objectivity and reproducibility [227-229], although their widespread adoption remains limited due to the lack of standardized, commercially available software. Together, these morphological approaches complement psychophysical assessments by providing an anatomical dimension to the study of taste function. Integrating structural indicators such as FPD with perceptual measures allows a more comprehensive understanding of individual differences in taste sensitivity and oral responsiveness.

However, because psychophysical methods are highly subjective, objective approaches are also required to complement them. Molecular approaches that determine genotypes of polymorphisms of specific genes involved in taste function have been studied to identify differences in gustatory sensitivity among individuals**.** The most widely studied are single-nucleotide polymorphisms (SNPs) in the *TAS2R38* gene, which are strongly associated with sensitivity to bitter compounds such as PROP. The variants in the *Gustin* (CA6) gene have been associated with taste bud function and density. Genetic variability also includes sweet and fat taste perception. For sweet taste, polymorphisms in the *TAS1R2* and *TAS1R3* genes, encoding the subunits of the sweet taste receptor, have been associated with differences in sucrose sensitivity. In particular, SNPs such as *rs12033832* and *rs35874116* in *TAS1R2*, and *rs307355* and *rs35744813* in *TAS1R3*, have been linked to variability in sweet detection thresholds and suprathreshold sensitivity [230-234]. Common variants in the *CD36* gene including *rs1761667*, *rs1527483*, and *rs3840546* have been associated with differences in oral fat sensitivity, preference, and obesity risk**.** These molecular analyses provide an objective means to explore the genetic basis of interindividual differences in taste perception and complement psychophysical and morphological assessments [15, 48, 90, 144, 220, 235, 236].

The fact that the psychophysical approaches can often lead to controversial results, being based on highly subjective evaluations that can produce significant measurement errors, and that molecular analyses are highly expensive and time-consuming, raises the necessity to use other kinds of objective approaches. Deep learning (DL) approaches based on Convolutional Neural Networks have shown great promise in the

analysis of biomedical images [237, 238]. In particular, the U-Net architecture has been widely applied in medical imaging for tasks such as tumor detection, organ segmentation, and cell counting, demonstrating robustness across various applications [239, 240]. Recent studies [227], have demonstrated the effectiveness of U-Net in segmenting FPs from tongue images, achieving strong correlations with manual counting methods. However, in this work, a limited dataset has been used to train the model. ML algorithms are designed to learn from data samples and can operate in different modes depending on the task. The algorithm is trained on labeled datasets and can then predict new subjects. Supervised learning can address regression problems, where the output is continuous, or classification problems, where the output is discrete (e.g., assigning a subject to one category). In taste perception research, ML models can integrate diverse biological and experimental variables such as sensory ratings, genetic markers, fungiform papillae density, demographic characteristics, and clinical data. By doing so, they could provide scalable and real-time classification, also highlighting the relative importance of each feature. In our laboratory, we were able to automatically recognize, with high precision, the PROP phenotype by using Machine Learning (ML). This allowed not only the objective discrimination between taster categories but also the validation of individual features that contribute most strongly to PROP sensitivity.

4. Taste impairment and health

Taste perception is fundamental not only for evaluating food quality and guiding dietary choices but also for overall health and disease susceptibility. Gustatory dysfunctions, such as hypogeusia and ageusia, are relatively common in the general population and increase with age, impacting nutritional status, body mass index (BMI), and quality of life, often contributing to depressive symptoms [241-260]. Individual differences in taste perception, including sensitivity to bitter compounds such as PROP and PTC, are associated with variations in general chemosensory sensitivity and broader health outcomes [90, 110, 111, 114, 126, 128, 131, 132, 163, 261-268]. Taste dysfunction has been increasingly recognized as a contributing factor in several pathological conditions that affect nutrition, metabolism, and overall health. Alterations in gustatory sensitivity can significantly influence eating behaviour, leading to unbalanced dietary habits and metabolic disorders such as obesity [255, 269-271]. Individuals with obesity frequently exhibit reduced taste sensitivity for sweet [272], umami [273], bitter, sour [259], and fatty acid stimuli [274], which may drive the preference for energy-dense foods such as fats and sugars [259, 275-280]. Conversely, improvements in taste sensitivity have been observed in obese subjects undergoing bariatric surgery, including enhanced taste identification and altered preferences toward low-calorie or less palatable foods [281-297]. These findings suggest that variations in gustatory perception may contribute to the success of weight-loss interventions by modulating food choice and intake [287]. Taste impairment has also been described in inflammatory and gastrointestinal diseases, particularly in Inflammatory Bowel Disease (IBD), although findings remain inconsistent [298-303]. Some studies report a generalized or selective reduction in taste function linked to zinc deficiency and decreased activity of the zinc-dependent salivary enzyme gustin/CAVI [300, 301, 304, 305], suggesting a biochemical contribution to altered taste perception.

Alterations in general oral perception represent a complex pathological condition resulting from disrupted multisensory integration among the gustatory, olfactory, and trigeminal systems [306, 307]. These sensory modalities, though anatomically distinct, interact at both peripheral and cognitive levels, and their dysfunction can profoundly affect food perception, dietary behavior, and overall quality of life [260, 267, 308-314]. Numerous diseases, medical interventions, and aging processes can impair oral sensitivity [260, 267, 309-312], leading to difficulties in detecting basic taste qualities and distinguishing between taste and flavor perception, the latter often being confounded by olfactory deficits [251, 315].

Dysfunctions in taste receptors, particularly type 2 taste receptors (T2Rs), have been associated with a variety of human diseases involving the respiratory, gastrointestinal, and nervous systems [316]. Genetic variants or epigenetic modifications, such as DNA methylation (DNAm), can influence the expression or sensitivity of these receptors, thereby affecting both taste perception and extraoral physiological functions, including innate immune defense, metabolism, and pathogen recognition [317-325]. Among these receptors, TAS2R38 is of particular interest due to its dual role in mediating bitter taste perception and contributing to the innate immune response of the respiratory tract through nitric oxide (NO) production upon microbial stimulation [326, 327]. Structural or regulatory alterations in *TAS2R38* caused by single-

nucleotide polymorphisms (SNPs) or changes in DNAm patterns may therefore underlie not only variations in taste sensitivity but also differences in susceptibility and severity of infections such as COVID-19 [328-332] .

Taste impairment is an increasingly recognized non-motor symptom of Parkinson's disease (PD), a neurodegenerative disorder, that affects over 10 million individuals worldwide [311, 333-337], characterized by the progressive loss of dopaminergic neurons in the substantia nigra pars compacta and the accumulation of misfolded α-synuclein within Lewy bodies [333, 338]. In addition to motor dysfunctions, PD patients frequently experience sensory alterations, including olfactory and gustatory deficits, which can precede motor symptoms and may serve as early biomarkers of disease progression [311, 339]. Taste disorders in PD ranging from hypogeusia and dysgeusia to complete ageusia are often correlated with disease severity and have been reported for all basic tastes, including sweet, salty, sour, bitter, and umami [340, 341]. These alterations can influence appetite, food preferences, and nutritional status, contributing to weight changes and reduced quality of life [342]. Although olfactory dysfunction is a well-established early marker of PD, the mechanisms underlying taste impairments remain poorly understood and inconsistently reported [343-345]. Emerging evidence suggests that taste receptor variants, particularly bitter taste receptors (T2Rs), may be implicated in PD pathophysiology [267, 346]. These receptors, which are expressed not only in the oral cavity but also in extraoral tissues, have been shown to interact with toll-like receptors (TLRs), key mediators of the innate immune system [316, 347]. Dysregulated TLR/T2R signaling has been linked to abnormal α-synuclein aggregation and neuroinflammation in PD [340, 348, 349]. Moreover, elevated salivary levels of oligomeric α-synuclein, as well as genetic variants in the SNCA gene, have been proposed as promising peripheral biomarkers of PD [350-352].

5. Aim of the Study

The main aim of this PhD thesis was to investigate the function of taste and its mechanisms controlling individual variability, and therefore health. Many studies that focused on this field have led to controversial results, often because methods to assess sensory parameters are based on highly subjective evaluations, which can produce significant measurement errors [180]. I conducted a multidisciplinary research work aimed at investigating the genetic, epigenetic, and computational determinants of human taste perception to clarify interindividual variability and explore its clinical implications. My work integrated molecular biology and psychophysical approaches with advanced machine learning and deep learning methods, addressing both fundamental aspects of sensory neuroscience and translational applications in health and disease.

Firstly, given the implications that the genetic variants of *TAS2R38* bitter receptor have in tasting and non-tasting functions and disorders [48, 120, 185, 252, 266, 267, 316, 326, 346, 353-359], we addressed the issue of assessing the efficacy of ML classifiers in the automatic and highly accurate distinction between *TAS2R38* genotypes, by exploiting psychophysical and biological features of participants which were used as predictive variables in the data set (**chapter 2**). In addition, the proposed approach was used to show the feasibility of machine learning as a cost-effective and time-saving alternative to traditional molecular assays for genotype identification, with implications for both basic research and clinical practice.

[*Naciri LC, Mastinu M, Crnjar R, Barbarossa IT, Melis M. Automated identification of the genetic variants of TAS2R38 bitter taste receptor with supervised learning. Computational and Structural Biotechnology Journal, 2023, 21, 1054-1065. DOI: 10.1016/j.csbj.2023.01.029*]

Secondly, to overcome the challenges and limitations associated with manual counting of FPs, we used and compared three different Convolutional Neural Net-works (Classic U-Net [239], MultiResUNet [360, 361], and an optimized version of U-Net that we designed to enhance the performance in detecting FPs even when it has to identify FPs in challenging input images characterized by different density and morphology (**chapter 3**). This work provided, for the first time, a reliable automated tool to assess papillae density and distribution, offering new opportunities for objective and large-scale analyses of fungiform papillae, with potential applications in both clinical diagnostics. The script is available and open source on GitHub.

[*Naciri LC, Cabini RF, Melis M, Roberto Crnjar R, Pizzagalli DU, Barbarossa IT. Automatic detection of fungiform papillae on the human tongue via Convolutional Neural Networks and identification of the best performing model. Computational and Structural Biotechnology Journal, 2025, 27, 1927-1934. DOI: 10.1016/j.csbj.2025.05.014*]

Furthermore, the third aim of this work was to apply supervised regression methods to analyze with high precision the overall taste statuses of healthy controls (HCs) and patients with chemosensory loss, and to characterize the combination of responses that would best predict the overall taste statuses of the subjects in the two groups (**chapter 4**). Considering that the oral perception that we experience when tasting food consists of the multimodal interactions of taste, smell, and the trigeminal system, we also assessed the efficacy of SL regression methods to analyze with high precision the subjective ratings of the oral sensitivity of healthy participants and patients with chemosensory loss (**chapter 5**). The proposed approach was also used to determine the significance and contribution to the oral sensitivity of the single components of taste, olfactory, and trigeminal, highlighting the differences between the two groups.
[*Naciri LC, Mastinu M, Melis, Green T, Wolf A, Hummel T, Barbarossa, IT. A Supervised Learning Regression Method for the Analysis of the Taste Functions of Healthy Controls and Patients with Chemosensory Loss. Biomedicines 2023, 11, 2133. DOI: 10.3390/biomedicines11082133*]
[*Naciri LC, Mastinu M, Melis M, Green, T, Wolf A, Hummel T, Barbarossa IT. A supervised learning regression method for the analysis of oral sensitivity of healthy individuals and patients with chemosensory loss. Scientific Report, 2023 13,17581. DOI: 10.1038/s41598-023-44817-w*]

My work also has investigated the role of epigenetic regulation in taste-related genes. At first, I analyzed the methylation status of the *Gustin* gene, which encodes a salivary protein with trophic functions for taste buds, to verify if *Gustin* gene methylation can affect the salivary levels of the protein, also concerning PROP bitter responsiveness and the polymorphism *rs2274333*, which is crucial for the full functionality of the protein **(chapter 6)**. Successively, since the *TAS2R38* is the T2R receptor primarily associated with the innate immune response of the respiratory system, we aimed to verify whether changes in *TAS2R38* DNAm patterns can contribute to shedding light on the involvement of *TAS2R38* in COVID-19 infection and symptoms severity **(chapter 7)**.
[*Melis M, Loi E, Mastinu M., Naciri LC, Zavattari P, Barbarossa I.T. Gene Methylation Affects Salivary Levels of the Taste Buds' Trophic Factor, Gustin Protein. Nutrients 2024, 16, 1304. DOI: 10.3390/nu16091304*]
[*Melis M, Loi E, Aru G, Sollai G, Mastinu M, Naciri LC, De Riu G, Vaira LA, Costanzo G, Firinu D, Cabras P, Caddori A, Crnjar R, Zavattari P, Barbarossa IT. TAS2R38 gene methylation is associated with syndrome Coronavirus 2 (SARS-CoV-2) infection and clinical symptoms. Scientific Reports 2025, 15, 14462. DOI: 10.1038/s41598-025-95879-x*]

A Supervised Learning (SL) model was also used to clarify the diagnostic significance of taste deficits in a complex neurological condition, such as Parkinson's disease (PD), and to automatically classify PD patients based on disease severity (**chapter 8**).
[*Naciri LC, Sollai G, Deligia S. Fenu G, Mellino P, Pinna B, Crnjar R; Cossu G, Barbarossa IT. A multi-dimensional study on taste deficits, α-synuclein genetic profiling, and Supervised Learning for diagnosis and disease severity stratification in Parkinson's disease (PD), accepted for publication in Neurobiology of Disease.*]

Chapter 2
Automated identification of the genetic variants of the TAS2R38 bitter taste receptor with supervised learning

1. Materials and Methods

1.1. Participants

Eighty-four participants (35 men and 49 women) were enrolled through traditional practices at the University of Cagliari, Italy. They were Caucasian and their age ranged from 18 to 40 years, with a mean of 25.07 ± 0.507. Participants were classified as non-smokers (n = 65) and smokers (n = 19) and as underweight (n = 10, BMI below 18.5 kg/m^2), normal weight (n = 58, BMI from 18.5 to 24.9 kg/m^2) and overweight (n = 16, BMI from 25.0 to 29.9 kg/m^2). Exclusion criteria: use of medications affecting taste sensitivity (e.g., antihistamines, steroids, and certain antidepressants), major systemic diseases, food allergies, pregnancy, and lactation. All participants signed a consent form before being accepted into the study. The study was authorized by the University Hospital of Cagliari's Ethical Committee and carried out in accordance with the Declaration of Helsinki's principles (protocol code: 451/09; date of approval: 5/2016).

1.2. Experimental Procedure

The following biological data, which have been associated with the PROP phenotype and/or genotype [48, 90, 109, 110, 117, 120, 139, 179, 181, 203, 252, 362-366], were collected from each participant over the course of two sessions on consecutive days: PROP and NaCl intensity ratings, scores for the five tastes, the density of fungiform papillae, BMI, age, *TAS2R38* genotypes, taste sensitivity status, gender and smoking, and BMI status.

Before starting the sensory analysis session, participants were asked to refrain from eating, drinking (excluding water), using dental care products or chewing gum for at least 2 h. They had to adapt to the environmental conditions (23–24 °C; 40–50% relative humidity) of the test room for 15 min. To prevent taste sensitivity alterations caused by the estrogen phase, women were assessed on the sixth or seventh day of menstrual cycle [367].

In the first visit, measurements of height (m) and weight (kg) were taken to determined BMI (kg/m^2). 2 mL of whole saliva samples were taken and were kept at − 80 °C until the molecular analyses were finalized. After a recovery period of 1 h, the ratings of the perceived taste intensity for NaCl and PROP were taken by using two approved psychophysical techniques (the Three-solution Test [117] and the Impregnated Paper Screening Test [179]).

On the second day, scores for the five basic taste qualities (salty, sweet, bitter, sour and umami) were assessed by using the Taste Strip Tests (TST and umami test, Burghart Messtechnik, Wedel, Germany) [209, 210, 368]. Fungiform papilla density was also determined.

Before each stimulation, each participant rinsed his/her mouth with spring water. The day before the session, the solutions were prepared, stored in the refrigerator, and then provided to the participant at room temperature.

1.3. Taste Assessments

1.3.1. PROP and NaCl Intensity Ratings and PROP Taster Status Classification

The ratings of the perceived intensity for PROP and NaCl were collected from each participant by two psychophysical methods (Three-Solution Test, [117] and the Impregnated Paper Screening Test [179]) which have been used in many studies [127, 159, 181, 185] and strongly correlate with the activation of peripheral taste system [207, 369, 370]. These two methods allowed to classify participants by their PROP taster status.

According to Tepper et al. [117], the Three-solution test was used as a first step to assess participants. Briefly, the ratings of perceived intensity for three solutions of NaCl (NaCl; 0.01, 0.1, 1.0 mol/L) (Sigma-Aldrich, Milan, Italy) and PROP (0.032, 0.32, and 3.2 mmol/L) (Sigma-Aldrich) at suprathreshold concentration were determined by applying the Labeled Magnitude Scale (LMS) [201]. Concentrations

(10 mL samples) were presented in random order with an interstimulus interval of 60 s. Participants who rated PROP lower than NaCl were categorized as non-tasters (NT), those who gave corresponding ratings were categorized as medium-tasters (MT) and those who gave higher ratings to PROP than to NaCl were categorized as super-tasters (ST). After a 1-h period of recovery, the appropriate belonging of a participant to a certain PROP taster group was confirmed by using the Impregnated paper screening test [179]. Thus, only participants categorized as alike were included in the other tests. In this second test, the perceived intensity ratings were collected using two paper disks impregnated with PROP (50 mmol/L) and NaCl (1.0 mol/L) that were applied on the tip of the tongue for 30 s according to Zhao et al. [179]. Participants who rated the PROP disk higher than 67 mm in LMS were categorized as ST, those who rated the PROP disk lower than 15 mm were categorized as NT, and the others were categorized as MT [179]. To validate the ST classification of participants who could overestimate the oral stimuli [90] by using LMS, the general labeled magnitude scale (gLMS) [202], which broadens the top anchor of the scale to encompass any sensation, was also used to assess ST participants. Based on their taster group assignments, 17 participants (6 M, 11 F) were NT, 16 were ST (5 M, 11 F), and 51 were MT (24 M, 27 F).

1.3.2. Taste Sensitivity for the Five Basic Qualities

Scores for the five taste qualities were collected by The Taste Strip Test and the Umami Test (TST, Burghart Messtechnik, Wedel, Germany) [209, 210, 368], which consist of the identification of taste qualities presented by filter paper strips impregnated with four concentrations of each stimulus (0.016, 0.04, 0.1, or 0.25 g/mL of NaCl; 0.05, 0.1, 0.2, or 0.4 g/mL of sucrose; 0.05, 0.09, 0.165, or 0.3 g/mL of citric acid; 0.0004, 0.0009, 0.0024, or 0.006 g/mL of quinine hydrochloride and 0.25, 0.1, 0.04, 0.016 g/mL of monosodium glutamate). Each correct identification was rated 1, therefore, the maximum score for each quality was 4, 16 for the four tastes (TST), and 20 when umami was incorporated (Overall TST). A participant was considered hypogeusic or ageusic if he/she scored< 9, normogeusic if he/she scored ≥ 9 according to Landis et al. [209]. The qualities were presented in a pseudo-randomized sequence and concentrations were tested in ascending order.

1.4. Papilla Density

The fungiform papillae were recognized according to Melis et al. [203]. The tip of the tongue dorsal anterior surface was stained by positioning (for 5 s) a disk (6 mm dia) of filter paper impregnated with a blue food dye (E133, Modecor Italiana, Italy). Three to ten photographs of the tongue surface were taken for each participant by using a Canon EOS D400 (10 megapixels) camera with an EFS 55–250 mm lens. In the stained area of the tongue surface, the fungiform papillae were identified by their very light staining and mushroom shape [221]. Their number in each photograph was determined by the consensus of five observers, and the density/cm^2 was determined for each participant.

1.5. Genetic Analysis

Using the QIAamp® DNA Mini Kit (QIAGEN S.r.l., Milan, Italy) in accordance with the manufacturer's instructions, DNA was extracted from saliva samples. Using an Agilent Cary 60 UV-Vis Spectrophotometer, readings at an optical density of 260 nm were used to determine the content of pure DNA (Agilent, Palo Alto, CA, USA).

Participants were genotyped for three single-nucleotide polymorphisms (SNPs), (*rs713598*, *rs1726866*, and *rs10246939)* of the *TAS2R38* gene, which caused three amino acid substitutions (Pro49Ala, Ala262Val and Val296Ile). Molecular analyses were performed by using TaqMan SNP Genotyping Assay (C_8876467_10 assay for the *rs713598*; C_9506827_10 assay for the *rs1726866* and C_9506826_10 assay for the *rs10246939*) according to the manufacturer's instructions (Applied Biosystems by Life Technologies Milan Italy Europe BV). Each reaction included three positive controls, two negative controls, and two replicates.

Based on molecular analyses of the *TAS2R38* locus, 20 participants were PAV/PAV homozygous, 43 were PAV/AVI heterozygous, and 21 were AVI/AVI homozygous. Participants with rare haplotypes were not included in the study to reduce confounding factors in taste sensitivity [205].

1.6. Supervised Learning

The automatic recognition of the *TAS2R38* genotype of participants was carried out with SL algorithms capable of distinguishing the three genotypes (PAV/PAV, PAV/AVI, and AVI/AVI), by using the participants' features presented in the data model as predictive variables, as already performed by Naciri et al. to identify PROP taster categories [371].

The following algorithms were used: Logistic Regression, Decision Tree, Random Forest, K-Nearest Neighbor (KNN), and CatBoost classifier according to Naciri et al. [371]. During training, the algorithms search for the correlation of the features with the *TAS2R38* genotype groups, then they take new unknown inputs and assign them to the appropriate category. Specifically, Logistic Regression is an algorithm that classifies data by considering outcome variables at the extremes and tries to make a logarithmic line between them [372]. The decision tree is an acyclic graph [373]: in each branching node of the tree, a specific feature is examined. When the value of the feature is below a certain threshold, the left branch is followed; otherwise, the right branch is followed. When the node of the leaf is reached, the decision is made about the class to which the example belongs. The random forest algorithm builds multiple decision trees on data samples, then makes the prediction from each of them, and finally selects the best solution [374]. It is a better method than a single decision tree because it reduces over-fitting by averaging the results. Contrary to other algorithms that allow for discarding training data after the model is built, KNN keeps all training data in memory [375] . When a new sample needs to be classified, the KNN algorithm finds all the closest training samples and returns the majority label. CatBoost is an algorithm for gradient boosting on decision trees, excels at handling small datasets, and produces the best results when a dataset contains many categorical features. Furthermore, it is well known that CatBoost can be used in a variety of settings and for a wide range of issues [376-378].

The evaluation of algorithms is performed by metrics, such as precision (1), accuracy (2), recall (3), F1-score (4), Receiver Operating Characteristic (ROC) curve, and Area Under Curve (AUC) [371].

$$\text{Accuracy} = \frac{\text{true positives} + \text{true negatives}}{\text{all samples}} \quad (1)$$

$$\text{Precision} = \frac{\text{true positives}}{\text{true positives} + \text{false positives}} \quad (2)$$

$$\text{Recall} = \frac{\text{true positives}}{\text{true positives} + \text{false negatives}} \quad (3)$$

$$\text{F1-score} = 2 \times \frac{\text{precision} \times \text{recall}}{\text{precision} + \text{recall}} \quad (4)$$

The ROC curve represents a classifier's diagnostic capability and is constructed by plotting the true positive rate (TPR) as a function of the false positive rate (FPR) at diverse threshold settings. The AUC shows which of the used models best predicts a category. AUC is evaluated by the micro-average that combines the contributions of all categories to compute the average metric and the macro-average that computes the metric independently for each group and then makes the average. The first is preferable in the presence of imbalanced categories.

The following data processing operations, which are an essential phase in the running of an SL project, were performed:

1. For each feature, the distribution in each genotype group and the correlations between each feature and the target were determined (Figure S1). It is important to note that all numerical features present a normal distribution and that the ratings obtained with the two tests were strongly correlated with each

other ($r > 0.43$; $p < 0.001$, Pearson's (r) coefficient analysis), as well as papilla density and rating of PROP paper disk ($r = 0.34$; $p = 0.0016$) and the scores of the TST and the overall TST were strictly correlated with the scores of each taster quality ($r > 0.43$; $p < 0.001$).

2. After analysis of the dataset, the handling of missing values was performed: the mean values of the column were used to approximate the BMI value in six rows where it was missing.

3. The dataset content was converted into a language that an algorithm can understand. This included: a) One Hot Encoding and Ordinal Encoding, which encodes categorical data into numerical data; b) normalization of the numerical data by converting the real range of numerical values into values between 0 and 1; c) the Synthetic Minority Oversampling Technique (SMOTE) [379], which allows the balancing of the number of observations among classes. This operation was necessary to prevent the algorithm from learning better from the majority class with respect to the minority ones. In the training process, after SMOTE, the 31 PAV/AVI, 14 AVI/AVI, and 13 PAV/PAV observations became 31 observations in each genotype class.

In order to solve problems of overfitting or underfitting that may occur in the training of SL algorithms, we removed all features not significantly correlated with the *TAS2R38* genotype groups and increased the regularization parameters. In addition, we used 3-fold Cross-Validation [380], which mixes and splits data into two groups: one group of data (67% of data) as the training data and the other (33% of data) as the test data. This process was done three times with distinct subsets of data.

The overall behavior of our classifiers was evaluated by the automatic optimization of their hyperparameters by the Grid Search Algorithm [381, 382]. Subsequently, the models were evaluated by means of the evaluation metrics described above.

In addition, we used the Shapley Additive exPlanations (SHAP) [383], which allows us to interpret the SL model outputs by linking feature importance with feature effects. It returns a SHAP summary plot that connects the significance of the features to their impacts. Each point on the chart is a SHAP value that allows us to understand the contribution of an input feature to that single prediction. In addition to indicating feature relevance, SHAP values also indicate whether a feature has a favorable or unfavorable influence on predictions.

1.7. Statistical Analysis

Fisher's Exact Test was used to compare differences in the distribution of PROP taster, gender, and smoker groups according to *TAS2R38* genotypes. One-way analysis (ANOVA) was used to compare differences in BMI, age, papilla density, intensity ratings for PROP or NaCl, and taste scores according to *TAS2R38* genotypes (AVI/AVI, PAV/AVI, and PAV/PAV). Statistical analyses were conducted using STATISTICA for WINDOWS (version 7; StatSoft Inc, Tulsa, OK, USA). *P* values< 0.05 were considered significant.

2. Results

Mean values± SE or the participant distribution according to the *TAS2R38* locus regarding the sensory, genetic, morphological, clinical, and demographic features are shown in Table 1. One-way ANOVA revealed that the fungiform papillae density, as well as the intensity ratings for PROP (0.032, 0.32, 3.2 and 50 mM), varies with *TAS2R38* genotypes ($F(2,81) = 6.269$; $p = 0.003$; $F(2,81) = 8.875$; $p = 0.0003$; $F(2,81) = 27.463$; $p < 0.00001$; $F(2,81) = 18.025$; $p < 0.00001$; $F(2,81) = 16.707$; $p < 0.00001$). Specifically, participants with the AVI/AVI genotype showed lower values of papilla density and gave lower intensity ratings for PROP (0.32, 3.2 and 50 mM) than PAV/PAV or PAV/AVI participants ($p < 0.008$; Fisher LDS test), who showed no difference from each other ($p > 0.05$). Instead, the intensity ratings for PROP (0.032, mM) were higher for PAV/PAV participants than for PAV/AVI and AVI/AVI participants ($p < 0.009$; Fisher LDS test). In addition, the PROP taster status of participants was associated with *TAS2R38* SNPs based on ST, MT and NT participant distribution in each genotype group ($\chi2 = 49.979$; $p < 0.0001$; Fisher's test). Post hoc comparisons distinguished all groups from one another ($\chi2 > 12.24$; $p < 0.0022$; Fisher's test). NTs were more frequent among participants with genotype AVI/AVI (88.23%), MTs were more frequent among participants with the genotype PAV/AVI (68.63%), while STs were more frequent in PAV/PAV participants

(62.5%). No difference related to *TAS2R38* locus in age, BMI, gender, smoking status, intensity ratings for NaCl, or taste scores was found ($p > 0.05$).

Table 1. Sensory, genetic, morphological, clinical, and demographic features of participants according to *TAS2R38* genotypes.

Features	**PAV/PAV (*n* = 20)**	**PAV/AVI (*n* = 43)**	**AVI/AVI (*n* = 21)**
Age (y)	26.00 ± 0.93	24.14 ± 0.64	26.09 ± 0.91
BMI (kg/m^2)	21.99 ± 0.74	21.91 ± 0.51	21.49 ± 0.72
Papilla density/cm^2	36.74 ± 3.05^a	31.94 ± 2.08^a	22.14 ± 2.98^b
Male/female *(n)*	10/10	16/27	9/12
Smokers/non *(n)*	2/18	14/29	3/18
Intensity ratings			
PROP (0.032 mM)	10.25 ± 1.59^a	3.64 ± 1.08^b	1.4 ± 1.55^b
PROP (0.32 mM)	42.95 ± 3.98^a	36.16 ± 2.65^a	6.47 ± 3.79^b
PROP (3.2 mM)	74.75 ± 4.99^a	64.63 ± 3.40^a	35.44 ± 4.87^b
NaCl (0.01 M)	3.59 ± 1.40	4.12 ± 0.95	5.19 ± 1.36
NaCl (0.1 M)	31.71 ± 4.09	29.36 ± 2.79	29.33 ± 3.99
NaCl (1 M)	59.10 ± 5.01	63.81 ± 3.41	61.86 ± 4.89
PROP disk (50 mM)	56.60 ± 5.04^a	50.16 ± 3.44^a	19.91 ± 4.92^b
NaCl disk (1 M)	21.35 ± 4.12	25.24 ± 2.81	26.40 ± 4.02
PROP taster status ST/MT/NT (*n*)	10/10/0^x	6/35/2 ^{y}	0/6/15^z
Taste scores			
Sweet	3.30 ± 0.15	3.53 ± 0.10	3.33 ± 0.14
Salty	3.45 ± 0.16	3.65 ± 0.11	3.52 ± 0.16
Sour	2.25 ± 0.21	2.42 ± 0.14	2.43 ± 0.21
Bitter	3.25 ± 0.24	3.23 ± 0.16	3.14 ± 0.23
Umami	0.80 ± 0.33	1.58 ± 0.23	1.28 ± 0.33
TST	12.40 ± 0.45	13.07 ± 0.31	12.62 ± 0.44
Overall TST	13.05 ± 0.64	14.42 ± 0.43	13.71 ± 0.62

Values are either means±SE or the total number of participants. Significant differences of mean values are shown with a, b, and c letters ($p \leq 0.009$; LSD test following one-way ANOVA), while differences in frequency distribution are shown with x, y, and z letters ($p < 0.0022$; Fisher's method).

The best hyperparameters for each model were evaluated by the metrics to estimate the training and performance of the SL algorithms. The high values of precision (88%), recall (83%), and F1-score (82%) revealed that the CatBoost algorithm allowed to achieve the objective discrimination of *TAS2R38* genotypes (Table 2). Since our data are unbalanced, the accuracy results are not shown as they are meaningless. The Logistic Regression, Decision Tree, Random Forest, and KNN algorithms also achieved the goal, but with lower values of evaluation metrics than the CatBoost.

Table 2: Evaluation metrics for each classifier model.

Classifiers	**Precision**	**Recall**	**F1-Score**
KNN	55%	55%	55%
Decision tree	61%	59%	59%
Logistic Regression	73%	72%	71%
Random Forest	80%	79%	79%
CatBoost	88%	83%	82%

The ROC curve and AUC of the three genotypes of *TAS2R38* (PAV/PAV, PAV/AVI, and AVI/AVI) obtained by the CatBoost model are shown in Figure 1. The ROC curve showed that the corrected predictions made by the model were 96%, 78%, and 82%, for the three genotypes (AVI/AVI, PAV/AVI, and PAV/PAV,

respectively). Besides, the AUC showed that the micro-average, which represents the average margin of error, was 90%. The macro-average, which represents the median percentage value of all genotype groups, was 87%, a value not significant because of the unbalanced data.

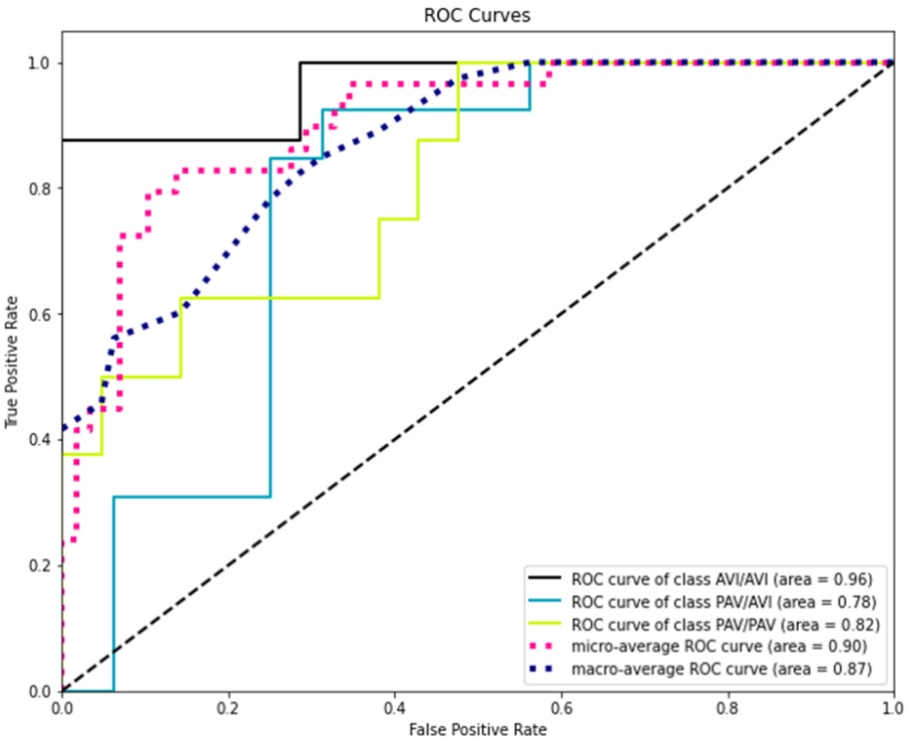

Figure 1. The ROC curve and the AUC determined with the CatBoost model. The ROC curve represents the percentage of error for each genotype of the *TAS2R38* gene. The line in black denotes the correct predictions of the AVI/AVI genotype, the line in light blue denotes the correct predictions of the PAV/AVI genotype and the line in yellow denotes the correct predictions of the PAV/PAV genotype. The dashed lines, in pink and blue, denote the value of the micro and macro-average, respectively.

Figure 2 shows an alluvial plot which represents the variations in network structure over the subject of *TAS2R38* groups recognized by different methods (*TAS2R38* genotyping and SL discrimination). This diagram graphically shows that 95.45% of subjects who had genotype AVI/AVI (n = 22) were allocated to the same genotype (n = 21) by SL discrimination, while 4.55% were allocated to PAV/AVI genotype (n = 1); 90.91% of subjects who had genotype PAV/AVI (n = 44) were allocated to the same genotype (n = 40) by SL discrimination, while 9.09% were allocated to AVI/AVI genotype (n = 2) or PAV/PAV genotype (n = 2); 76.19% of subjects who had genotype PAV/PAV (n = 21) were allocated to the same genotype (n = 16) by SL discrimination, while 23.81% were allocated to PAV/AVI genotype (n = 5) by SL discrimination.

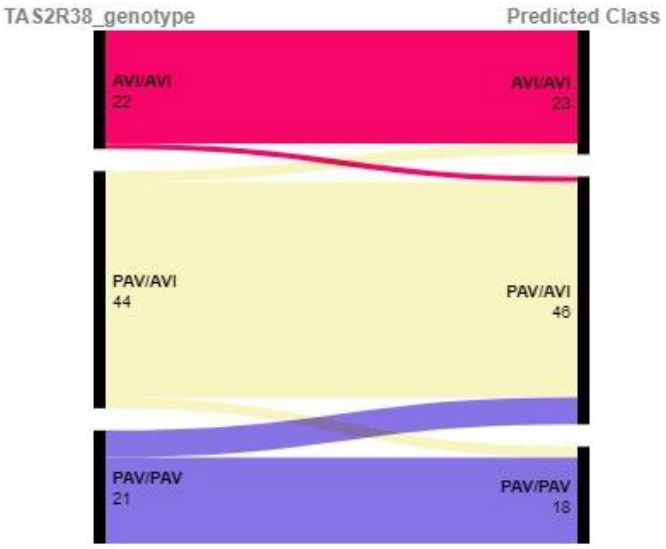

Figure 2. The alluvial plot graphically shows the variations in network structure over the subject of *TAS2R38* groups recognized by different methods (*TAS2R38* genotyping and SL discrimination). The magnitude of the components present in the two blocks connected by a stream is represented by the height of the stream. The number of subjects for each cluster is shown by a number.

The CatBoost classifier established the order of importance of the features in facilitating the learning of the model to detect the three *TAS2R38* genotypes (Figure 3). Specifically, the figure shows the importance of features for training the PAV/PAV genotype, the AVI/AVI genotype, and the PAV/AVI genotype. The intensity rating for the PROP solution (0.32 mM) was the most significant feature in the training model. This feature was followed in order of importance by ratings of intensity for the PROP solution (0.032 mM) and PROP paper disk (50 mM), and MT category, ratings of intensity for NaCl solution (0.01 M) and NaCl paper disk (1 M), and age. It is intriguing to observe that the score for umami was the most important in facilitating the learning of the model (ninth significant feature) among the scores for other taste qualities. Also, papilla density was a significant feature (eleventh in order of importance).

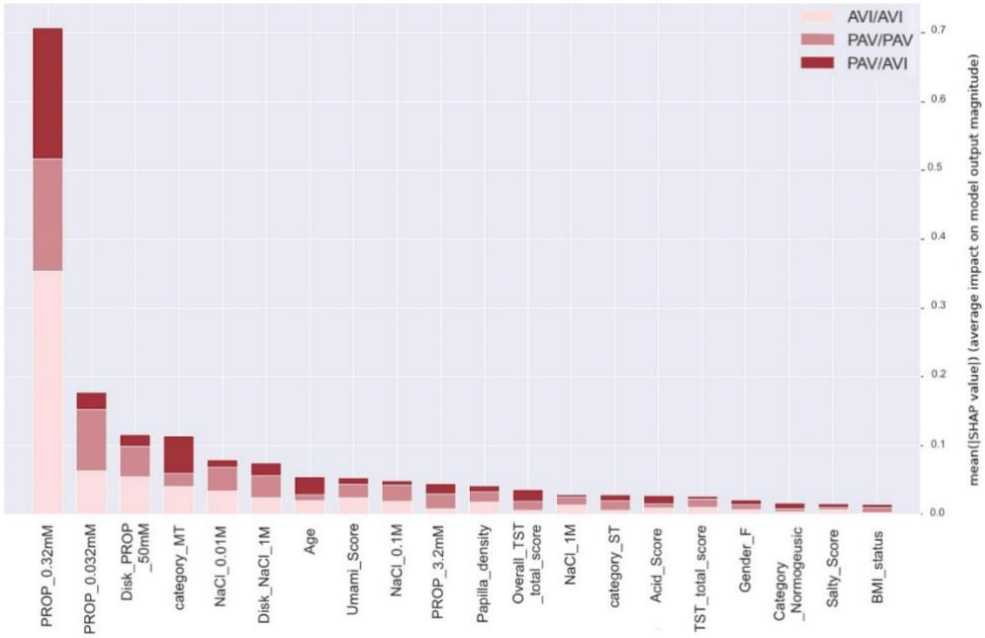

Figure 3. Importance of the features in training the CatBoost classifier. The X-axis denotes the order of importance of the features to discriminate each *TAS2R38* genotype, while the average impact on the model output is represented in the Y-axis.

Figure 4. shows that by including the first three features (the rating of perceived intensity for PROP solutions (0.32 mM), PROP solutions (0.032 mM) and PROP paper disk (50 mM)), the F1-Score rises to a value of 0.84, then reaches 0.90 by including the successive three features (MT category, intensity rating for NaCl solution (0.01 M) and NaCl paper disk (1 M)) and reaches 0.95 after adding age, umami score and intensity rating for NaCl solution (0.1 M).

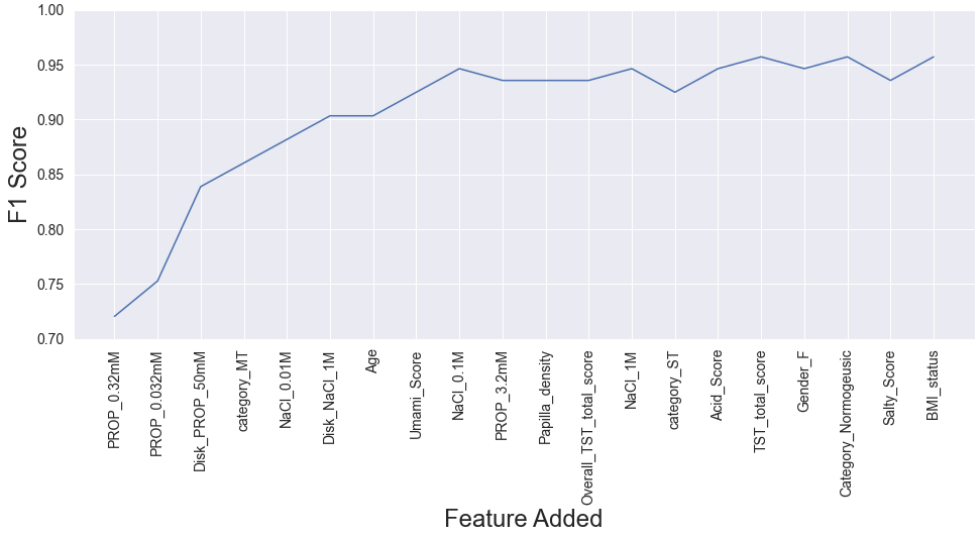

Figure 4. The learning progress curve of the CatBoost model when the features are included one by one based on their importance in learning the model.

The use of the SHAP algorithm provided an overview of the importance of features and how they affect the model prediction. The SHAP summary plot showing the linking between the importance of features and the effects of features for PAV/PAV genotype is shown in Figure 5. Specifically, the plot highlights that the rating of the perceived intensity for PROP solutions (0.32 mM) was the most important feature for the model, and high and medium estimated values (red and violet, respectively) were strongly and positively correlated with PAV/PAV genotype. The rating of perceived intensity for the PROP solutions (0.032 mM) was the second in order of importance for the PAV/PAV genotype, and high and medium estimated values (red and violet, respectively) had a high impact on making a PAV/PAV genotype prediction. Low values (blue) of these two features mostly pushed the model prediction toward other genotypes. The ratings of perceived intensity for NaCl paper disk (1 M) and NaCl solution (0.01 M) were the third and fourth significant features for PAV/PAV genotype, and low estimated values (blue) positively correlated with it, while high and medium estimated values (red and violet) pushed the prediction of the model towards other genotypes. The rating of intensity for paper disk (50 mM) was the fifth significant feature, and high estimated values positively correlated with a PAV/PAV genotype prediction. The salty score was the more important (sixth in order of importance) among those given to taste qualities, and low estimated values positively correlated with PAV/PAV genotype, while high values pushed the model towards the other genotypes. The classification as normogeusic or MT was the seventh and eighth important features and correlated negatively and moderately with this genotype, while the ST category was less important, but positively correlated with PAV/PAV genotype.

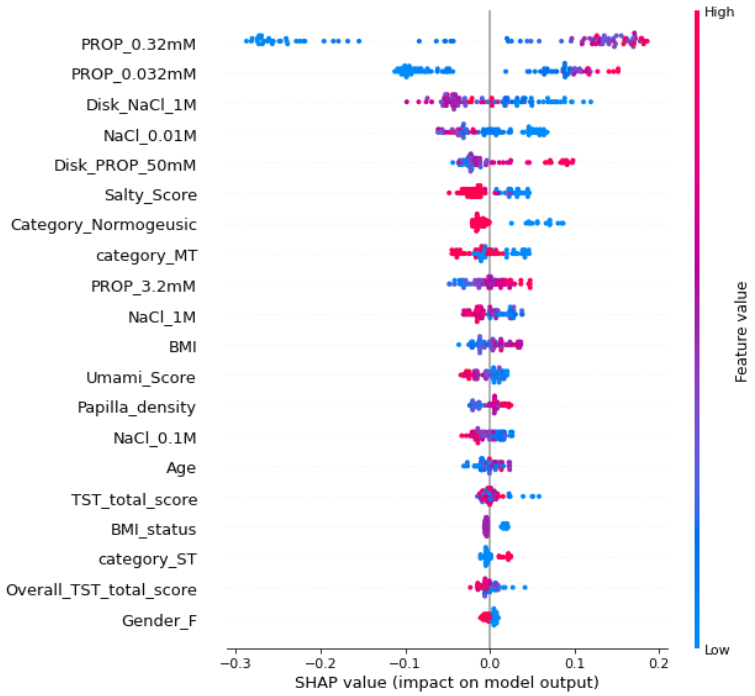

Figure 5. SHAP summary plot of PAV/PAV genotype. The descending order of importance of the features (from the most significant at the top to the less significant at the bottom) is shown on the left of the Y-axis; the impact on the model output (SHAP value) is shown on the X-axis. The color in the line at the right of the graph represents the feature value: high value (red color), medium value (violet color), and low value (blue color).

The SHAP algorithm provided an overview of the importance of features and how they affect a PAV/AVI genotype prediction (Figure 6). Also, in the case of this genotype, the rating of intensity for PROP solutions (0.32 mM) was the most significant feature for the model. High and medium values (red and violet, respectively) were positively and strongly correlated with this genotype; low values (blue), however, shifted the prediction in favor of the other genotypes. Interestingly, the classification of participants as MT, which was the second significant feature, had a high impact on making a prediction of PAV/AVI genotype, while age (third feature) correlated negatively. The intensity rating for the PROP solutions (0.032 mM) was the fourth feature for the PAV/AVI genotype, and low estimated values (blue) correlated moderately and negatively with this genotype. The rating of intensity for the PROP paper disk (50 mM) was the successive important feature. Medium estimate values pushed the model to predict PAV/AVI genotype, while low and high values were negatively correlated with it and pushed the model to make another prediction. The score for umami was the most important (sixth in importance order) among those for taste qualities, and high and medium estimated values (red and violet, respectively) were moderately and positively correlated with this genotype. Again, the classification of participants as normogeusic was a significant feature that positively and moderately correlated with this genotype.

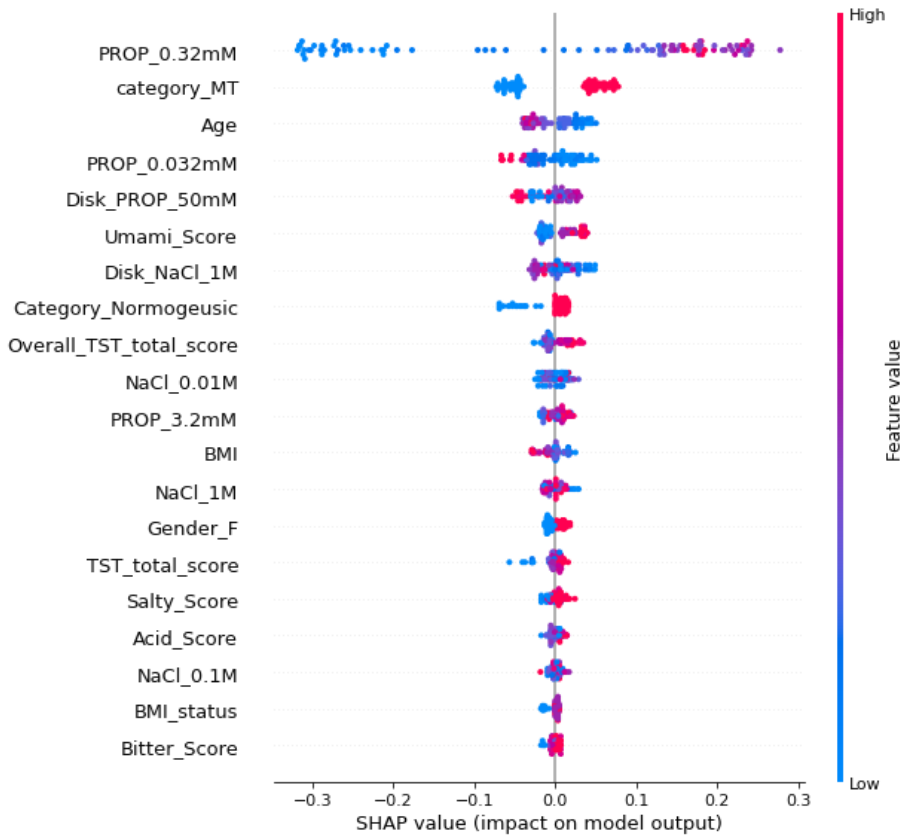

Figure 6. SHAP summary plot of PAV/AVI genotype. The descending order of importance of the features (from the most significant at the top to the less significant at the bottom) is shown on the left of the Y-axis; the impact on the model output (SHAP value) is shown on the X-axis. The color in the line at right of the graph represents the feature value: high value (red color), medium value (violet color) and low value (blue color).

Figure 7 shows the SHAP summary plot for the AVI/AVI genotype. Also, in this case, the rating of perceived intensity for PROP solutions (0.32 mM) was the most important feature for the model, and low estimated values (blue) had a high impact to make an AVI/AVI genotype prediction. On the other hand, high and medium estimated values of this feature (red and violet) strongly pushed the prediction of the model towards the other genotypes. The PROP solution (0.032 mM) intensity rating was the second feature for this genotype, and low estimated values (blue) were positively and moderately correlated with the AVI/AVI genotype. The intensity ratings for NaCl paper disk (1 M) and NaCl solution (0.01 M) were the third and fifth features in order of importance, and high and medium estimated values (red and violet, respectively) moderately pushed the model prediction towards AVI/AVI genotype. The classification of participants as MT, which was the fourth feature in order of importance, negatively impacted to make an AVI/AVI genotype prediction. The intensity rating for PROP solutions (3.2 mM) and PROP paper disk (50 mM) were significant features and low estimated values (blue) positively and moderately correlated with AVI/AVI genotype prediction, while high values pushed toward the other genotypes.

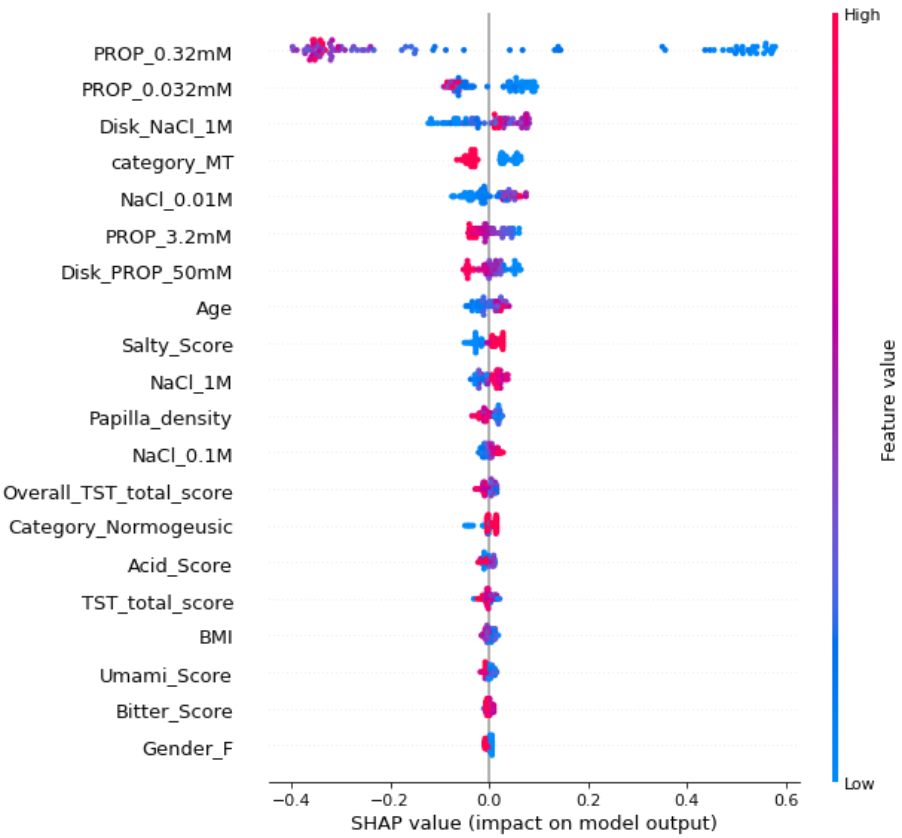

Figure 7. SHAP summary plot of AVI/AVI genotype. The descending order of importance of the features (from the most significant at the top to the less significant at the bottom) is shown on the left of the Y-axis; the impact on the model output (SHAP value) is shown on the X-axis. The color in the line at right of the graph represents the feature value: high value (red color), medium value (violet color) and low value (blue color).

3. Discussion

The primary aim of the present work was to develop an SL model capable of automatically identifying and, with high precision, identifying the genetic variants of the *TAS2R38* bitter receptor, given their importance in taste and health [48, 90, 120, 185, 266, 267, 316, 326, 346, 353-359, 384, 385]. Our approach, the effectiveness of which was verified, also allowed us to understand the importance and the impact of each feature to make a prediction, which was used as input in the data model.

The processing of the dataset and the analysis of correlations between features used as predictive variables were critical phases to improve the dataset quality and obtain improved results. We found robust correlations between the intensity ratings for PROP and NaCl, between fungiform papillae density and PROP ratings or taste perception scores. PROP sensitivity greatly varied between *TAS2R38* genotype groups: AVI/AVI participants perceived the PROP with little intensity, and PAV/PAV and PAV/AVI participants more intensely. We also found a robust link between *TAS2R38* genotype groups and PROP taster status: STs never had AVI/AVI genotype, and NTs never had PAV/PAV genotype. Instead, PAV/PAV and PAV/AVI genotypes could be determined in both MTs and STs.

For our purpose, we used five different algorithms (Logistic Regression, Decision Tree, Random Forest, KNN, and the CatBoost classifier) and we compared their performance. The higher evaluation metric values obtained with the CatBoost algorithm, as compared to those of other models, indicated that this algorithm was the best model for the automatic identification of the *TAS2R38* genotypes, even though the other algorithms did achieve the objective. The CatBoost algorithm allowed us to reach the goal with a high precision level (88%), recall (83%), and F1 score (82%). These results were also confirmed by the best ROC curve that showed a small error for the prediction of each genotype group (18% of error for the PAV/PAV genotype, 4% of error for the AVI/AVI genotype and 22% of error PAV/AVI genotype prediction), the best average margin of error (90%, micro-average) and the large overlap in the network structure over subject of *TAS2R38* groups identified by molecular analysis and SL model. The best performance of the CatBoost

model was not surprising, as it is a method that handles small datasets containing a large number of categorical features better than other types [376-378].

The sensory, morphological, genetic, clinical, and demographic features that we used as predictive variables in facilitating the model learning and understanding of the differences between the three *TAS2R38* genotype groups were all parameters previously determined from participants, which have been associated with PROP genotype or phenotype in a large number of studies [48, 90, 109, 110, 117, 120, 139, 179, 181, 203, 252, 362-366]. Among them, the perceived intensity ratings for different amounts of PROP or NaCl were the most important ones. These measures have been commonly and reliably used for a long time in PROP phenotyping methods [109, 117, 179, 181], can be employed outside of traditional laboratories [117, 179], and can be easily and quickly administered to large groups of participants at a minimal cost and without creating discomfort. Our findings showed that, by using the CatBoost classifier, we were able to identify six of these measures as the most relevant in facilitating the model learning targeted at comprehending the differences between the three genotype groups. In order of importance, they were the intensity ratings for PROP solution (0.32 mM), for PROP solution (0.032 mM), for PROP paper disk (50 mM), MT category, the intensity ratings for NaCl solution (0.01 M), and NaCl paper disk (1 M). All measures were performed by the Impregnated Paper Screening Test [179] and the Three-Solution Test [117], which are the simplest and fastest psychophysical approaches for PROP phenotypic determination. This finding is relevant because it shows that the two tests provide the best features for training a model to make *TAS2R38* genotype predictions for novel samples, further validating their use for PROP phenotyping and genotyping of participants. Furthermore, since PROP taste variability is mostly controlled by the genetic variants of the TAS2R38 receptor [48, 120], which mediate the detection of PROP [48], it is worth noting that the best four features in the training of the model to make predictions on the *TAS2R38* genotype of new samples were ratings of PROP bitterness. The analysis of the evaluation of the performance of the algorithm by including, one by one, the features in order of importance in learning the model seems to suggest that the ratings of PROP solutions (0.32 mM), PROP solutions (0.032 mM) and PROP paper disk (50 mM) may be considered the minimum threshold to predict the *TAS2R38* genotype with an F1-score of 0.84 when there is a lack of resources for conducting molecular analysis.

The SHAP algorithm allowed us to correlate, with high precision, the feature relevance with its effect on the model's predictions for each *TAS2R38* genotype group. Particularly, the SHAP findings very clearly showed the impact they had on making a prediction of the PROP solution (0.32 mM) intensity rating, which was also the most important feature in training the model, thus understanding the differences between the three genotype groups. Medium and high estimated values strongly pushed the model to make PAV/PAV and PAV/AVI predictions, while low values powerfully pushed toward AVI/AVI predictions. Similarly, high values of the PROP solution (0.32 mM) intensity rating strongly pushed the model to make PAV/PAV predictions, while low values pushed toward AVI/AVI predictions. These results indicate that the two PROP solutions at the lowest concentrations used in the Three-Solution Test [117] are the best predictors to identify the genotype of participants for the specific bitter receptor TAS2R38. Conversely, low values of the intensity ratings for NaCl paper disk (1 M) and NaCl solution (0.01 M), which are used as standard controls in the two tests, pushed the model towards PAV/PAV genotype predictions, while high and medium values pushed it towards the AVI/AVI one.

Our results showed that among the three PROP taster categories (ST, MT, and NT), MT was the most critical feature (the fourth in importance order) for the training model to learn to discriminate among genotype groups and was effective in making precise PAV/AVI predictions. SHAP algorithm showed that the MT category had a strong impact on predicting PAV/AVI genotype, while it did not have a favorable impact on predicting AVI/AVI or PAV/PAV genotypes. On the other hand, the SHAP technique showed that the ST category was less important, but positively and moderately pushed the model towards the PAV/PAV predictions. These findings are in line with previous research showing that having two PAV haplotypes, as opposed to one, does not add benefits for PROP bitter detection [115]. Our results also showed that age was a significant feature for the training model to learn to discriminate among the three genotype groups, and low SHAP values moderately pushed the model to make PAV/AVI predictions, while high values moderately pushed toward AVI/AVI predictions. These results are consistent with data showing that the penetrance of the *TAS2R38* gene (i.e. the degree to which environmental factors impact the phenotypic

expression of a trait), varies with age [386]. Furthermore, gender was also a critical feature: females, who have been shown to have a stronger sensitivity to PROP [109, 187, 387], were more relevant in terms of training the model.

Also, the scores that the participants attributed to tastes (that are not specifically mediated by the *TAS2R38* receptor) were significant features in facilitating the model learning to discriminate the *TAS2R38* genotype groups, according to results showing associations between perception for the five tastes [108, 128-133, 162, 370, 388] and that for PROP. Umami was the most important quality, and its high values significantly impacted the model to make a PAV/AVI prediction. Future research may look at this aspect. On the other hand, the SHAP approach showed that low expected values of salty perception moderately pushed the model toward PAV/PAV predictions, while high values toward AVI/AVI predictions. This is consistent with the fact that in the psychophysical assessments used to classify participants for PROP taster status, NaCl is used as a standard reference, indicating that the perceived intensity rating for this stimulus is unaffected by the PROP phenotype of participants [117].

The fungiform papilla density was also a significant feature for the training model and was effective in making the specific PAV/PAV predictions. Indeed, the SHAP algorithm revealed that high estimated papilla density values are positively associated with PAV/PAV genotype, while low values pushed the model toward an AVI/AVI prediction. These results are in agreement with previous studies that found that STs, who predominantly have a PAV/PAV genotype, possess a larger number of fungiform papillae than PROP NTs, who had the AVI/AVI genotype [109, 124, 126, 150, 181, 203].

Chapter 3
Automatic Detection of Fungiform Papillae on the Human Tongue Via Convolutional Neural Networks and Identification of the Best Performing Model

1. Materials and Methods

1.1. FPs identification and measurements

Identification and measurements of FPs were performed on one hundred and seventy-five young, healthy Caucasian subjects (62 male, 113 female) from Sardinia, Italy, recruited at the local university. The mean age was 24.77 ± 4.74 y, ranging from 18 to 42 y; 22 subjects were smokers and 153 were non-smokers. A structured history was taken for each subject. They had a normal body mass index (BMI) ranging from 20.2 to 25.2 kg/m^2. The exclusion criteria included: major systemic diseases, otolaryngology disorders, neurodegenerative diseases, use of drugs interfering with taste or smell, pregnancy or lactation, and food allergies. Taste and olfactory impairment were ruled out by using the Taste Strips and Sniffin' Sticks test (Burghart Messtechnik, Wedel, Germany). All subjects provided a signed informed consent form before being enrolled in the study. The study was conducted according to the guidelines of the Declaration of Helsinki and approved by the Ethical Committee of the University Hospital of Cagliari (protocol code: 451/09; date of approval: 5/2016).

A standardized procedure was used to identify the FPs on the tongue of these subjects [203]. Briefly, the tip of the anterior tongue surface was dried using filter paper and stained with a blue food dye (E133, Modecor Italiana, Italy) on the left side of the midline of the tongue. Multiple photographs (3−10) of the stained area were taken using a Canon EOS D400 (10 megapixels) camera equipped with an EFS 55–250 mm lens. After transferring the images to a computer, they were analyzed by the zoom function in GIMP Software. The FPs were identified in a 6 mm diameter circle of stained and dried area according to Melis [203]. This circular area provides reliable measurements of the density of FPs in high correlation with their total number on the tongue [223]. The FPs were identified by their mushroom shape and lighter staining, which allowed them to be distinguished from the darker-stained filiform papillae. The number of FPs in the stained area of 6 mm diameter was counted by three trained observers, who independently evaluated the image. The final measurements were based on the consensus of all observers.

1.2. Deep Learning methods

To automatically identify the FPs on the tongue images of 175 healthy subjects, considering natural variations in morphology and distribution among subjects, we used and compared three different Convolutional Neural Networks (Classic U-Net, MultiResUNet, and an Optimized U-Net). Our workflow is illustrated in Figure 1. It starts with the Initial Image of the tongue (selected as the best image of each subject). Then, it follows with a second image (Ellipse Detector) showing the circular region of interest where the FP measurements are performed. In this image, an ellipse detector was employed to identify the ellipse, which was subsequently cropped into a square centered around this ellipse (Crop Image). The Crop Image is then standardized to a uniform resolution of 250 × 250 pixels. Finally, Contrast Limited Adaptive Histogram Equalization (CLAHE) is applied for image normalization, enhancing the visibility of the FPs. The processed images and Ground Truth Images, generated as described below, are then fed to the end-to-end DL models, which generate output images featuring bright spots at the center of the FPs.

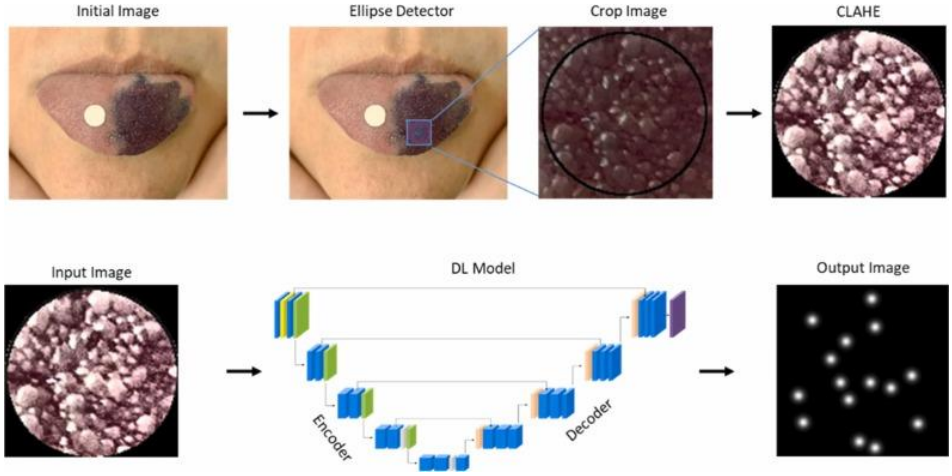

Figure 1. Workflow of the automatic identification of the FPs by Deep Learning architectures. Initial Image, the best image of each subject; Ellipse Detector shows the circular region where the FP measurements are performed; Crop Image, the previous image cropped after applying an ellipse detector; Contrast Limited Adaptive Histogram Equalization (CLAHE) image after normalization and enhancing the visibility of the FPs.

1.2.1. Generation of ground truth images

Three steps were followed to generate the Ground Truth Images needed to train the models (Figure 2). With this pipeline, we obtained a uniform and high-quality dataset to train the three models. The three steps were:

1. The normalized images were manually annotated by marking the position of all FPs using GIMP Software.
2. Isolation of the points indicating each FP position.
3. Creation of Ground Truth Image using Peak Local Maxima Detection [389] and Gaussian kernels [390].

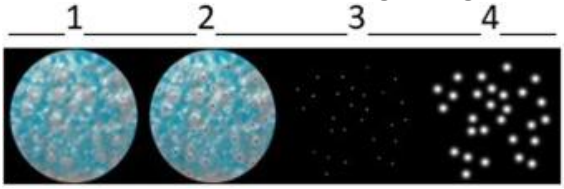

Figure 2. Image processing pipeline for creating the Ground Truth images. Three steps were followed: 1 → 2, manual identification of all FPs using GIMP Software; 2 → 3, isolation of the points indicating each FP position; 3 → 4, creation of Ground Truth Image using Peak Local Maxima Detection and Gaussian kernels.

1.2.2. Deep learning architectures for FP identification

The three architectures (Classic U-Net, MultiResUNet, and an Optimized U-Net) have been used as a regression task, with a high probability of bright spots at the center of the FPs that gradually decreases toward the borders. To this end, we used a linear activation function in the final layer of all architectures [240].

Classic U-Net [239] : a standard U-Net architecture, composed of an encoder-decoder structure, each composed of 4 blocks of 2D convolutional layers. The encoder progressively downsamples the input image to extract relevant features, while the decoder upsamples the feature maps from the encoder to gradually reconstruct the original image resolution. A middle block of convolutional layers connects the encoder and the decoder. The encoder progressively doubles the number of the convolutional filters in each block, starting with 64 filters in the first block and reaching 1024 filters in the middle block.

MultiResUNet [360]: an advanced U-Net architecture incorporating multi-resolution convolutional blocks within the encoder and decoder. These blocks allow the network to extract features at different scales, improving the model's ability to capture fine-grained details at various resolutions.

Optimized U-Net: The improvements made in the Classic U-Net to enhance the performance in the detection of FPs were: reducing the number of filters in the encoder and decoder blocks to 64 convolutional filters in the first two blocks, 128 in the third, 256 in the fourth, and 512 in the middle block,

incorporating Batch Normalization layers after each convolution to stabilize and speed up training, and adding Dropout layers to mitigate overfitting.

1.2.3. Training a deep learning model

After processing the data, to train and validate the models, we used the K-fold cross-validation strategy [391]. The k-fold cross-validation is a technique for the statistical evaluation of DL models that trains and assesses them on data subsets. This procedure was repeated five times (k = 5): each subset was randomly used once as a validation set and the remaining four for training. At each of these five times, the model runs for 500 epochs with a batch size of 2. This approach provided robust model evaluation by assessing performance across different training-validation splits, enhancing the reliability of the results.
In addition, we used the Mean Squared Error (MSE) as the loss function and the Mean Absolute Error (MAE) as the error quantification after each epoch. They were optimized with the Adam optimizer (learning rate: 1e-3). The training data were augmented with rotations, flips, and intensity adjustments to improve the model's generalization. Final performance metrics are reported as the mean and standard deviation across the five hold-out folds.

1.2.4. Evaluation of results of deep learning models

To evaluate the overall performance of the three models used to predict the position of each FP we first used the Mean Absolute Error (MAE), which quantifies the average of errors between the Ground Truth and the prediction made by each model [392] after the end of training. Second, we used the Structural Similarity Index Measure (SSIM), which evaluates the overall structural similarity between the Ground Truth and the prediction [393].
In addition, we performed two deeper analyses (Dice Coefficient, DC, and Local Peak Detection, LPD) to compare the prediction that the model returns with the corresponding Ground Truth. The DC calculates the degree of the overlap between predictions and the Ground Truths, summing the pixels that coincide between them. DC = 0 means no overlap, DC = 1 means perfect overlap. LPD allowed us to extract the coordinates of the spots and calculate the rate of True Positive (TP), the rate of Untrue Positive (UP), and the rate of Untrue Negative (UN) with respect to the Ground Truth for all predicted FPs of each model evaluated.
Final performance metrics are reported as the mean and standard deviation across the five hold-out folds.

Table 1. Meaning of True Positive (TP), Untrue Positive (UP), and Untrue Negative (UN) of the prediction of FPs that the models return with the corresponding Ground Truth True image.

Model prediction	**Meaning**
True Positive (TP)	Correct prediction
Untrue Positive (UP)	Incorrect prediction: The model identified an FP that does not exist.
Untrue Negative (UN)	Unrecognized FPs: The model did not identify an FP that exists.

1.3. Statistical Analysis

One-way analysis of variance (ANOVA) was used to analyze differences in mean values ± SD of the number of FPs in the Ground Truths and those predicted by each model. Post hoc comparisons were conducted with Tukey HSD test. Statistical analyses were conducted using STATISTICA for WINDOWS (version 7; StatSoft Inc, Tulsa, OK, USA). P values ≤ .05 were considered significant.

2. Results

Figure 3 shows the values of over 500 epochs (the history) of MSE, as the loss function (left graphs), and MAE, as the error quantification after each epoch (right graphs) monitored for a representative fold of the Classic U-Net (A), the MultiResUNet (B), the Optimized U-Net (C) to evaluate the training and validation of models. In all the models, we observed a quick decrease in MSE and MAE during the first epochs, which indicates effective early learning. Specifically, the Classic U-Net model showed higher convergence for both training and validation metrics than the MultiResUNet model, which indicates better performance. The MultiResUNet model shows that the training values decrease and those of validation remain constant,

which suggests overfitting, and a slightly unstable training process, highlighted by the oscillations in the MSE and MAE validation values. The optimized U-Net model achieved the most balanced performance and stability because the curves show consistent trends in both training and validation, with small deviation and small stabilized MSE and MAE values.

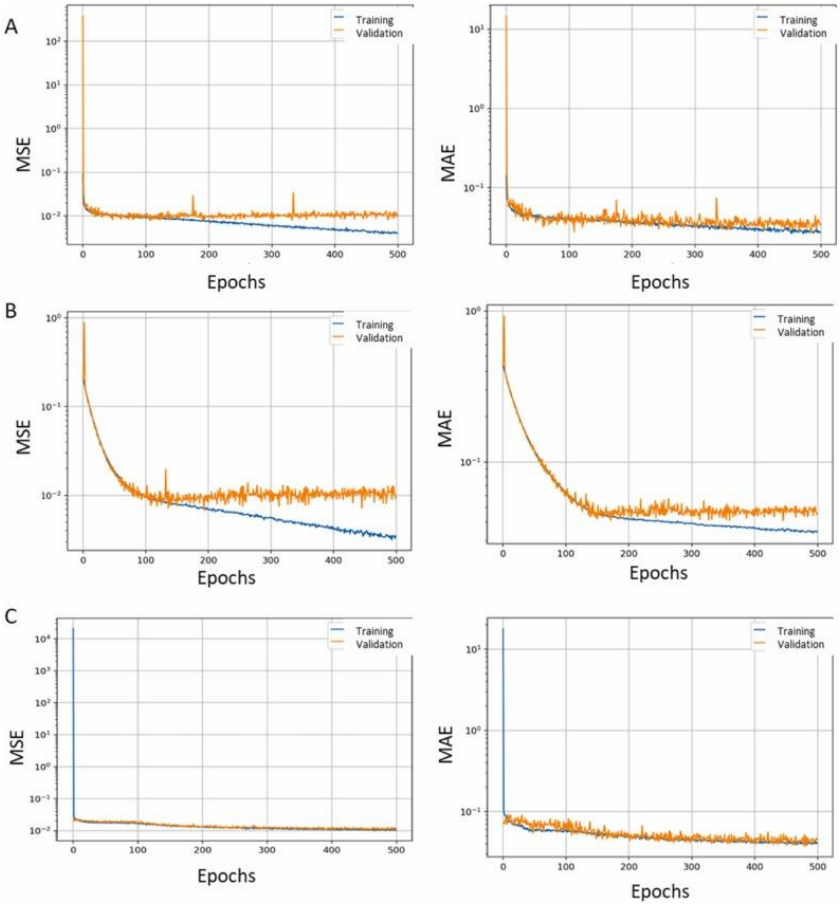

Figure 3. The history of the Mean Squared Error (MSE), as the loss function (left graphs), and the Mean Absolute Error (MAE), as quantification of error after each epoch (right graphs) for a Representative Fold of the Classic U-Net (A), the MultiResUNet (B), the Optimized U-Net (C). The blue curve represents training, and the orange one represents validation. The X-axis represents the number of epochs, and the Y-axis represents the logarithmic scale, which illustrates the variation of the metric values.

Table 2 shows the mean values ± SD of MAE, SSIM, and DC across the five hold-out folds, the metrics used to evaluate the overall performance of the three models to predict the position of each FP. The Optimized U-Net showed the best performance by achieving the lowest value of MAE, which quantifies the average of errors between Ground Truths and the predictions, the highest SSIM values, which evaluate the similarity between Ground Truths and predictions, and a DC value (0.712) that indicates a very good overlap between Ground Truths and predictions.

Table 2. Mean values ± SD of Mean Absolute Error (MAE), Structural Similarity Index Measure (SSIM), and Dice Coefficient (DC), across the five hold-out folds, for each model.

DL Model	MAE ± SD	SSIM ± SD	DC ± SD
Classic U-Net	0.036 ± 0.029	0.666 ± 0.084	0.713 ± 0.058
MultiResUNet	0.047 ± 0.002	0.258 ± 0.027	0.702 ± 0.055
Optimized U-Net	0.034 ± 0.001	0.755 ± 0.047	0.712 ± 0.033

Table 3 shows the mean values ± SD of the number of FPs in the Ground Truths and those predicted by each model. One-way ANOVA showed that the number of FPs in Ground Truths and those predicted by other models was significantly different ($F_{(3,\ 696)} = 63.818$, $p = 0.0000$). However, the post hoc comparison showed that the number of FPs predicted by the Classic U-Net was higher than that of Ground Truths or

that predicted by the other two models ($p < 0.000008$; Tukey HSD test). No significant difference in the number of FPs predicted by the MultiResUNet or Optimized U-Net was found when compared to that of Ground Truths ($p \geq 0.827$; Tukey HSD test) or between them ($p = 0.947$; Tukey HSD test).

Table 3. Mean values ± SD of the number of FPs in the Ground Truths and those predicted by each model.

Ground Truths	Classic U-Net	MultiResUNet	Optimized U-Net
16.96 ± 7.67	29.25 ± 13.18*	17.84 ± 8.15	18.40 ± 7.76

* Indicate significant differences compared to the other values (p < 0.000008; Tukey HSD test, after one-way ANOVA).

LPD analysis by extracting the coordinates of the spots in each image allowed us to calculate the rate of True Positive (TP), the rate of Untrue Positive (UP), and the rate of Untrue Negative (UN) with respect to the Ground Truth for all predicted FPs by each model. Five representative examples of the ability of each model to identify the FPs in challenging input images characterized by different FP densities and morphology are shown in Figure4. TPs (green points), UPs (red points), and UNs (blue points) for each model are highlighted. The predicted number of True Positives (TPs), Untrue Negatives (UNs), and Untrue Positives (UPs) calculated with respect to Ground Truth by each model for FPs in five representative examples of input images are shown in Table 4. The Optimized U-Net showed the best balance prediction across all examples.

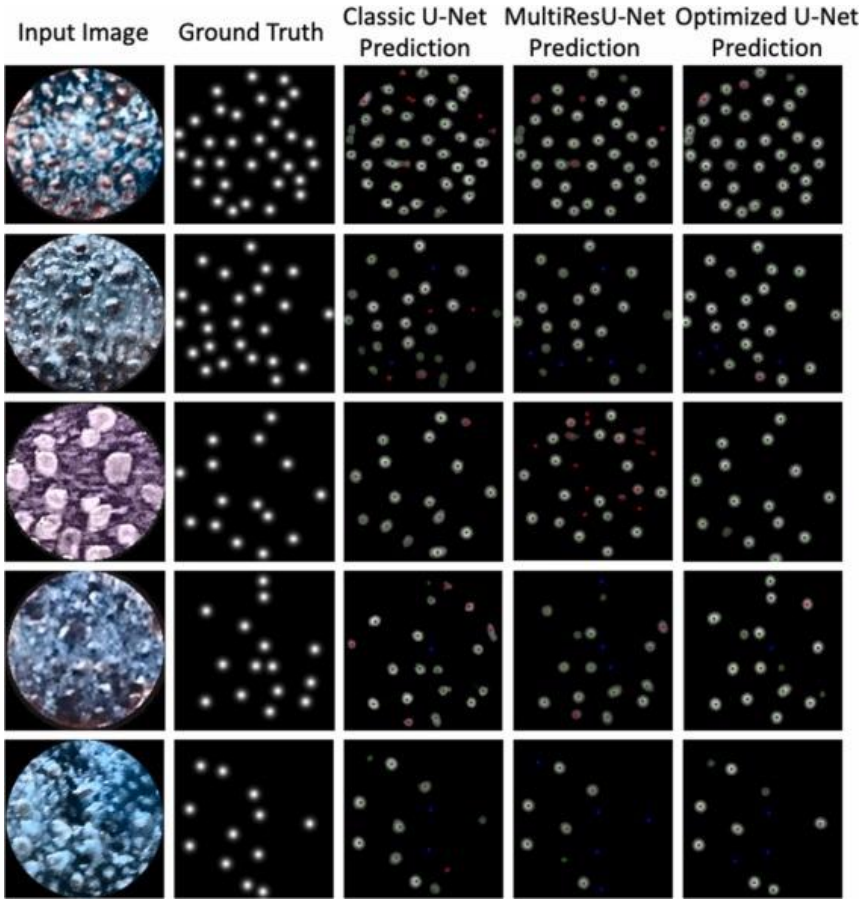

Figure 4. Representative examples showing the prediction of the three models the Classic U-Net, the MultiResUNet and the Optimized U-Net. Green points indicate True Positives (TPs), red points indicate Untrue Positives (UPs) and blue points indicate Untrue Negatives (UNs).

Table 4. The predicted number of True Positives (TPs), Untrue Negatives (UNs), and Untrue Positives (UPs) calculated with respect to Ground Truth by each model for FPs in five representative examples of input images.

Example	Ground Truth	DL Model	TPs	UNs	UPs
1	32	Classic U-Net	32	0	7
		MultiResUNet	32	0	4
		Optimized U-Net	32	0	2
2	24	Classic U-Net	22	2	4
		MultiResUNet	20	4	0
		Optimized U-Net	21	3	1
3	15	Classic U-Net	15	0	1
		MultiResUNet	15	0	15
		Optimized U-Net	15	0	0
4	15	Classic U-Net	14	1	5
		MultiResUNet	13	3	2
		Optimized U-Net	14	1	1
5	12	Classic U-Net	10	2	1
		MultiResUNet	7	5	0
		Optimized U-Net	9	3	0

Table 5 shows the mean values ± SD across the five hold-out folds of the number of FPs of the Ground Truths and the predicted rate of True Positives (TPs), Untrue Negatives (UNs), and Untrue Positives (UPs) calculated by each model for FPs of 175 images. The table also shows the percentages of TPs, UNs, and UPs calculated across the five hold-out folds, taking into account the real number of FPs in each fold. Specifically, the Classic U-Net model gave the highest rate of TPs and UPs and the lowest rate of UNs. The MultiResUNet gave the highest rate of UNs, the lowest rate of TPs, and the lowest rate of UPs. Finally, the Optimized U-Net model showed intermediate values that were more equilibrated than those of other models: a slightly lower rate of TPs than that of Classic U-Net, a lower rate of UNs than that of MultiResUNet, and a lower rate of UPs than that of Classic U-Net.

Table 5. The mean values ± SD across the five hold-out folds of the number of FPs of the Ground Truths and the predicted rate of True Positives (TPs), Untrue Negatives (UNs), and Untrue Positives (UPs) calculated by each model for FPs of 175 images.

Ground Truths ± SD	DL Model	TPs ± SD %	UNs ± SD %	UPs ± SD %
592.8 ± 69.75	Classic U-Net	515.6 ± 59.98 87.06 ± 4.22	77.2 ± 26.46 12.92 ± 4.22	212 ± 130.57 37.33 ± 24.79
	MultiResUNet	444 ± 83.86 74.51 ± 6.13	148.8 ± 28.30 25.48 ± 6.13	98.4 ± 21.197 16.77 ± 4.02
	Optimized U-Net	469.4 ± 42.43 79.41 ± 3.77	123.4 ± 33.36 20.57 ± 3.77	136.8 ± 75.14 24.31 ± 15.06

The percentage of TPs (TPs/Ground Truth*100 %), that of accurate count (TPs/TPs+UPs*100 %), and complete accuracy (TP/TP+UP+UN*100 %) calculated by the three models are shown in Table 6. Specifically, the Classic U-Net model gave the highest percentage of TPs and the lowest of accurate count and complete accuracy. The MultiResUNet gave the lowest percentage of TPs, the highest percentage of the accurate count, and an intermediate value of complete accuracy. The Optimized U-Net gave an intermediate percentage of TPs and the accurate count, while the complete accuracy was the highest value compared to the other two models.

Table 6. The percentage of TPs (TPs/Ground Truth*100 %), and that of accurate count (TPs/TPs+UPs*100 %), and complete accuracy (TP/TP+UP+UN*100 %) calculated by the three modes.

DL Model	TPs/Ground Truth* 100 %	TPs/(TPs+UPs)* 100 %	TP/(TPs+UPs+UNs)* 100 %
Classic U-Net	87.06	69.98	63.40
MultiResUNet	74.51	81.62	63.81
Optimized U-Net	79.41	76.56	63.89

3. Discussion

The main aim of this work was to provide an efficient, reliable, and automatic method for identifying FPs on the tongue, also considering physiological variations in morphology and distribution among subjects. To achieve this aim, we used and compared three different Convolutional Neural Networks capable of generating a probability map as a regression task, with a high probability at the center of the FPs that gradually decreases toward the borders. Our results showed that the modifications made in the Classic U-Net architecture allowed us to stabilize and speed up its training, mitigate overfitting, and improve prediction by identifying the best-performing model. The metrics used to evaluate and compare the training and validation of the models and assess their performance in learning and prediction showed that the Optimized U-Net had superior accuracy and robustness than the other two DL models. Specifically, the history of over 500 epochs of the metrics used to evaluate the training and validation of the models, MSE as a loss function, and MAE as an error quantification after each epoch, showed a rapid decrease during the first epochs, which indicates successful early learning for all models. The Classic U-Net showed a better performance than that of MultiResUNet, as shown by the higher convergence of the curves. Instead, the non-convergence and the higher oscillations of the values obtained by MultiResUNet suggest overfitting and a slightly unstable training process for this model. On the other hand, the metric curves determined with the Optimized U-Net showed consistent trends in both training and validation, with modest deviation and stable MSE and MAE values, indicating that this model achieved the most balanced performance, good stability, and no overfitting.

Our results also showed that the Classic U-Net predicted a significantly higher number of FPs than that obtained by the manual counting (Ground Truths), while the MultiResUNet or Optimized U-Net predicted a number of FPs not different from that of the manual counting. It is important to note that our approach, by identifying the number of the FPs in the small circular area (6 mm in diameter) stained with the blue food dye, provides reliable density measurements in the whole tongue. Indeed, it is known that the density measurements in this area are in high correlation with their total density on the tongue [223]. Additionally, the metrics used to evaluate the overall performance of the models showed notable differences in the learning process for identifying FPs. In particular, the Classic U-Net showed a stable performance. The values of MAE, which quantify the error after each epoch, the DC, which calculates the overlap between predictions and the Ground Truths, and the SSIM, which evaluates the overall structural similarity between the Ground Truths and the predictions, indicate a better accuracy of the Classic U-Net in predicting the FPs compared to MultiResUNet. However, the Classic U-Net showed the highest ability to identify TPs, but also the highest rate of UPs and a low rate of UNs, as well as the lowest of accurate count and complete accuracy, suggesting that it tends to confuse other types of papillae with the Fungiform ones. Hence, the high rate of TPs does not mean that it has effectively learned to recognize the morphology of FPs. These findings suggest that further refining of this model is needed to lower the rate of UPs. The MultiResUNet showed the highest MAE and the lowest SSIM and DC, which indicate a weaker performance in capturing fine details and accurately predicting the positions of the FPs compared to other models. In addition, even though MultiResUNet showed the highest accurate count and intermediate values of complete accuracy and the lowest rate of UPs, the lowest rate of TPs and the highest rate of UNs, confirm an observable difficulty in accurately detecting FP positions. The Optimized U-Net outperformed the other two models. Specifically, it achieved the lowest error (MAE), the highest similarity (SSIM), and an overlap (DC) very close to maximum, indicating the highest accuracy and precision of this model in predicting the FPs. The Optimized U-Net also showed intermediate values of TPs, UNs, UPs and accurate count, and the highest

complete accuracy, indicating a more balanced detection of TPs, UNs and UPs compared to other models. Interestingly, this last value was much lower than that of the Classic U-Net, indicating fewer errors, while the UN rate was lower than that of the MultiResUNet, indicating fewer FP position misdetections. The percentage of accurate counts would seem to indicate that MultiResUNet is the most recommendable model. However, the evaluation of the performance of a model cannot be captured by a single metric, but it needs to be evaluated by looking at all metrics collectively. Therefore, although MultiResUNet showed a better accurate count (81.62 % vs 76.56 %), the Optimized U-Net showed a higher sensitivity (TPs/Ground Truth: 79.41 % vs 74.51 %), identifying approximately 5 % more FPs present in the images, and showed a slight superiority of the complete accuracy that also considers the UNs. Our results also showed that the Optimized U-Net had a higher stability, compared to MultiResUNet, with a lower SD of TPs (3.77 % vs 6.13 %) and a superior performance in case of high morphological variability, as shown in the five examples of Figure 4 and Table 4.

Although the Optimized U-Net demonstrated the best performance among the three models, there is potential for further improvement. The procedure that uses blue food dye for coloring the tongue offers the advantage of allowing the identification of FPs by their mushroom shape and lighter staining, distinguishing them from the darker-stained filiform papillae. However, other methods that make the images sharper could be evaluated. A limitation of our method is that the tongue surface is non-flat, making it difficult to distinguish FPs for creating the Ground Truths, which were used for learning the models. Future studies would benefit from a method for flattening the tongue. Our future work should focus on reducing both the UP and UN rates by adding more images to the dataset that could further enhance the model's performance. Convolutional Neural Network architecture typically require large datasets to achieve optimal performance. Testing the model on diverse datasets, potentially from other domains, would also be valuable to assess its robustness and generalizability. Finally, exploring alternative architectures could provide new solutions to the FP identification problem.

Chapter 4
A Supervised Learning Regression Method for the Analysis of the Taste Functions of Healthy Controls and Patients with Chemosensory Loss

1. Materials and Methods

1.1. Subjects

One hundred and fifty-three individuals aged 18 to 81 years (38.3 ± 14.3 years; 103 females) were recruited at the Department of Otorhinolaryngology of the TU Dresden from February 2021 to January 2022. Of these, 51 were patients of the Smell and Taste Clinic who self-reported a chemosensory dysfunction. The remaining study sample comprised 102 healthy controls as a reference group. For this cross-sectional study, patients were enrolled regardless of the etiology of the taste dysfunction or their smoking habits. The exclusion criteria were: pregnancy, allergy to substances used in the present study, unmedicated hypo/hyperthyreosis, uncontrolled diabetes mellitus, renal dysfunction, and significant cardiovascular issues. Informed written consent was obtained from all participants before their inclusion in the study. The research protocol was approved by the Ethics Review Board at the University Clinic of the Technische Universität Dresden, application number BO-EK-25012021.

1.2. Experimental Procedure

The experimental procedure took place in a single session from February 2021 to January 2022. Subjects were requested to abstain from drinking (except water), eating, and chewing gum or using oral care products for at least 1 h prior to testing. Their taste sensitivity of the four primary qualities (sweet, sour, salty, bitter) and sensations of astringency and spiciness were assessed as described below. Before the session, the health statuses of participants were ascertained with detailed medical histories. Weight (kg) and height (m) were recorded in order to calculate the subjects' BMI (kg/m^2). Additionally, all participants were screened for depression using the 5-item World Health Organization Well-Being Index (WHO-5) [394, 395]. The questionnaire consists of five positively phrased items concerning being in good spirits, feeling relaxed, having energy, waking up fresh and rested, and being interested in things. Each of the five items is rated on a 6-point Likert scale from 0 to 5. The theoretical raw score ranges from 0 to 25. A high score in the WHO-5 indicates a high level of well-being, while a score below 13 indicates poor well-being [394, 395]. Subjects were also asked to indicate their preference for consuming spicy foods.

Authors had no access to information that could identify individual participants during or after data collection.

1.3. Sensory Measurements

All taste measurements were performed using the same "taste strips" that are used in the validated "Taste Strip Test" (TST, Burghart Company, Wedel, Germany) [209, 210]. Taste strips used in the assessments consisted of filter papers impregnated with two concentrations of stimuli representative of four basic taste qualities (sweet, sour, salty, bitter) and of sensations of astringency and spiciness. Taste qualities were presented in a semi-random order, with trigeminal stimuli presented last due to their persistent sensations. Before every new test, participants were asked to rinse their mouths with tap water. The evaluation did not include umami sensation due to the low familiarity in the European population [396].

The following two concentrations (one low and one high) for each stimulus were used: 0.4 and 0.05 g/mL sucrose; 0.3 and 0.05 g/mL citric acid; 0.25 and 0.016 g/mL sodium chloride; 0.006 and 0.0004 g/mL quinine hydrochloride; 0.1 and 0.2 g/mL tannin; 2.47×10^{-5} and 2.47×10^{-4} g/mL capsaicin. After placing each filter paper on the tongue, subjects had to evaluate the perceived intensity for each stimulus using a visual analog scale from 0 to 5 (0 = no taste at all, 5 = extremely strong taste). The ratings of the perceived taste intensity for the two concentrations of each stimulus were called: sweet_low_int and sweet_high_int, sour_low_int and sour_high_int, salty_low_int and salty_high_int, bitter_low_int and bitter_high_int, astring_low_int and astring_high_int, and hot_low_int and hot_high_int. The overall taste status, which is the target of the regressor model, was calculated in each subject as the mean value of intensity ratings for the low and the high concentrations of the six stimuli (score_lowhigh_capsadstr_int1). Subjects of both

sexes also had to identify the taste quality of each stimulus by choosing from a list of six possible answers (sweet, sour, salty, bitter, astringent, and hot) in a forced choice procedure [209]. Each correct answer was rated 1; the number of correctly identified tastes was summed up in the total taste score (score_lowhigh_capsadstr1) whose maximum value was 12. The scores of the correct answer for the two concentrations of each stimulus were labeled as follows: salty_low_taste_correct; salty_high_taste_correct; sweet_low_taste_correct; sweet_high_taste_correct; sour_low_taste_correct; sour_high_taste_correct; bitter_low_taste_correct; bitter_high_taste_correct; hot_low_taste_correct; hot_high_taste_correct; astring_low_taste_correct; and astring_high_taste_correct.The complete procedure required 20 min for each subject.

1.4. Supervised Learning

The automatic prediction of the overall taste status of healthy controls and patients with chemosensory loss was carried out from January to October 2022 by SL algorithms exploiting the subjects' parameters that were presented in the data model as predictive variables (features). We used the SL regressors because they are specific to predict continuous outcomes such as the overall taste status of subjects [397]. The SL regressors learned and created automatic regressor models that assessed between-subjects differences and returned, with high accuracy, a value prediction of the overall taste status in healthy controls or patients with chemosensory loss. The following algorithms were used: logistic regression, random forest regressor, and CatBoost regressor. During training, the different algorithms learn the hidden patterns in the structured dataset and then take new unforeseen inputs (test dataset) to predict the target value (the overall taste status). In order to analyze the overall taste status of healthy controls and patients with chemosensory loss and identify specific stimuli or their combination that can best predict the overall taste status of the two groups, it was necessary to apply the regressor model separately to the dataset of healthy controls and patients with chemosensory loss. Therefore, we performed two SL regressor experiments: experiment 1 included healthy controls (n = 102) and experiment 2 included patients with chemosensory loss (n = 51).

The interpretation of the results of the random forest regressor model has been performed by using Shapley additive explanations (SHAPs) [383], which is a game-theoretic method that allows us to link the importance of each feature with its effect. SHAPs return a specific plot for each random forest regressor experiment, representing the impact of each feature in that experiment.

The following data processing operations, which are a crucial phase in the performance of an SL project, were applied:

1. The correlations between numerical parameters and those between each numerical feature and the target, which were a fundamental step to understand the data structure, were also considered to include a feature in the dataset (Figure 1).
2. The choice of features that are used by the algorithm as predictive variables of the target: The set of parameters most suitable for our case study was selected as features by expert researchers in taste physiology and ML engineering, based on their domain knowledge, from a database of the sensory, clinical, and demographic parameters [398]. In addition, since two features strongly correlated with each other have almost the same effect on the dependent variable, one of them was dropped to reduce the noise that could impact algorithm performance [399]. Specifically, the sum of the scores of the correct answer for the two concentrations of salty, sweet, sour, bitter, hot, and astringency; the sum of the scores of the correct answers for the two concentrations of salty, sweet, sour, and bitter; and the intensity ratings for the two concentrations of salty, sweet, sour, and bitter strongly correlated with each other. The first summated variable that included evaluations of all stimuli was selected, and the latter two were excluded.
3. Handling of missing values: Every line of the subject that represents lacking information in some column was eliminated.
4. Elimination of duplicate values: In fifty-eight subjects of the control group, all sensory measurements were repeated twice. The column relative to these repeated measures, and those of the overall taste status and total taste score calculated in these subjects (twenty-nine columns in total) were eliminated from the dataset.

5. Converting the dataset content into a language that an algorithm can understand: This included the one hot encoding, which encodes categorical data into numerical data and the normalization of the numerical data, which consist of transforming a real range of numerical values in a range between 0 and 1.

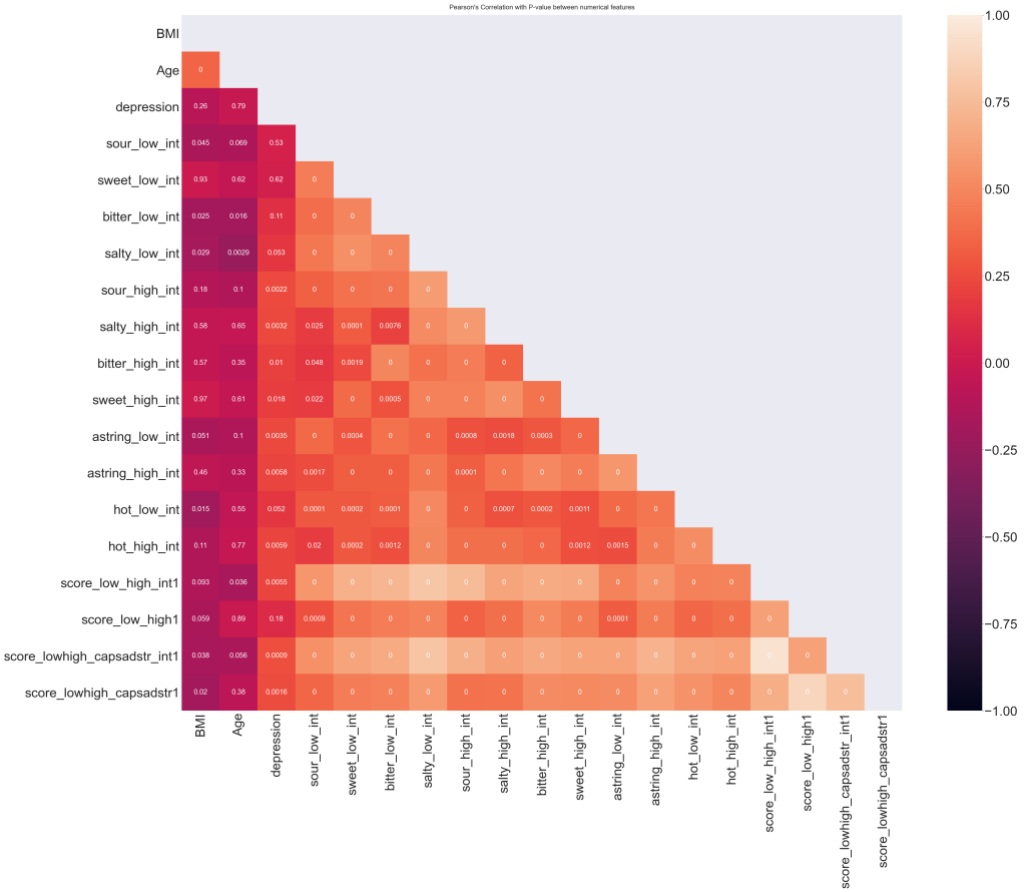

Figure 1. Linear correlation analysis between the numerical features of the dataset and those between the numerical features and the target. The bar color on the right side on the Y axis represents the value of linear correlation between features. *p-values* are indicated inside each square and derived from Pearson's coefficient analysis.

After data processing operations that included the removal of all non-significant and correlated features, we increased the parameters of the number of estimators and the maximum depth of the SL regressors. Moreover, we used a 3-fold cross-validation, which mixes and splits data into two groups (training data, 66.66% and test data, 33.33%) three times using different subsets of data each time.

The evaluation of the performance of the algorithms was conducted by metrics, such as mean absolute percentage error (MAPE) and mean squared error (MSE), that assess the differences between the observed and predicted values. In particular, MAPE represents the error percentage of predicted values, while MSE represents the average of the summation of the squared difference between the actual output value and the predicted output value. The overall behavior of our regressors was subsequently evaluated by the automatic optimization of their hyperparameters by grid search algorithm.

1.5. Statistical Analysis

Fisher's exact test was used to analyze differences between healthy controls and patients with chemosensory loss regarding the frequency of correct answers for the two concentrations of each stimulus, gender, and preference for spicy foods. *T*-test was used to compare differences between healthy controls and patients with chemosensory loss in age, BMI, depression, taste intensity ratings for each stimulus, and total taste score. Statistical analyses were conducted using STATISTICA for WINDOWS (version 7; StatSoft Inc, Tulsa, OK, USA). *p-values*< 0.05 were considered significant. *p-values* of the T-test were adjusted by

Bonferroni correction (adjusted $p = p$/number of groups being compared) (p values < 0.0031 were considered significant).

2. Results

Mean values ± SD or frequencies of the sensory, clinical, and anthropometric parameters determined in healthy controls and patients with chemosensory loss are shown in Table 1. The *T-test* adjusted by Bonferroni correction showed that ratings of the taste intensity in response to low concentrations of each stimulus and high concentrations of sweet, sour, and astringent, as well as the total taste score of healthy controls, were higher than those of patients with chemosensory loss ($p \leq 0.0006$). The depression level was higher in patients with chemosensory loss than in healthy controls ($p < 0.0001$). The number of correct answers for the low concentrations of salty, bitter, hot, and astringent, and the high concentrations of sweet, sour, and astringent, alongside the number of subjects who enjoy spicy foods, were higher in healthy controls than in patients with chemosensory loss ($\chi 2 \geq 4.79$; $p \leq 0.041$; Fisher's test). No differences in the ratings of taste intensity in response to high concentrations of salty, bitter, and hot, age, BMI, gender, or in the number of correct answers for low concentrations of sweet and sour, and high concentrations of salty, bitter, and hot were found between the two groups ($p > 0.05$).

Table 1. Sensory, clinical, and anthropometric parameters of healthy controls and patients with chemosensory loss.

Features	Healthy Controls (n = 102)	Patients with chemosensory loss (n = 51)	p-value
Numerical type			
astring_low_int	2.24 ± 1.32	0.84 ± 1.10*	< 0.0001
bitter_low_int	2.40 ± 1.49	1.06 ± 1.26*	< 0.0001
hot_low_int	2.04 ± 1.30	0.84 ± 1.24*	< 0.0001
salty_low_int	3.03 ± 1.07	1.92 ± 1.18*	< 0.0001
astring_high_int	3.53 ± 1.09	2.43 ± 1.43*	< 0.0001
score_lowhigh_capsadstr1	9.37 ± 1.92	7.18 ± 2.47*	< 0.0001
sour_high_int	3.90 ± 0.85	3.27 ± 1.05*	0.0001
sweet_low_int	1.99 ± 1.18	1.22 ± 1.14*	0.0002
sweet_high_int	3.58 ± 0.89	2.90 ± 1.38*	0.0003
sour low int	1.37 ± 1.22	0.68 ± 0.97*	0.0006
bitter_high_int	3.15 ± 1.43	2.57 ± 1.43	0.018
hot_high_int	3.54 ± 1.16	3.04 ± 1.33	0.018
salty_high_int	3.79 ± 0.89	3.45 ± 1.27	0.054
depression	17.15 ± 3.62	14.14 ± 5.18*	< 0.0001
BMI (kg/m2)	23.66 ± 4.02	25.61 ± 5.55	0.014
Age (y)	36.70 ± 14.43	40.45 ± 12.62	0.116
Categorial type			
astring_low_taste_correct/non (n)	78/24	15/36#	< 0.0001
astring_high_taste_correct/non (n)	86/16	24/27#	<0.0001
hot_low_taste_correct/non (n)	77/25	18/33#	<0.0001
salty_low_taste_correct/non (n)	87/15	33/18#	0.0039
sour_high_taste_correct/non (n)	93/9	36/15#	0.0014
bitter_low_taste_correct/non (n)	63/39	22/29#	0.0221
sweet_high_taste_correct/non (n)	100/2	46/5#	0.0415
sour_low_taste_correct/non (n)	32/70	10/41	0.0877
sweet_low_taste_correct/non (n)	72/30	32/19	0.2122
hot_high_taste_correct/non (n)	97/5	46/5	0.2061
bitter_high_taste_correct/non (n)	77/25	39/12	0.531

Values are means ± SD, or number of correct answers, or number of subjects. Body mass index, BMI; significant differences in mean values between healthy controls and patients with chemosensory loss are indicated by * ($p \leq 0.0006$; T test adjusted by Bonferroni correction), while differences in frequency distribution are indicated by # ($p < 0.041$; Fisher's method).

The metrics of evaluation of the performance of the algorithms, MAPE and MSE, which measure the accuracy of a forecast system, showed that the random forest regressor was the best algorithm to predict the values of the overall taste status with high precision. The scatterplots showing experimental values vs. predicted values of the overall taste status obtained with the random forest regressor in healthy controls, and patients with chemosensory loss are shown in Figure 2. The values of MSE, which evaluate how estimated values are close to experimental values, were 0.019 and 0.014 in the two groups. Furthermore, the MAPE values, which represent the error percentage of predicted values, were 4.55% and 8.40% in healthy controls and patients with chemosensory loss, respectively.

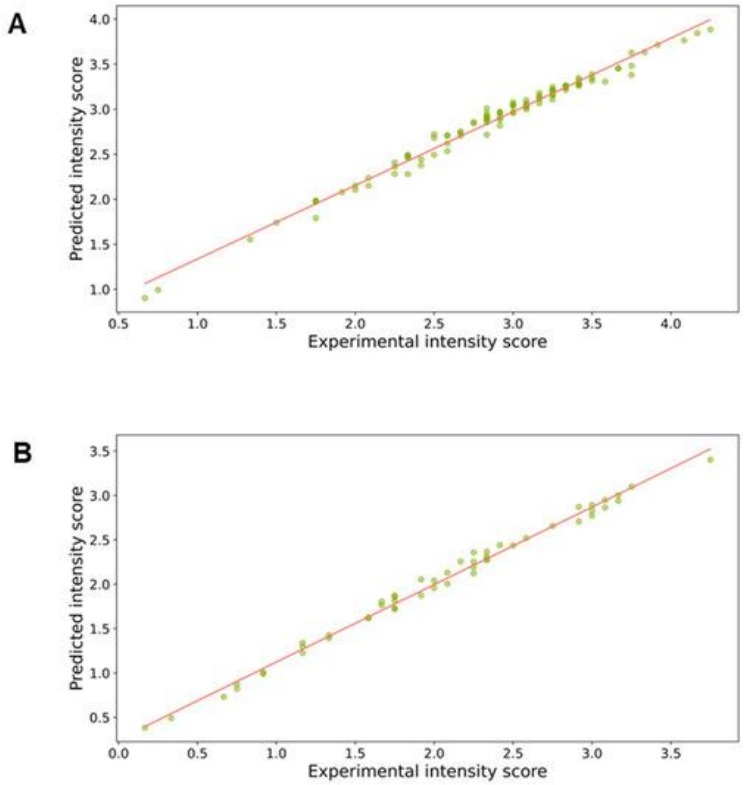

Figure 2. Scatterplots of experimental values vs. predicted values (dots) of the overall status obtained with the random forest regressor in healthy controls (*n* = 102) (**A**) and in patients with chemosensory loss (*n* = 51) (**B**). The lines represent the relationships between the predictive and experimental (independent and dependent) variables.

The random forest regressor allowed us to determine the order of importance and the contribution of the sensory, clinical, and anthropometric features on the prediction of the overall taste status in the two groups, and the interpretation by SHAP algorithm allowed us to obtain an overview of their impact on the prediction. Specifically, the rating of the perceived taste intensity for low concentrations of salt was the most important feature for model learning in healthy controls, and its contribution on the prediction of the overall taste status, estimated as the average impact on the model, was 0.079 (Figure 3A). This feature was followed in order of importance from second to tenth by: the intensity rating for high concentrations of sour, for low concentrations of bitter, for high concentrations of sweet, for high concentrations of bitter, for low concentrations of hot, for high concentrations of salty, for low concentrations of astringency, the total taste score, and the intensity rating for low concentrations of sweet. It is interesting to note that depression status was a significant feature (sixteen in importance order). These features had an average impact on the model lower than 0.057. The link between importance and the effect of the features on the overall status of healthy controls is shown in the SHAP summary plot (Figure 3B). The plot highlights that high estimated values (pink) of the perceived taste intensity rating for low concentrations of salt and high concentrations of sour had a strong and positive impact on predicting high values of the overall taste status, and the low estimated values (blue) of these features strongly pushed the model prediction toward low values of the overall taste status. The mean values of the positive impacts of these two features were 0.052 and 0.040, while those of the negative impacts were −0.155 and −0.106, respectively. High estimated values (pink) of the successive eight features had a positive impact (≤0.057) to predict high values of the

overall taste status; medium values (violet) impacted the model to predict medium values of the overall taste status; and low estimated values (blue) of these features pushed the model prediction toward low values of the overall taste status (negative impact ≤ −0.069).

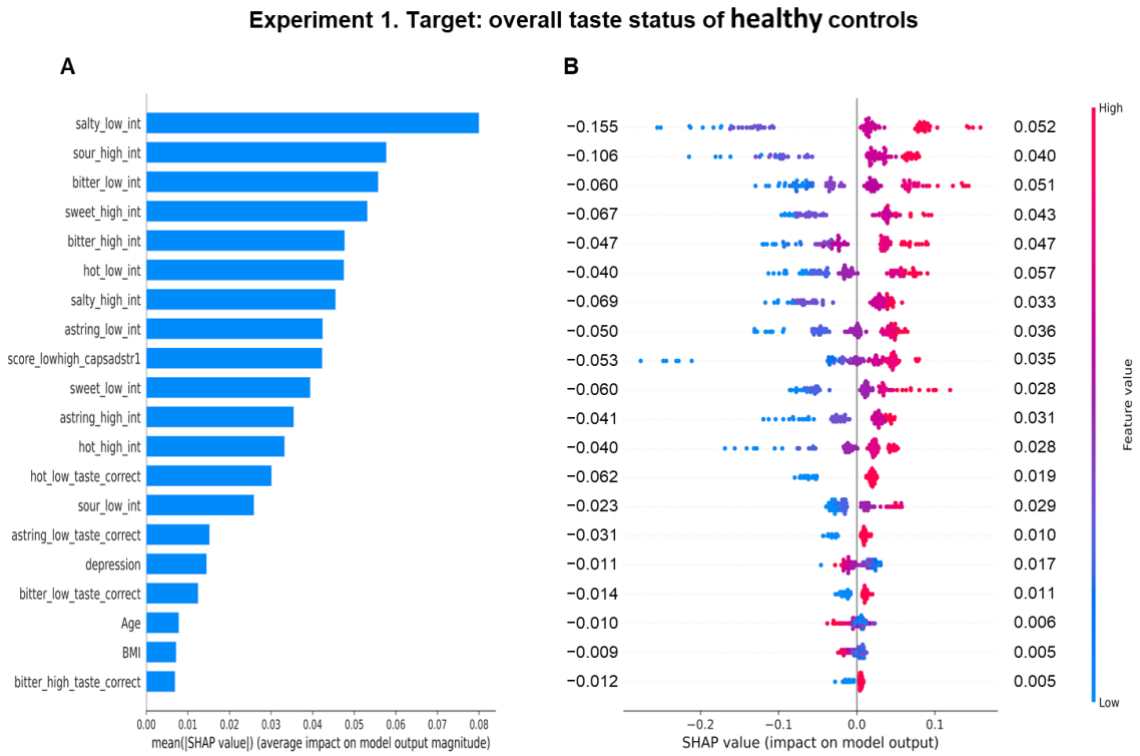

Figure 3. Importance and impact of the sensory, clinical, and anthropometric features on the overall taste status prediction determined with a random forest regressor in healthy controls. Importance of features in the learning of the model to understand the overall taste status (**A**). The Y axis represents the order of the importance of features, while the average impact on the model output is represented on the X axis. The SHAP summary plot in the healthy controls (**B**). The left-hand side of the Y axis represents the descending order of importance; the X axis represents the SHAP value, i.e., the impact on the output model. The color represents the feature value: high values have a pink color, while low values have a blue one. Numbers indicated for each line represent the mean of the positive impact values and the negative impact of each feature.

The importance of features in facilitating the learning of the random forest regressor to predict the overall taste status, and an overview of how the most important features impact it to make a prediction in patients with chemosensory loss are shown in Figure 4. In this case, the ratings of the perceived taste intensity for high concentrations of bitter and for high concentrations of astringency were the first two most important features for the model to predict the overall taste status of this group, resulting in a similar contribution on the model prediction of the overall taste status, whereby the average impacts were 0.105 and 0.100, respectively (Figure 4A). These were followed in order of importance from the third to the tenth by: the total taste status, the intensity rating for low concentrations of salty, for high concentrations of sweet, for low concentrations of bitter, for low concentrations of sweet, for high concentrations of sour, for high concentrations of salty, and for low concentrations of sour. These features had an average impact on the model of lower than 0.077. The SHAP summary plot highlights that high estimated values (pink) of the rating of the perceived taste intensity for high concentrations of bitter and for high concentrations of astringency had a strong and positive impact to predict high values of the overall taste status, and the low estimated values (blue) of these features strongly pushed the model prediction toward low values of the overall taste status (Figure 4B). The mean values of the positive impacts of these two features were 0.085 and 0.096, while those of the negative impacts were −0.134 and −0.105, respectively. High estimated values (pink) of the successive eight features had a positive impact (≤0.098) to predict high values of the overall taste status; medium (violet) and low (blue) estimated values of these features impacted the model to predict medium and low values of the overall taste status (negative impact ≤ −0.105).

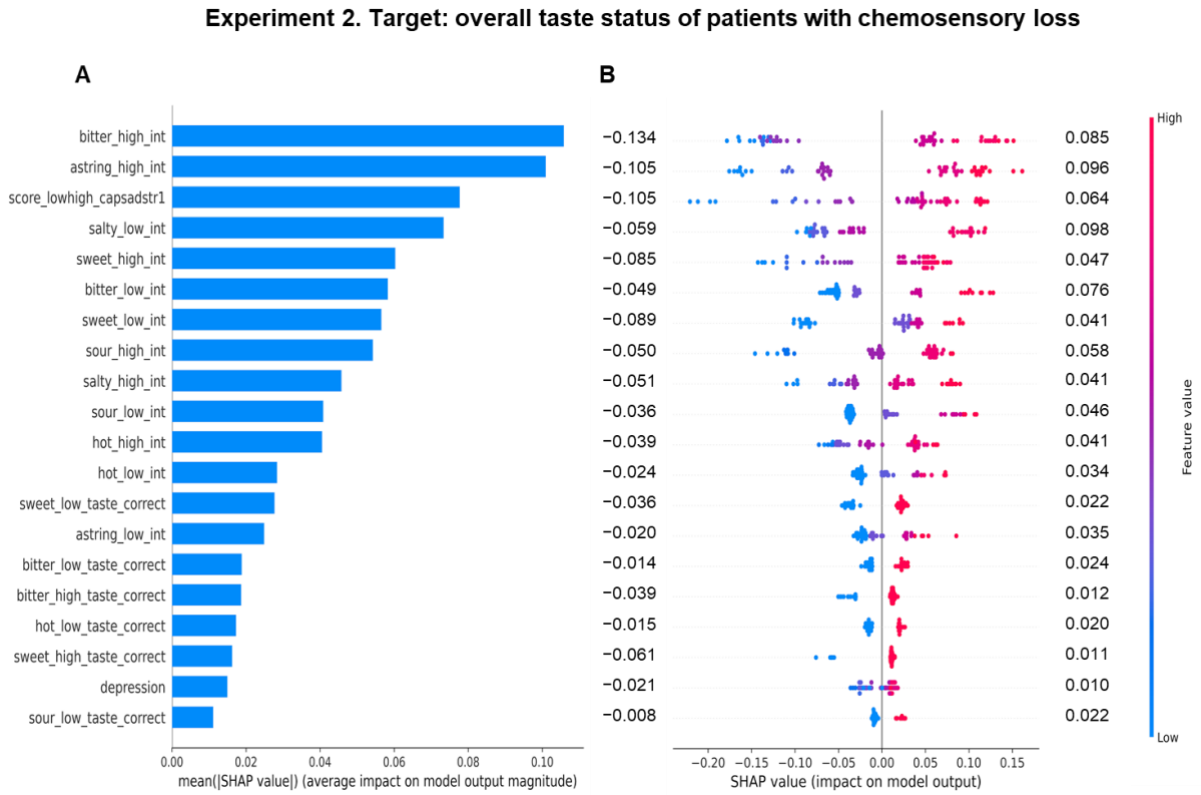

Figure 4. Importance and impact of the sensory, clinical, and anthropometric features on the overall taste status prediction determined with a random forest regressor in patients with chemosensory loss. Importance of features in the training model to understand the overall taste status (**A**). The Y axis represents the order of importance of the features, while the average impact on the model output is represented on the X axis. The SHAP summary plot in patients with chemosensory loss (**B**). The left-hand side of the Y axis represents the descending order of importance; the X axis represents the SHAP value, i.e., the impact on the output model. The color represents the feature value: high values have a pink color, while low values have a blue one. Numbers indicated for each line represent the mean of the positive impact values and the negative impact of each feature.

The error percentage of predicted values of the overall taste status (MAPE values) calculated in the datasets of the two groups by using as inputs for the algorithm only the most important feature for the two groups (the intensity rating for low concentrations of salt in healthy subjects and high concentrations of bitter in patients), was 12.35% and 17.94% in healthy controls and patients with chemosensory loss, respectively. When the second important features were also included in the model (high concentrations of sour for healthy subjects and high concentrations of astringency for patients), the error percentage of predicted values of the overall taste status was 11.05% and 17.16% in healthy controls and patients with chemosensory loss, respectively.

3. Discussion

This study used the SL regression method to establish which combination of sensory, clinical, and anthropometric parameters best predicts the overall taste status of healthy controls or that of patients with chemosensory loss. The subjects included as patients with chemosensory loss were selected based on what they reported. The values of the sensory parameters, which were used as predictive variables of the overall taste status, as well as the correlation between them and the target, confirm that they showed a lower taste sensitivity compared to the subjects of the control group. The low taste sensitivity of these subjects was linked to their higher depression status according to what was already reported [248].

The random forest regressor was the best model to deeply understand differences among subjects and obtain, with high precision, the value of the overall taste status of subjects. Moreover, the random forest regressor allowed us to establish the impact of each parameter based on prediction, identifying the combination of the biological parameters that could best predict the overall taste status of healthy subjects or that of patients with chemosensory loss. The performance of our approach was tested by the metrics of evaluation, MAPE and MSE, which allowed us to verify that the estimated values by the random forest

regressor were strictly close to experimental values with an error percentage of 4.55% and 8.40% in healthy controls and patients with chemosensory loss, respectively. In addition to these advantages of the SL method adopted, which are further outlined below, it is necessary to point out some disadvantages or limitations of this approach. First, it is known that machine learning methods need big data to fit the algorithms, and bias is expected to be larger for smaller datasets. Although dataset size is not necessarily a barrier to a high-performing model, as shown by the metrics of evaluation, our results were obtained in small-sized datasets, mainly that of patients. Therefore, it would be useful to confirm our results in larger datasets. Second, the interpretation of the results of the regressor model used has been performed by using the SHAP algorithm, which allows us to link the importance of each feature with its impact on the prediction. Although SHAP is the best algorithm to achieve this goal, other algorithms can also be used [400]. These two limitations of the study need to be further explored and will be the topic of future research projects.

The random forest regressor also allowed us to achieve the order of importance of each feature on the prediction of the overall taste status of the subjects of the two groups. The regressor identified the rating of the perceived taste intensity for low concentrations of salt to be the most important parameter in healthy subjects, while the rating of the perceived taste intensity for high concentrations of bitter was the most significant in patients with chemosensory loss. Moreover, the interpretation of the link between the importance and the effect of parameters showed that high estimated values of the perceived intensity for low concentrations of salt had a strong and positive impact on predicting high values of the overall taste status in healthy subjects. On the other hand, high estimated values of the rating of the perceived taste intensity for high concentrations of bitter had a strong and positive impact on predicting high values of the overall taste status in patients with chemosensory loss. Low values of these two parameters strongly pushed the model prediction toward low values of the overall taste status in both groups. The fact that the most important parameter to predict the overall taste status in healthy controls was the rating of the perceived intensity for low salt concentrations is not surprising since, as we can see from experimental values shown in Table 1, low concentrations of salt evoked the highest response compared to low concentrations of other stimuli, and a high percentage of subjects (85.3%) recognized it correctly. The rating of the perceived taste intensity for high concentrations of bitter, which was the most important feature in patients with chemosensory loss, was correctly recognized by 76.5% of patients. The bitter taste was also an important stimulus in healthy controls, ranking third in importance order at low concentrations, and was correctly recognized by 61.8% of subjects. The difference in the importance of bitter taste that we found in the two groups may be explained by possible genetic differences between the two groups. In our pilot study, we found that, unlike healthy controls, in patients with taste disorders, a taster haplotype in the gene coding for bitter TAS2R38 receptor is not sufficient to exhibit high responses, suggesting that the genetic constitution may represent a risk factor for the development of taste disorders [346]. Furthermore, based on the findings, which suggest that the TAS2R38 pathway is an immune response target [266, 326], patients with the non-taster haplotype, who show lower responsiveness, could have a higher susceptibility to oropharyngeal infections, which may contribute to their chemosensory loss.

The second most important parameter in learning the model in healthy controls was the perceived intensity rating for high concentrations of sour, which was the stimulus that evoked the highest response, and which 91.2% of subjects correctly recognized. High estimated values had a positive impact on predicting high values of the overall taste status, while low estimated values strongly pushed the model prediction toward low values of the overall taste status. Less important was the impact that sour had on the prediction of the overall taste status in patients with chemosensory loss, in which it was the eighth feature in order of importance, suggesting that the impact of sour on taste function may be more relevant in subjects who have no pathologies that cause chemosensory loss.

The second most important parameter in the model's learning in the patients with chemosensory loss was the perceived intensity rating for high concentrations of astringency, which strongly impacted the prediction of the overall status of this group in a way equivalent to that which was performed by the most important feature, high concentrations of bitter (the values of their contribution to the model prediction were 0.105 and 0.100, respectively). Less important was the contribution and impact that astringency (eighth in importance order at low concentrations and eleventh at high concentrations) had on the

prediction of the overall taste status in healthy subjects, in which low estimated values pushed the model prediction toward low values of the target. These results allow us to speculate that the impact of astringency on taste function could be more important in subjects with low sensitivity. This result deserves to be further investigated in future studies.

It is interesting to note that the performance of our model applied in the datasets of the healthy controls and that of patients, by using as inputs for the algorithm only the most important features for the two groups, allowed us to verify that the estimated values were strictly close to experimental values with an error percentage of 12.35% and 17.95%, respectively. By also including in the model the second important features as the predictive variables, the error percentages of the predicted values of the overall taste status decreased of 1.3% and 0.79%, in healthy controls and patients, respectively. The low error percentage of the predicted values that we found by including in the model low concentrations of salt and high concentrations of sour for healthy subjects, and high concentrations of bitter and high concentrations of astringency stimuli for patients, offers the great advantage of having identified the two most important stimuli that can predict the overall taste status in the two groups. This is extremely important because it allows for the reduction in the experimentation times from 20 min to 3 min for each subject, with respect to the complete procedure of the “12-taste strip test”, which lasts 20 min.

Chapter 5
A supervised learning regression method for the analysis of oral sensitivity of healthy individuals and patients with chemosensory loss

1. Materials and Methods

1.1. Participants

One hundred fifty-two individuals aged 18 to 81 years (38.3 ± 14.3 years; 103 females) have been invited to participate in the study. They were recruited at the Department of Otorhinolaryngology of the TU Dresden. A chemosensory impairment was self-reported by 50 participants who were Smell and Taste Clinic patients. One hundred and two healthy individuals were included in the study's sample as a control group if they self-reported a good sense of taste. They were recruited from the TU Dresden community and matched by age. In all subjects, a structured history was taken. The study size was determined by the statistical power analysis using the software G*Power, Dusseldorf, Germany. Pregnancy, an allergy to study-related substances, untreated hypo- or hyperthyroidism, uncontrolled diabetic mellitus, kidney failure, and serious cardiovascular conditions were among the exclusion criteria. Before their enrollment in the study, all participants gave their informed, written consent. The research protocol was approved by the Ethics Review Board at the University Clinic of the Technische Universität Dresden, application number BO-EK-25012021, and it was performed in accordance with the Declaration of Helsinki.

1.2. Study Design

The experimental value of self-rated oral sensitivity was calculated in each participant as the mean value of self-rated taste sensitivity, self-rated sensitivity for spiciness, and self-rated sensitivity for astringency. The prediction values of the self-rated oral sensitivity of control individuals and patients with chemosensory loss were obtained by the SL regressors. The SL regressors learn from data (presented in the model as predictive variables), create automatic regressor models that evaluate the differences among participants, and return a high-precision prediction of the target in the participants of the two groups. To this aim, the dataset was randomly divided into training data (80%) and test data (20%). During training, the algorithm searches for patterns that correlate with the target in the two groups, then it takes new unknown inputs (in the test data) to determine the predictive values of the target in the two groups. The following algorithms were used: Logistic Regression, Random Forest Regressor, and CatBoost Regressor. Two SL experiments were performed: the first included control individuals (n = 102), and the second included patients with chemosensory loss (n = 50). The data presented in the model as predictive variables were the biological features that were previously recorded from each participant, as described below. Figure 1 shows the study design of each SL experiment.

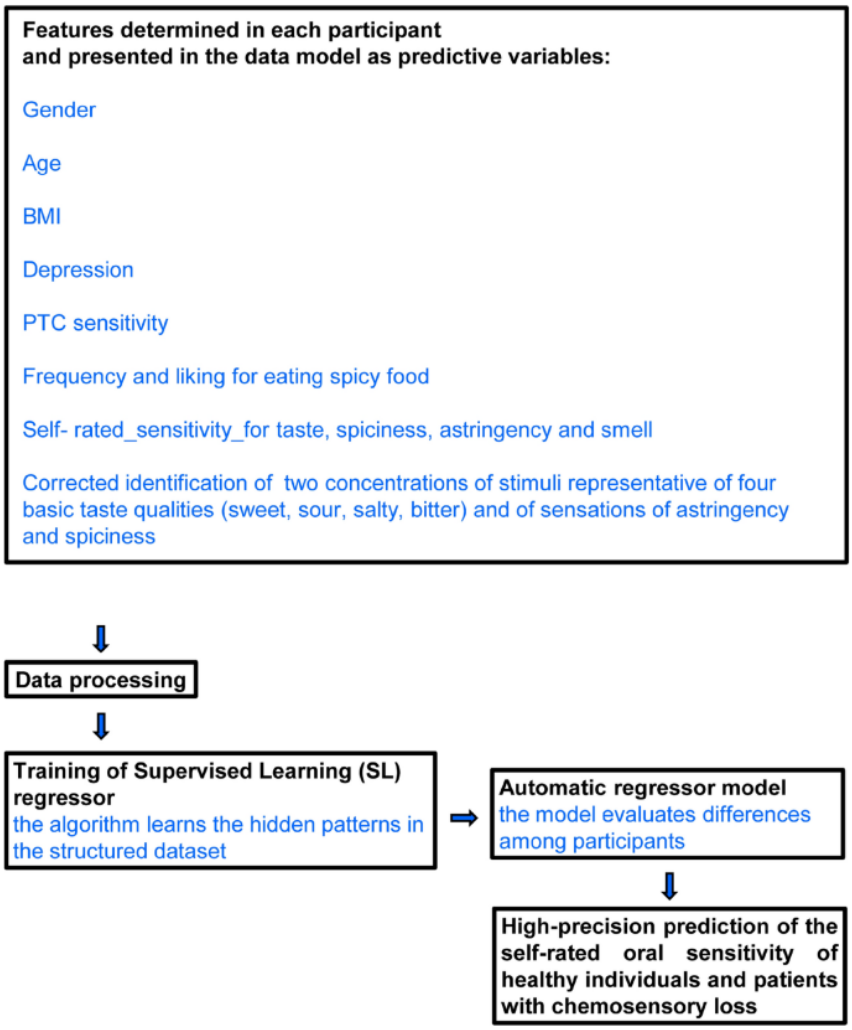

Figure 1. A graphic diagram representing the study design

Data processing operations and the resolution of the overfitting or underfitting problems, which are crucial phases in the running of an SL experiment, were performed according to Naciri et al. [371, 401]. They included handling of missing values; elimination of duplicate values; the conversion of the dataset's content into a structure that machine learning algorithms can employ; the models' hyperparameter optimization that allows finding the optimal value of the number of model iterations, learning rate, and depth of the SL regressors.

Symmetric Mean Absolute Percentage Error (SMAPE) and Mean Squared Error (MSE), which denote the differences between the observed and predicted values, were used to evaluate the performance of the algorithms. Specifically, SMAPE assesses the error percentage of predicted values, and MSE assesses the average of the sum of the squared differences between the observed and the predicted values.

The interpretation of the output of the best SL model (CatBoost regressor) was evaluated by the Permutation explainer method, which is a default model-agnostic explainer used for structured datasets, that has important performance optimizations and does not require regularization parameter tuning. The Permutation explainer works by iterating over complete permutations of the features forward and reversed. The permutation of one feature at a time ensures the efficiency of the original model that we choose to use for the approximation of the contribution of a feature value. The Permutation explainer can be used for Local Interpretability and Global Interpretability [402, 403]:
-In the case of Local Interpretability, which regards a single instance, the Permutation explainer returns the plot of the single instance representing the importance and contribution of features in the CatBoost

regressor model learning to predict the target value. In the plot, the average of the predicted values of the dataset (E[f(x)]) is the starting point to determine the contribution of each feature.
-In the case of Global Interpretability, which regards the whole dataset, the Permutation explainer returns the global summary plot representing the average of the importance and the contribution (mean of SHAP values) of features in the learning of the CatBoost regressor model to predict the values of the target.

1.3. Experimental Procedure for the Biological Feature Measurements

The experimental procedure for the biological feature measurements was completed in a single session. For at least half an hour prior to testing, participants were instructed to refrain from eating, drinking anything save water, and using chewing gum or other dental care items. Participants' health status was evaluated before the session using a thorough medical history. Participants were asked to self-report their weight (kg) and height (m) to determine their BMI (kg/m^2). All participants self-rated their sensitivity for taste, spiciness, astringency, and smell using a 7-point Likert-type scale and they were requested to indicate their frequency and liking for eating spicy food. Moreover, participants were tested for their depression status by using the 5-item World Health Organization Well-Being Index (WHO-5) [394, 395]. Each item response was rated on a 6-point Likert scale from 0 to 5, based on the severity, giving scores ranging from 0 to 25. A high score denotes a high level of well-being, whereas a score of less than 13 denotes a low level of well-being [394, 395].

1.4. Sensory Measurements

All measurements of oral sensitivity were performed by a modification of the "Taste Strip Test" (TST, Burghart Company, Holm, Germany) [209, 210]. Briefly, the filter papers were impregnated with two concentrations (one low and one high) of stimuli representative of four basic taste qualities (sweet, sour, salty, bitter) and of stimulants capable of evoking sensations of astringency and spiciness. The two concentrations for each stimulus were: 0.4 and 0.05 g/mL sucrose; 0.3 and 0.05 g/mL citric acid; 0.25 and 0.016 g/mL sodium chloride; 0.006 and 0.0004 g/mL quinine hydrochloride; 0.1 and 0.2 g/mL tannin; 2.47 × 10–5 and 2.47 × 10–4 g/mL capsaicin. After placing each filter paper on the tongue, each participant had to identify the taste quality of each stimulus by choosing from a list of six possible choices (sweet, sour, salty, bitter, astringent and hot) in a six-alternative forced-choice procedure (compare to [209]). Taste stimuli were presented in a semi-randomized manner. However, trigeminal stimuli were presented as last due to their persistent effect. Participants were instructed to rinse their mouths with tap water before each new test. For each participant, the entire process took 20 min.
Each correct answer was rated 1, thus the maximum score given when all stimuli were correctly identified was 12. The features that represent the score given for each stimulus are called from now on salty_low_taste_correct; salty_high_taste_correct; sweet_low_taste_correct; sweet_high_taste_correct; sour_low_taste_correct; sour_high_taste_correct; bitter_low_taste_correct; bitter_high_taste_correct; hot_low_taste_correct; hot_high_taste_correct; astring_low_taste_correct; astring_high_taste_correct. Whereas the feature that represents the sum of scores given for all stimuli is called score_lowhigh_capsadstr1.

PTC-impregnated filter paper (phenylthiocarbamide test paper; Sensonics, Philadelphia, PA, USA) [404] was used to assess the bitter taste of PTC, whose taste sensitivity is highly correlated to the bitter perception of 6-n-propylthiouracil (PROP) [115, 405]. To re-focus the participant's attention on the experimental procedures, the intensity of the PTC-related bitterness was rated on a different scale than the other tastes, ranging from 0 to 10 (where 10 denoted the most intense bitterness).

1.5. Statistical Analysis

Fisher's Exact Test was used to analyze differences between control individuals and patients with chemosensory loss, in the frequency of correct answers for the two concentrations of each stimulus, gender, and liking for eating spicy food (liketoeatspicy). Data were checked for normality with Shapiro–Wilk test and Kolmogorov–Smirnov test. Since the normality was violated the Mann–Whitney U Test was used to

compare differences, between the two groups, in age, BMI, depression, total taste score (score_lowhigh_capsadstr1), self-rated taste sensitivity (selfratedsensitivitytaste), self-rated sensitivity for spiciness (selfratedsensitivityspicyness), self-rated sensitivity for astringency (selfratedsensitivityastringency), self-rated smell sensitivity (selfratedsensitivitysmell) and frequency for eating spicy food (spicyfoodmealspermonth), and the relationships between the self-rated oral sensitivity data and oral sensitivity data obtained by "Taste Strip Test" (score_lowhigh_capsadstr1) in the two groups were assessed using Spearman's correlation analysis. Statistical analyses were conducted using STATISTICA for WINDOWS (version 7; StatSoft Inc, Tulsa, OK, USA). P values < 0.05 were considered significant.

2. Results

Table 1 shows the differences in mean values ± SE or the number of correct answers or participants' frequency of biological features between control individuals and patients with chemosensory loss. Mann–Whitney U Test showed that the total taste score (score_lowhigh_capsadstr1), as well as the self-rated sensitivity for taste, spiciness, astringency and smell were higher in control individuals than in patients with chemosensory loss ($p < 0.0001$). Instead, the BMI and depression status were higher in patients than in controls ($p \leq 0.035$). The number of correct answers for the low concentrations of salty, bitter, hot and astringency and the high concentration of sweet, sour and astringency, as well as the number of participants who like to eat spicy, were higher in controls than in patients ($\chi^2 \geq 4.94$; $p \leq 0.039$; Fisher's test). No differences in the low concentrations of sweet and sour, and high concentrations of salty, bitter and hot or in PTC ratings, frequency of eating spicy food, age and gender were found between the two groups ($p > 0.05$).

Table 1. Differences in biological features between control individuals and patients with chemosensory loss.

Features	Controls (*n* = 102)	Patients (n = 50)	p-value
score_lowhigh_capsadstr1	9.37 ± 0.21	7.14 ± 0.30	< 0.001
PTC1	5.42 ± 0.36	4.55 ± 0.52	0.146
Age (years)	36.70 ± 1.38	40.34 ± 1.97	0.074
BMI (kg/m^2)	23.66 ± 0.46	25.60 ± 0.65	0.035
depression	17.15 ± 0.42	14.20 ± 0.60	< 0.001
Self-rated sensitivity taste	3.79 ± 0.11	1.90 ± 0.15	< 0.001
Self-rated sensitivity spiciness	4.09 ± 0.11	2.80 ± 0.16	< 0.001
Self-rated sensitivity astringency	3.77 ± 0.11	2.64 ± 0.16	< 0.001
Self-rated sensitivity smell	3.62 ± 0.12	1.90 ± 0.15	< 0.001
Spicy food meals per month	4.92 ± 0.59	1.70 ± 0.17	0.379
salty_low_taste_correct/non (n)	87/15	32/18	0.003
salty_high_taste_correct/non (n)	90/12	44/6	0.579
sweet_low_taste_correct/non (n)	72/30	31/19	0.189
sweet_high_taste_correct/non (n)	100/2	45/5	0.039
sour_low_taste_correct/non (n)	32/70	9/41	0.058
sour_high_taste_correct/non (n)	93/9	35/15	0.001
bitter_low_taste_correct/non (n)	63/39	21/29	0.017
bitter_high_taste_correct/non (n)	77/25	38/12	0.557
hot_low_taste_correct/non (n)	77/25	17/33	0.000
hot_high_taste_correct/non (n)	97/5	46/4	0.346

Features	Controls (*n* = 102)	Patients (n = 50)	p-value
astring_low_taste_correct/non (n)	78/24	15/35	< 0.001
astring_high_taste_correct/non (n)	86/16	24/26	< 0.001
Male/Female *(n)*	37/65	14/36	0.203
Liketoeatspicy/non (*n*)	66/36	22/28	0.010

Values are means ± SE, or numbers of correct answers, or of participants. Significant differences in mean values were determined by Mann–Whitney U Test ($p \leq 0.035$), while significant differences in the number of correct answers or participants' frequency were determined by Fisher's method ($p < 0.039$).

Figure 2 shows the scatterplots depicting the relationships between the self-rated oral sensitivity data and oral sensitivity data obtained by the "Taste Strip Test" (score_lowhigh_capsadstr1) in the control individuals (**a**) and in patients with chemosensory loss (**b**). Spearman's correlation analysis showed that the self-rated oral sensitivity data were correlated with the oral sensitivity data obtained by the "12 Taste Strip Test" ($r \geq 0.34$; $p \leq 0.017$) in the two groups. No correlation was found between self-rated oral sensitivity data and PTC bitterness ($p > 0.05$).

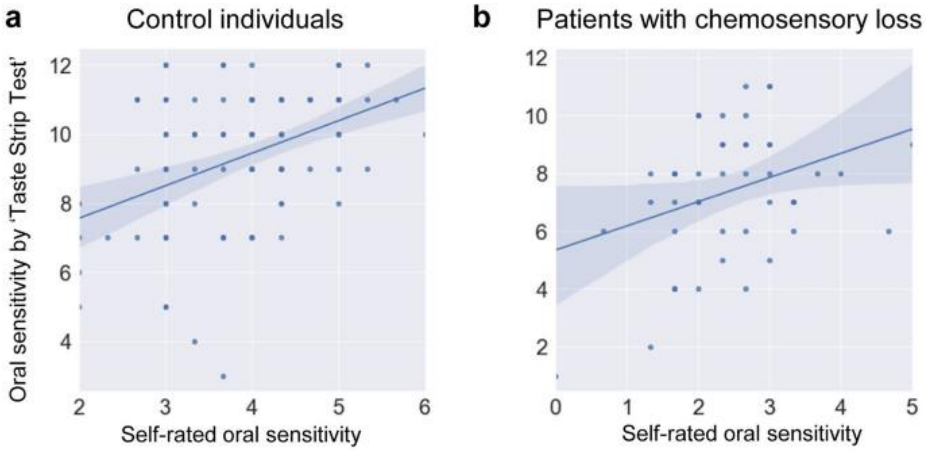

Figure 2. Relationships between the self-rated oral sensitivity data and oral sensitivity data obtained by the "Taste Strip Test" (score_lowhigh_capsadstr1) in the control individuals (n = 102) (**a**) and in patients with chemosensory loss (n = 50) (**b**).

The metrics of evaluation of the training and performance of the algorithms, SMAPE and MSE, showed that the CatBoost regressor algorithm was the best algorithm to predict the values of the self-rated oral sensitivity with high precision. The scatterplots in Figure 3 show experimental values vs. predicted values of the self-rated oral sensitivity obtained with the CatBoost regressor in controls (a) and patients with chemosensory loss (b). The values of the MSE, which assesses the average squared difference between the experimental and predicted values, were 0.025 and 0.034 in controls and patients, respectively. The values of the SMAPE, which represent the error percentage of predicted values, were 5.39% and 27.81% in control individuals and patients with chemosensory loss, respectively.

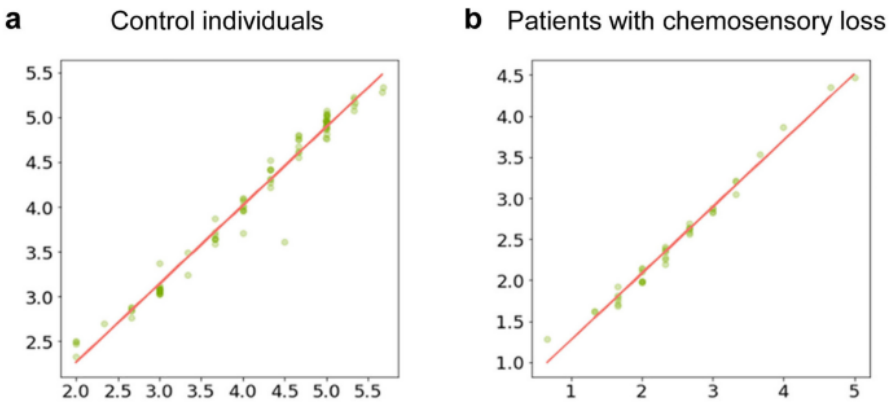

Figure 3. Scatterplots of the self-rated oral sensitivity experimental values vs. predicted values obtained with the CatBoost regressor in the control individuals (n = 102) (**a**) and in patients with chemosensory loss (n = 50) (**b**).

Figure 4 shows the plots of single instances representing the importance and contribution of features in the CatBoost regressor model learning to predict the self-rated oral sensitivity value in a representative control individual (a), in which the experimental value was 5 and the predicted value was 4.999, and in a representative patient (b), in which the experimental value was 2 and the predicted value was 1.938. The average of the predicted values in the control group (E[f(x)]) was higher (3.987) than that of the patient group (2.537). In addition, in the control individual, the self-rated sensitivity for astringency (selfratedsensitivityastringency), spiciness (selfratedsensitivityspicyness), taste (selfratedsensitivitytaste) and smell (selfratedsensitivitysmell) were the four important features and gave a contribution of + 0.41, + 0.33, + 0.15 and + 0.04. The successive five features in importance order were: depression, salty high_taste_correct, age, sweet_low_taste_correct, and astringency_high_taste_correct. Differently, in the patient, the self-rated sensitivity for astringency (selfratedsensitivityastringency), spiciness (selfratedsensitivityspicyness), PTC, and taste (selfratedsensitivitytaste) were the four important features and gave a contribution of − 0.37, − 0.2, − 0.04, and + 0.02. The successive five features in importance order were: BMI, hot_high_taste correct, age, sour high_taste_correct, and sex.

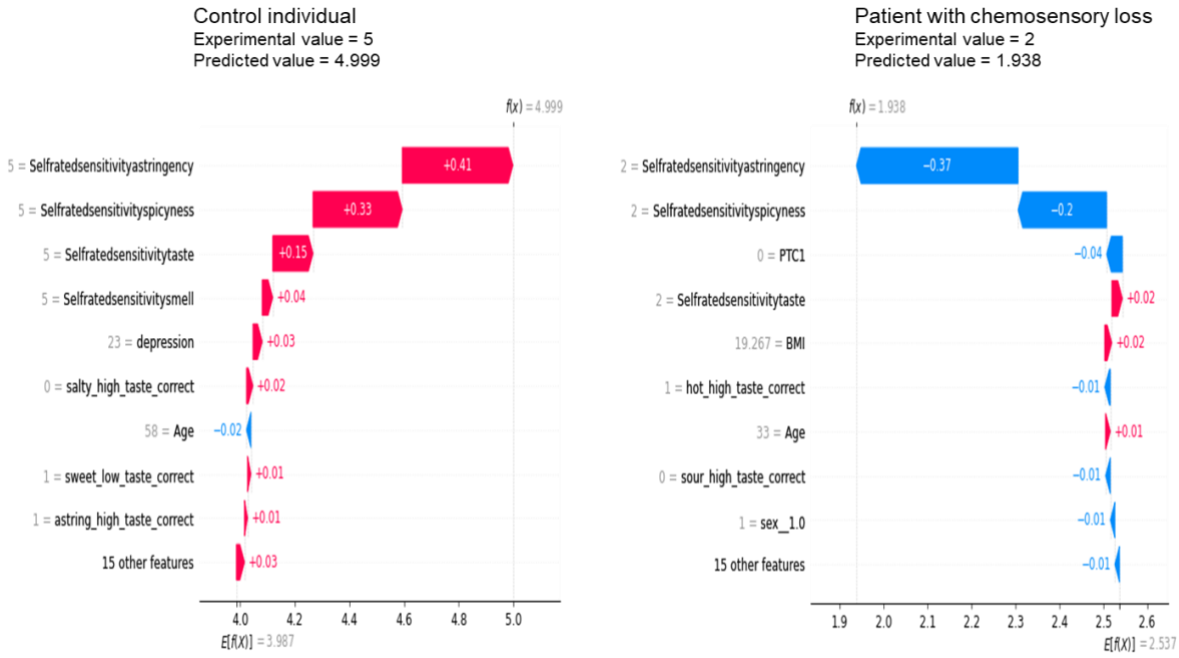

Figure 4. Plots of single instances representing the importance and contribution of features in the learning of the CatBoost regressor model to predict the value of the self-rated oral sensitivity in a control individual (**a**) and in a patient with chemosensory loss (**b**). The Y axis represents the order of the features' importance, while the X axis represents the contribution of features. Below the X axis, (E[f(x)]) is the average of the predicted values of the dataset which is the starting point to determine the contribution of each feature. At the top of the plot, f(x) is the predicted value in the single instance. The numbers next to each bar represent each feature's contribution values.

Figure 5 shows the global summary plots representing the average of the importance and contribution (mean of SHAP values) of features in the learning of the CatBoost regressor model to predict the values of the self-rated oral sensitivity in control individuals (a) and in patients with chemosensory loss (b). The self-rated sensitivity for astringency (selfratedsensitivityastringency) was the most important feature and gave a similar contribution in the two groups (+ 0.29 and + 0.27). The self-rated sensitivity for spiciness (selfratedsensitivityspicyness) was the second important feature in both groups, but contributed more in facilitating the learning of the model in control individuals (+ 0.28) than in patients (+ 0.19). The self-rated taste sensitivity (selfratedsensitivitytaste) was the third important feature in the two groups and contributed more in control individuals (+ 0.18) than in patients (+ 0.07). The self-rated smell sensitivity (selfratedsensitivitysmell) was the fourth feature in both groups, giving a similar contribution in the learning of the model (+ 0.03 and + 0.02). The successive five features in order of importance were different in the two groups and were: astring_high_taste_correct, depression, sweet_low_taste_correct, age and sweet_high_taste correct in control individuals and PTC1, age, BMI, Hot_high_taste correct and sex in patients with chemosensory loss.

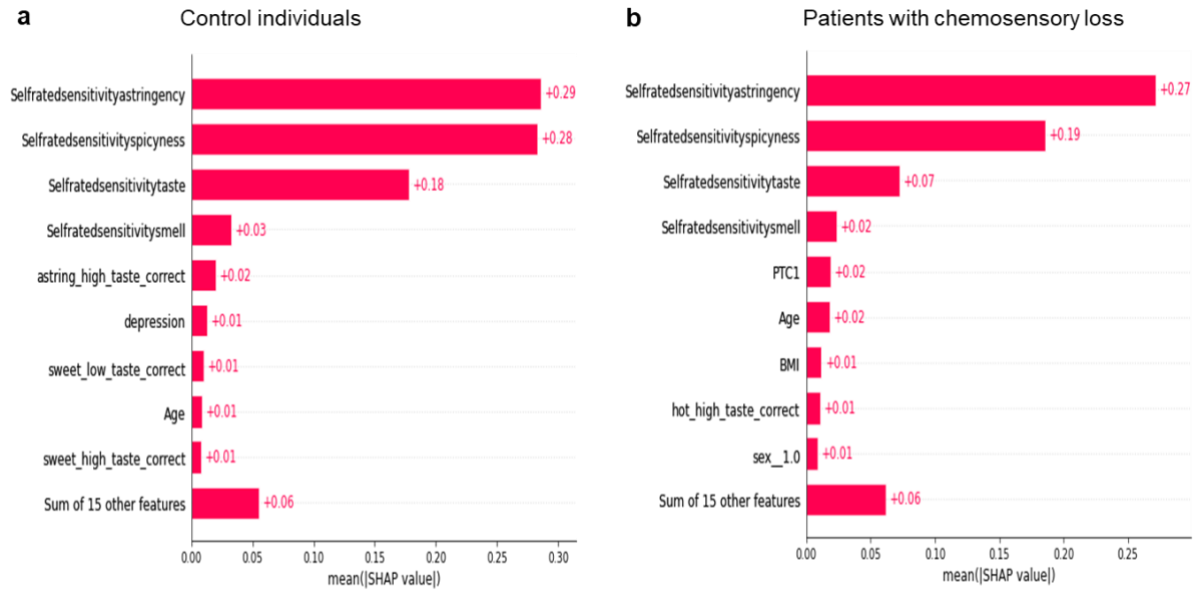

Figure 5. Global summary plots representing the average of the importance and the contribution of features in the learning of the CatBoost regressor model to predict the values of the self-rated oral sensitivity in control individuals (**a**) and in patients with chemosensory loss (**b**). The Y axis represents the order of the features' importance, while the average contribution to the model output is represented in the X axis. The numbers next to each bar represent the mean values of the contribution of features.

3. Discussion

The primary aim of the present work was to build an SL model capable of automatically analyzing with high precision the subjective ratings of the oral sensitivity of healthy individuals and patients with chemosensory loss, considering its three components: gustatory, olfactory, and trigeminal functions. To this aim, the prediction values of the self-rated oral sensitivity of control individuals and patients with chemosensory loss were obtained by the Supervised Learning (SL) Regression. The following SL Regression algorithms (Logistic Regression, Random Forest Regressor, and CatBoost Regressor) were used as they are specifically designed to forecast continuous outcomes like self-rated oral sensitivity [397]. In the proposed approach, the algorithms learn from data that were participants' biological features previously determined (presented in the model as predictive variables), create automatic regressor models that evaluate the differences among participants, and return a high-precision prediction of the self-rated oral sensitivity in the participants of the two groups. The self-rated oral sensitivity that we used as the target was calculated in each participant as the mean value of the self-rated taste sensitivity, self-rated sensitivity for spiciness, and self-rated sensitivity for astringency. The approach allowed us to deeply understand the importance and contribution of the taste, olfactory, and trigeminal components of oral sensitivity, highlighting the

differences between the two groups. In addition, the method enabled us to determine the importance and impact on the model output of the six stimuli presented to each participant, as well as of their concentration, and other parameters that may influence oral sensitivity. To achieve the goal of this work, we performed two SL experiments, one included control individuals and the other included participants who were selected based on their self-reported chemosensory impairments. The lower values of the total taste, the self-rated taste sensitivity, the self-rated sensitivity for spiciness, the self-rated sensitivity for astringency, and the self-rated smell sensitivity, as well as the average of the predicted values (E[f(x)]) in these participants, compared to those of participants of the control group, confirmed that they had chemosensory impairments. These participants showed a higher BMI. This was expected because reductions in taste sensitivity for sweet, umami, bitter and sour, and fatty acids [273], and impaired olfactory performance have been observed in people with obesity [406-408], or increased BMI [110, 187, 194, 272, 274, 363]. However, other reports have produced conflicting evidence [409-413]. These participants also showed lower levels of well-being according to what has already been reported in other studies [248].

In our approach, self-rated data were used as predictive variables even though they are highly subjective evaluations that may produce large errors of measurement. Not with standing this limitation, self-rated evaluations, as well as all psychophysical testing procedures, are the only procedures in use in human studies since they are of simple application to large populations at a low cost and without causing inconvenience. In addition, the strong correlation that we found between self-rated oral sensitivity data and those obtained by the complete procedure of the "12-taste strip test" in the two groups is indicative of the fact that self-rated data can effectively be used. Moreover, the training and performance of our approach were tested by the metrics of evaluation, SMAPE, and MSE, which allowed us to verify, in both SL experiments, that the predicted values by the CatBoost regressor algorithm are strictly close to experimental values, the error percentages were 5.39%, and 27.81% and the average squared differences were 0.025 and 0.034 in control individuals and patients with chemosensory loss, respectively. These results indicated that the CatBoost regressor could efficiently learn from this kind of data and return a high-precision prediction of the target in the two groups, even if they had a low size (mostly the group of patients) and were unbalanced in number and gender. However, Machine Learning techniques are known to require large datasets to fit the algorithms, and bias is expected to be larger for smaller datasets. Therefore, it would be beneficial to confirm our findings in larger samples.

The Permutation explainer method allowed us to achieve the importance and contribution of features in the learning of the CatBoost regressor model to predict the self-rated oral sensitivity in the Local Interpretability, which regards a single instance, and the Global Interpretability, which regards the whole dataset. For the Local Interpretability, we have chosen the two more representative instances of the two groups, i.e., those in which the predicted values were close to experimental values. In the instance of the control group, the experimental value was 5, and that predicted 4.999; in the instance of the patient group, the experimental value was 2, and that predicted 1.938. The smaller distance between the two values in the control individual could depend on the fact that in the control group, the CatBoost regressor learned better, thanks to the larger number of observations. However, the metrics of evaluation of the training and performance of the algorithm computed in the patient group indicated that the algorithm predicted values of the self-rated oral sensitivity with high precision also in this group, and the evidence is that the predicted values of patients are very close to the experimental ones, as shown by the value of MSE (0.034) in this dataset. The local interpretability of the permutation explainer allowed us to identify in the control individual, the self-rated sensitivity for astringency, the self-rated sensitivity for spiciness, the self-rated taste sensitivity, and the self-rated smell sensitivity as the four features most important to predict the value of the self-rated oral sensitivity, positively contributing with respect to the average of the predicted values of the whole dataset. Differently, in the patient instance, the self-rated sensitivity for astringency and the self-rated sensitivity for spiciness, and PTC ratings, which were the three most important features, provided a negative contribution to the predicted value of the self-rated oral sensitivity of this patient. The successive features in order of importance were different in the two instances: depression, the correct identification of high concentration of salt, age, the correct identification of low concentration of sweet, and the correct identification of high concentration of astringent stimulus in the control individual and the

self-rated taste sensitivity, BMI, the correct identification of high concentration of capsaicin, age, the correct identification of high concentration of sour, and sex in the instance of the patient group.
In the Global Interpretability, the Permutation Explainer allowed us to identify the average of the importance and contribution of features in the learning of the CatBoost regressor model to predict the values of the self-rated oral sensitivity in the whole dataset of the control group and in the whole dataset of the patient group. It is interesting to note that only the self-rated sensitivity for astringency, the self-rated sensitivity for spiciness, and the self-rated taste sensitivity shared more than 75% of explanatory power in both groups (83.33% in control individuals and 77.94% in patients). However, in control individuals, the self-rated sensitivity for astringency and the self-rated sensitivity for spiciness had a similar impact on the model output (32.22% and 31.11% were their explanatory power), and the self-rated taste sensitivity had a lower impact (20% was the explanatory power). Differently, in patients, the self-rated sensitivity for astringency was the most important feature with an explanatory power of 39.7%, while the self-rated sensitivity for spiciness had a lower impact, with 27.94% explanatory power. The self-rated taste sensitivity was the third significant feature with a 10.29% explanation power. The self-rated smell sensitivity was the fourth feature in both groups, but it had an extremely low explanatory power (about 3% in both groups). Also, the Global Interpretability highlighted that the other features that significantly impacted the model output were different in the two groups, though they had a very low explanatory power. They were the correct identification of the high concentration of astringent stimulus, depression, the correct identification of low concentration of sweet, age, the correct identification of high concentration of sweet in the control group, and PTC ratings, age, BMI, the correct identification of high concentration of capsaicin and sex in the patient group.
It is noteworthy that the average level of well-being was a significant feature in predicting the self-rated oral sensitivity in control individuals who had higher levels, while the BMI was significant in the patients, who showed higher values.

Chapter 6
Gene Methylation Affects Salivary Levels of the Taste Buds' Trophic Factor, Gustin Protein

1. Materials and Methods

1.1. Volunteers and Experimental Procedure

Sixty-six Caucasian volunteers (48 females and 18 males, ages 24.76 ± 4.80) were recruited at the University of Cagliari using standard procedures. They were originally from Sardinia, Italy. Volunteers were normal weight with a body mass index (BMI) ranging from 20.2 to 24.8 kg/m^2. Exclusion criteria included pregnancy, lactation, major metabolic diseases (diabetes, kidney disease, etc.), food allergies, and the usage of drugs that would have impaired their ability to taste or smell (e.g., steroids, antihistamines, or anti-depressants). Their taste function for the four basic tastes was evaluated using the taste strip test (Burghart Messtechnik, Wedel, Germany) to rule out any taste impairment. All volunteers were informed regarding the purpose and procedure of the study. All volunteers provided written informed consent. The current study was carried out following the most recent version of the Helsinki Declaration, and all methods were authorized by the University Hospital Company's (AOU) Ethical Committee in Cagliari, Italy (protocol code 451/09, date of approval May 2016).

All volunteers were instructed to abstain from eating, drinking (except water), using dental care products, or chewing gum for at least two hours before testing. Each volunteer was required to arrive in the experiment room fifteen minutes before the test's scheduled start time (9.30 a.m.) to adapt to the environmental conditions (23–24 °C; 40–50% relative humidity and light with standard solar light 15,000 lux) that were kept constant throughout the experimental session. The environment was maintained relatively quiet and odor-free. For each volunteer, multiple photographs of the tongue surface were taken to determine the density of fungiform papillae. All were assessed for their PROP responsiveness and two samples of the whole-unstimulated saliva (1 mL each) were collected as described below. To prevent alterations in taste function caused by the estrogenic phase, women were tested around the sixth day of the menstrual cycle [367].

1.2. PROP Responsiveness Measurements

PROP responsiveness of each volunteer was assessed by a scaling method for their taster status classification. The impregnated paper screening test [179], which had been tested for validity and reliability [181, 207, 414], was used. The test is based on the ratings of two paper disks, placed for 30 s on the tip of the tongue, impregnated with sodium chloride, NaCl (1.0 mol/L), and PROP solution (50 mmol/L), respectively. Intensity ratings for PROP or NaCl were collected using the Labeled Magnitude Scale (LMS) [415]. Volunteers were trained in the use of the LMS before testing. This scale gives volunteers the freedom to rate the perceived taste intensity for each stimulus relative to the "strongest imaginable" oral stimulus they had ever experienced in their lives. The interstimulus interval was set at 5 min. Volunteers who evaluated the PROP disk higher than 67 mm in LMS were classified as PROP super-tasters (STs), those who evaluated the PROP lower than 15 mm on the scale were classified as PROP non-tasters (NTs), and those who rated the PROP disk with intermediate ratings were classified as medium-tasters (MTs) [179]. Volunteers who rated the PROP disk as borderline (≅15 mm) and rated NaCl significantly higher (≅30 mm discrepancy on the LMS) were classified as NT. Likewise, volunteers who rated the PROP disk as borderline (≅67 mm) and rated NaCl much lower were classified as ST. Based on their taster group assignments, 27 volunteers were classified as ST (40.91%), 29 were MT (43.94%), and 10 were NT (15.15%).

1.3. Density Assessments of the Fungiform Taste Papillae

Fungiform papillae density was determined according to Melis et al. 2013 [203] on the anterior tongue surface's tip, at the left side of the midline. This area provides measurements of the fungiform papillae density which are highly correlated with the total number on the tongue [223]. The tip of the tongue was dried with filter paper and stained by placing (for 3 s) a piece of filter paper (circle 6 mm in dia) that was impregnated with blue food coloring (E133, Modecor Italiana, Cuvio, Italy). Multiple photographs of the

stained area were taken using a Nikon Coolpix P520 Digital Camera (Nikon Corporation, Konan, Minato-ku, Tokyo) (18.1 megapixels). After downloading the digital photos to a computer, the "zoom" feature of Adobe Photoshop CS2 version 9.0 (Adobe Systems Incorporated, San Jose, CA, USA) was used to evaluate the pictures. The fungiform papillae in the stained area were identified by their mushroom shape and distinguished by their very light staining in contrast to filiform papillae which stained dark [221]. The number of papillae was counted for each volunteer separately by three trained observers who were blind to the genotype of SNP analyzed and to the PROP taster status of volunteers [203, 207, 223]. Final measurements were based on the consensus of all observers which then calculated the density/cm^2.

1.4. Salivary Levels of Gustin Protein

1.4.1. Saliva Collection and Treatment

Using a soft plastic aspirator, two samples (1 mL) of whole unstimulated saliva were collected, within less than a minute, from the anterior floor of the mouth of each volunteer. One tube was directly stored at −80 °C until the DNA extraction, and the second was immediately treated for the immunoblot procedure for *Gustin* protein quantification before storage. A protease inhibitor cocktail solution [mix of 1 tablet/1.4 mL of cOmplete® Protease Inhibitor Cocktail (Roche Diagnostics, Indianapolis, IN, USA) and 175 mM NH_4HCO_3 (Ammonium Bicarbonate, Sigma-Aldrich, St. Louis, MO, USA) was added to saliva in a 1:2 *v/v* ratio.

1.4.2. Salivary Protein Quantification

Bicinchoninic Acid (BCA) Protein Assay Kit (Sigma-Aldrich, St. Louis, MO, USA) was used to quantify the total protein content of the saliva samples according to the manufacturer's instructions. The total concentration of salivary protein was used to normalize the protein levels in the dot blot analysis.

The quantification of the *Gustin* protein salivary levels was performed using the semi-quantitative dot-blot technique, where the protein samples were spotted directly onto a PVDF membrane (0.2 µm pore size; Immun-Blot® PVDF Membrane, Bio-Rad Laboratories, Inc., Segrate, Italy). To prepare an assay for dot blot, the treated saliva samples were first diluted with Tris Buffered Saline (TBS: 20 mM Tris-HCl, pH 7.6, 150 mM NaCl) to ensure that every sample had the same amount of total protein content (adjusted to 0.42 µg/µL). The recombinant Human Carbonic Anhydrase VI Protein (code: 2939-CA-010, R&D Systems, Minneapolis, MN, USA) was used as a standard in 5 concentrations (0.2, 0.3, 0.4, 0.6, and 0.8 µg/µL).

Before transferring the samples onto the PVDF membrane, it was pre-wetted with methanol for 1 min, and then transferred to TBS for 2 min. All samples (2 µL of volume) and standards (1 µL of volume) were spotted onto the wet PVDF membrane in triplicate. The membrane was blocked with a blocking agent of 5% of BSA (Bovine serum albumin, Sigma Aldrich, St. Louis, MO, USA) in TBS-T buffer (20 mM Tris-HCl, pH 7.6, 150 mM NaCl, 0.05% Tween 20) for 1 h at room temperature. Subsequently, the membrane was incubated for 2 h at room temperature with primary antibody (0.5 µg/mL, Human Carbonic Anhydrase VI antibody, Monoclonal Mouse IgG3 clone #401819, Catalog: MAB2939 R&D Systems) in 0.5% of BSA in TBS-T buffer. Three washes for 5 min with TBS-T buffer were performed, and the membrane was incubated for 1 h with secondary antibody (dilution 1:5000; Rabbit anti-Mouse IgG, Secondary Antibody, HRP Thermo Fisher Scientific, Waltham, MA, USA). After three further washes with TBS-T and one wash with TBS (5 min), the membrane was incubated for 5 min with ECL substrate (Clarity Western ECL Substrate, Bio-Rad Laboratories, Inc., Segrate, Italy) to develop fluorescence signals and captured on the iBright™ CL1500 Imaging System (ThermoFisher Scientific, Waltham, MA, USA). Analysis of images obtained was performed using iBright Analysis Software Desktop Version 5.2.0 (ThermoFisher Scientific, Waltham, MA, USA). Signals of samples were identified and shown as intensity values, which were transformed by the software into value of concentration (µg/µL) for each sample by using the standards as references. Each sample was analyzed three times, with a reasonable coefficient of variation (CV%) set as below 15%.

1.5. Genotyping for Gustin (CA6) Gene Polymorphism rs2274333

DNA was extracted from saliva samples using the standard salting-out procedure. The concentration of purified DNA was estimated by measuring the optical density at 260 nm with a NanoDrop™ One/OneC

Microvolume UV-Vis Spectrophotometer (Thermo Scientific™, Life-Technologies Italia, Milan, Italy, Europe BV, Monza, Italy). Volunteers were genotyped for the single-nucleotide polymorphism (SNP) *rs2274333* (A/G) of the *Gustin* gene located in the exon 3 that resulted in a substitution of amino acid Ser90Gly in the protein sequence by using TaqMan® SNP Genotyping Assay technique, using the assay with code: C_1739329_1 (ThermoFisher Scientific, Waltham, MA, USA). The plates were read using a StepOne™ Real-Time PCR System following the manufacturer's instructions (Applied Biosystems by Life Technologies, Milan, Italy, Europe BV, Monza, Italy). The results were analyzed by allelic discrimination of the sequence detector software (TaqMan® Genotyper Software v1.7.1, Applied Biosystems, Inc., Foster City, CA, USA). Replicates, two negative and three positive controls (one for each genotype), were included in all reactions. The PCR reactions were run on 96-well plates with fast thermal cycling conditions and included: 1X TaqMan® genotyping master mix (code: 4371355), 1X TaqMan® genotyping assays (C_1739329_1, Catalog number: 4351379), and 10 ng of DNA and nuclease-free water.
In total, 39 (59 %) participants had the AA genotype (16 were classified as STs, 19 MTs, and 4 NTs), 21 (32 %) had the AG genotype (10 STs, 8 MTs, and 3 NTs), and 6 (9 %) had the GG genotype (1 ST, 2 MTs, and 3 NTs). Although Allele A was more frequent in STs and MTs (78% and 79%) than in NTs (55%), no significant differences were found based on the genotype distribution or allelic frequency of the *Gustin* (CA6) gene polymorphism *rs2274333* (A/G) (Genepop software version 4.2; online software: **http://genepop.curtin.edu.au/genepop_op3.html** (accessed on 23 February 2024); Montpellier, France).

1.6. Gustin Gene Methylation Profiling

Focusing on the promoter region, there are some scattered CpG loci that could be involved in the regulation of gene expression. In particular, in an interval of 1000 bp upstream of the beginning of the coding sequence, there are eight CpG loci distant from each other, except the two closest to the ATG (33 and 36 bp upstream of it), and very close to each other (3 bp). This allowed us to design an assay for MethyLight that interrogated at least two CpG loci, as is very often done even when designing an assay within a CpG island. We designed a MethyLight assay (amplicon size 128 bp) to interrogate the DNA methylation status of two CpG sites (cg06962067 and cg00198750) located in the region (chr1:8945775-8945902, hg38) upstream of the coding sequence (CDS) of the Gustin gene (Table 1). The two selected CpG loci are located 36 bp and 33 bp upstream of the ATG. The designed assay involves the use of primers that hybridize to regions not influenced by methylation (not containing CpG loci) and a probe that hybridizes in the stretch of sequence containing the two CpG loci described above, capable of discriminating the methylated from the unmethylated state.

Table 1. Gustin methylation assay.

Type	Seq (5'→3')	Tm (°C)
Primer Forward	AAGGGTGGTTTAGTTAGTTGGGTAG	57.1
Primer Reverse	ACACCAAAACCCTCATAATACTACACA	58.0
Probe	5'6-FAM AAGAAGAGTTTCGTCGGAAT	68.0

We carried out two reactions for each sample: one for the target assay and one for the bisulfite-dependent methylation-independent control (ALU-C4) that was used to normalize the quantity of the input DNA sample [416]. Each reaction was performed in triplicate and contained: 1X TaqMan® Genotyping Master mix (Applied Biosystems, Foster City, CA, USA), 900 nM of each primer, 250 nM of probe, and 30 ng bisulfite-converted DNA in a final volume of 20 µL. The experiment was conducted on Rotor-Gene Q (Qiagen, Venlo, The Netherlands) using the following thermal conditions: 95 °C for 10 min, followed by 45 cycles of 95 °C for 15 sec and 60 °C for 1 min. The methylation levels were expressed as Δ cycle threshold (Ct), calculated as the difference between Ct of the target assay and Ct of the ALU-C4 control (higher ΔCt means a lower methylation level and vice versa).

1.7. Statistical Analyses

One-way ANOVA was used to analyze the effect of *Gustin* gene polymorphism *rs2274333* on the density of fungiform papillae and salivary levels of *Gustin* protein and to compare the differences in salivary levels of *Gustin* protein among ST, MT, and NT volunteers. Post hoc comparisons were conducted with Fisher's least significant difference (LSD) test. The relationships between salivary levels of *Gustin* protein and ΔCt values were assessed using Pearson linear correlation analysis. The same analysis was conducted separately in the three *Gustin* genotypes and PROP taster groups.

Statistical analyses were conducted using STATISTICA for WINDOWS (version 7; StatSoft Inc., Tulsa, OK, USA). *p* values ≤ 0.05 were considered significant.

2. Results

The mean values of the densities (±SEM) of the fungiform papillae of participants with genotypes AA, AG, and GG of the *Gustin* gene are shown in Figure 2. One-way ANOVA revealed that the fungiform papillae density was associated with *Gustin* gene polymorphism ($F_{(2,63)}$ = 3.788; p = 0.029). Specifically, the values of the fungiform papillae density were lower in volunteers with the GG genotype than in those with the AA genotype (p = 0.019; Fisher LSD test). The values of the AG genotypes were not different from those of the other groups ($p > 0.05$).

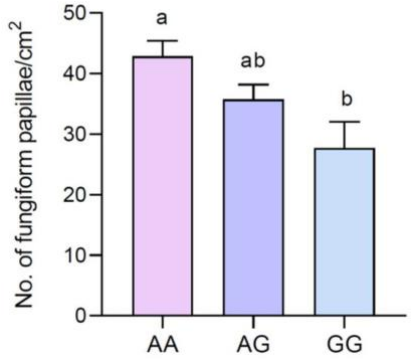

Figure 2. Mean values ± SEM of the density of fungiform papillae (No./cm^2) of volunteers with AA, AG, and GG genotypes of *Gustin* polymorphism *rs2274333* (A/G). *n* = 66. Different letters indicate a significant difference (p = 0.019; Fisher LSD test after one-way ANOVA).

Figure 3 shows the mean values of the salivary levels of the *Gustin* protein (μg/μL) of PROP ST, MT, and NT (A) volunteers and with the AA, AG, and GG genotypes of the *Gustin* gene (B). ANOVA revealed that the salivary levels of the *Gustin* protein were associated with PROP responsiveness ($F_{(2,63)}$ = 4.408; p = 0.016). A post hoc comparison showed that the salivary levels of the *Gustin* protein were higher in NT volunteers than those in MT and ST volunteers ($p \leq 0.042$, Fisher LSD test). A post hoc comparison also showed that the salivary levels of the *Gustin* protein were higher in volunteers with the GG genotype than in those with the AA or AG genotypes ($p \leq 0.037$, Fisher LSD test), but there was no difference between the AA and AG volunteers ($p > 0.05$).

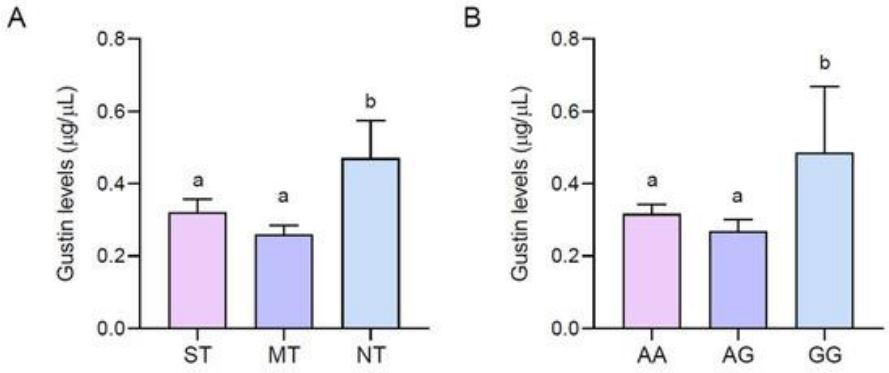

Figure 3. Mean values ± SEM of salivary levels of Gustin protein (μg/μL) for STs, MTs, and NTs (**A**) and for volunteers with genotypes AA, AG, and GG (**B**) of Gustin polymorphism *rs2274333* (A/G) *n* = 66. Different letters indicate a significant difference ($p \leq 0.037$; Fisher LSD test after one-way ANOVA).

Figure 4 shows the scatterplots depicting the relationships between the salivary levels of the Gustin protein (µg/µL) and ΔCt values in the whole sample (A), in the three *Gustin* genotype groups (B), and the PROP taster groups (C). A linear correlation analysis showed that the salivary levels of the *Gustin* protein (µg/µL) were linearly correlated with the ΔCt values in the whole sample (r = 0.304; p = 0.015), in volunteers with the AA genotype (r = 0.380; p = 0.018), and PROP ST (r = 0.490; p = 0.011). No correlation was found between the salivary levels of the *Gustin* protein and the ΔCt values in the AG and GG groups or MT and NT volunteers (p > 0.05).

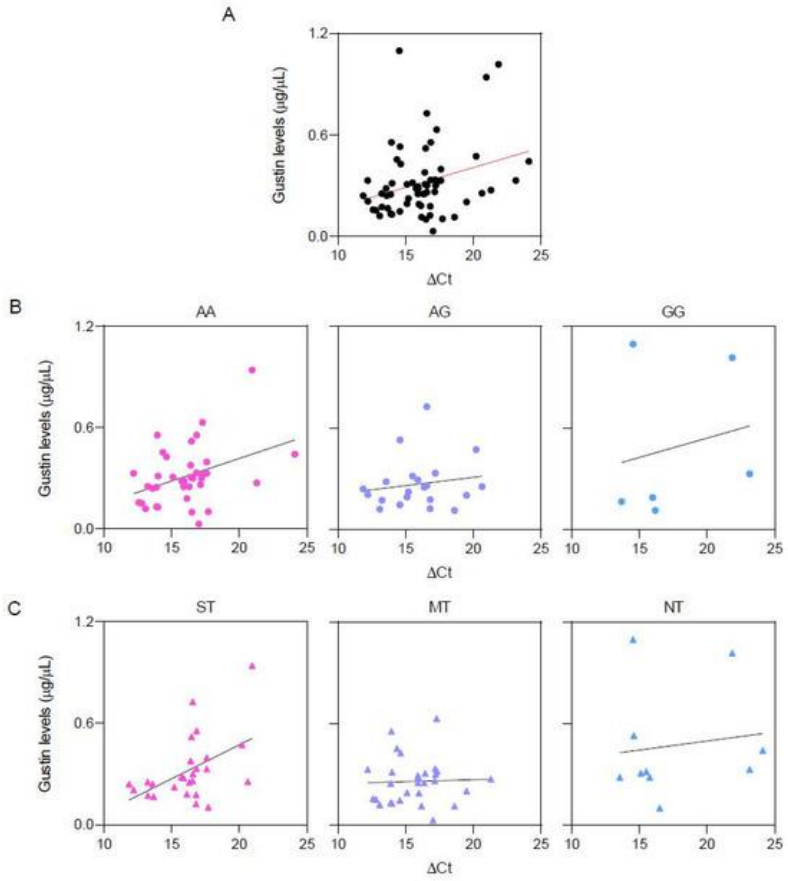

Figure 4. Pearson linear correlation analysis between the salivary levels of Gustin protein (µg/µL) and ΔCt values. (**A**) Relationship in the whole sample (r = 0.304; p = 0.015). (**B**) Relationships in the three Gustin genotype groups (genotype AA: r = 0.380; p = 0.018; genotype AG: r = 0.152; p > 0.05; genotype GG: r = 0.201; p > 0.05). (**C**) Relationships in the three PROP taster groups (ST: r = 0.490; p = 0.011; MT: r = 0.056; p > 0.05; NT: r = 0.127; p > 0.05). n = 66.

3. Discussion

The primary aim of the present work was to verify whether variations in *Gustin* gene expression, which could be influenced by different methylation patterns, could represent a confounding factor for the effect of the polymorphism *rs2274333* (A/G) gene (Ser90Gly in the protein sequence) on the fungiform papillae density and taste function, which may explain discrepant findings across the population.

First of all, it has been fundamental to select the two CpG sites (*cg06962067* and *cg00198750*), located in the region upstream of the coding sequence (CDS) of the Gustin gene, whose methylation status could potentially affect gene expression. We found a direct correlation between the ΔCt values and the salivary levels of the Gustin protein in the whole sample, indicating higher methylation associated with a lower amount of protein. Therefore, this result strongly indicates a potential involvement of these two CpG sites in regulating gene expression. This is not surprising since it is generally known that methylation in the region upstream of the CSD significantly influences gene expression [417] and is more strictly linked to the silencing of gene expression than methylation in the promoter region [418, 419].

In our previous works, we studied the effect of the *rs2274333* (A/G) polymorphism in the Gustin gene (Ser90Gly in the protein sequence) on PROP responsiveness and its role as a trophic factor for cell development and the maintenance of fungiform papillae in a genetically homogeneous cohort. First,

Padiglia et al. 2010 [127] revealed that the GG genotype was associated with structural alterations and the decreased functionality of the protein, and PROP NTs were more likely to possess this genotype. Afterward, Calò et al. 2011 [185] showed that having two A alleles increased the PROP bitterness intensity regardless of the genotype groups of the specific receptor *TAS2R38*. Finally, Melis et al. 2013 [203], in vivo and in vitro experiments, showed that the polymorphism of the Gustin gene influences PROP responsiveness by acting on the fungiform papillae density and maintenance, and the treatment of isolated cells with the active isoform of the *Gustin* protein increased cell division and metabolic activity. Otherwise, other authors failed to find associations between Gustin polymorphism and PROP responsiveness or papillae density in ethnically mixed populations in Brazil [180] and in the U.S. [225]. Specifically, Feeney and Hayes 2014 [225] found no difference in PROP bitter taste perception and fungiform papillae density for the Gustin genotypes. Also, they failed to find any evidence that Gustin's effects on taste perception can be due to differences in the fungiform papillae density. Genick et al. 2011 [180], in a genome-wide study, showed no associations between Gustin and PROP phenotypes.

The results of the present work confirm our earlier observations by showing that volunteers carrying the AA genotype, who should express the functional form of the Gustin protein, had a greater density of fungiform taste papillae, whereas those carrying the GG genotype, who should express a less functional isoform, showed a lower density. We also found variations in protein levels in the three genotype groups, which can limit the effect of the genotype on papillae density. Gustin protein levels were higher in volunteers carrying the GG genotype (who have the less functional isoform of protein and show a lower density) compared with volunteers carrying the AA or AG genotypes (who have the functional isoform of protein and show a higher density). Interestingly, Gustin protein salivary levels were higher in volunteers who showed low PROP responsiveness (NT) than in volunteers who showed higher PROP responsiveness (MT and ST).

In addition, our results showed an inverse relationship between Gustin gene methylation and the salivary levels of the *Gustin* protein, indicating higher methylation (and thus usually the lower expression of the gene) associated with a lower amount of protein. We found high ΔCt values associated with the high salivary levels of the Gustin protein and low ΔCt values associated with low protein levels (a higher ΔCt means a lower methylation level and vice versa). It is worth noting that this was particularly evident in AA volunteers who are carriers of the functional isoform of the Gustin protein. This suggests that the levels of the DNAm, and thus of the salivary protein, are important in contributing to the effect of *Gustin* as a trophic factor in those volunteers who are carriers of the functional form of the protein. On the other hand, the levels of DNAm seem to be insignificant in volunteers carrying the non-functional form (AG and GG volunteers). Therefore, even when the levels of methylation are low, determining a high amount of the protein (GG volunteers), its effect as a trophic factor is not observable because it is in its nonfunctional form. These findings should be confirmed in a larger population and in ethnically mixed populations to verify this hypothesis. The effect of DNAm was particularly evident also in ST volunteers who showed the highest PROP responsiveness. Since PROP tasting is considered a paradigm of general taste function and an oral marker for food preferences [90], this result suggests that the methylation of the *Gustin* gene, and thus its expression, is important for the volunteers who have a more developed gustatory function.

Chapter 7
TAS2R38 gene methylation is associated with syndrome Coronavirus 2 (SARS-CoV-2) infection and clinical symptoms

1. Materials and Methods

1.1. Participants

Eighty-four Caucasian subjects were recruited in Sardinia Island, Italy. They consisted of two groups closely similar in age and sex. The first group included fifty-one participants of which 44 were infected by SARS-CoV-2, as proven by a positive real-time reverse transcriptase-PCR assay (RT-PCR) of a nasopharyngeal swab specimen for SARS-CoV-2 RNA. They displayed severe COVID-19 (*n* = 16) and mild-to-moderate COVID-19 (*n* = 24) or were asymptomatic (*n* = 4). This group also included 7 participants who were post-COVID at the time of sample collection. They were referred to the study from the Santissima Trinità Hospital (Cagliari, Italy) and the University Hospital "Policlinico Duilio Casula" (Monserrato, Italy).The second group included 33 post-COVID-19 participants, as proven by an initial positive real-time reverse transcriptase-PCR assay (RT-PCR) of a nasopharyngeal swab specimen for SARS-CoV-2 RNA, followed by a negative one. They were asked to answer a questionnaire with more detailed questions on their symptoms during the disease, to include them in the following three groups: severe COVID-19 (*n* = 6), mild-to-moderate COVID-19 (*n* = 13), and asymptomatic participants (*n* = 14). They were referred to the study from the Department of Medicine, Surgery, and Pharmacy of the University of Sassari, Italy. All participants were categorized based on disease symptoms according to the already validated classification [420].

All participants were informed about the study's objectives and methodology and gave their written informed consent. The present work was conducted following the most recent edition of the Helsinki Declaration. For the first group, the protocol was approved by the Ethics Committee of "ATS Sardegna" (224/2020/CE) for the second group, by the University Hospital Company's (AOU) Ethical Committee in Cagliari, Italy (PG/2021/5471).

1.2. Genotyping for TAS2R38 polymorphisms

For the first group, nasopharyngeal swabs, containing sinonasal epithelial cells that express *TAS2R38* [326, 421], were collected from participants and immediately stored in a tube with TRIzol reagent (Thermo Fisher Scientific, Waltham, Massachusetts, USA). The protocol of DNA isolation from nasopharyngeal samples is described in [422]. For the second group, DNA was extracted from saliva samples of participants by using the QIAamp® DNA Mini Kit (QIAGEN S.r.l., Milan, Italy) according to the manufacturer's instructions. Briefly, saliva samples were lysed under denaturing conditions at 56 °C for two hours with proteinase K and a lysis buffer. The lysate was then applied to a silica membrane column, where DNA was selectively bound under denaturing salt conditions. After sequential washes to eliminate impurities and inhibitors, DNA was eluted using 20 µL of elution buffer. The purity and the concentration of purified DNA were estimated by measuring the optical density at 260 nm with a NanoDrop One/One Spectrophotometer (Thermo Fisher Scientific) and by fluorometric reading (Qubit dsDNA BR (Broad-Range) Assay kit). Participants were genotyped for the three single-nucleotide polymorphisms (SNPs) *rs713598*, *rs1726866*, *and rs10246939* of the *TAS2R38* locus, which cause three amino acid substitutions (Pro49Ala, Ala262Val, and Val296Ile). These three loci result in two major haplotypes, PAV and AVI, and three uncommon haplotypes (AAI, AAV, and PVI). Molecular analyses were carried out by using a TaqMan® SNP Genotyping Assay (C_8876467_10 assay for the *rs713598*; C_9506827_10 assay for the *rs1726866* , and C_9506826_10 assay for the *rs10246939*) according to the manufacturer's specifications (Applied Biosystems by Life Technologies Milano Italia, Europe BV). The reactions were run on 96-well plates with fast thermal cycling conditions, and the reagent concentrations were 1X TaqMan® genotyping master mix (code: 4371355), 1X TaqMan® genotyping assays, 10 ng of DNA, and nuclease-free water. The plates were read on a StepOne™ Real-Time PCR System, and the results were analyzed by allelic discrimination of the sequence detector software (Genotyping—Applied Biosystems, version v2.3; by Life-Technologies Italia, Europe BV, Monza, Italy). Replicates and positive and negative controls were included in all reactions.

1.3. TAS2R38 gene methylation profiling

Notably, *TAS2R38* is a mono-exonic gene, lacking CpG islands in the promoter region and along the gene body. However, probes interrogating the methylation status of specific CpG sites associated with this gene are included in the commercially available methylation arrays, such as Illumina EPIC arrays. Accordingly, to choose the site where to analyze the *TAS2R38* gene methylation profiling, we checked the methylation levels of the CpG loci interrogated by the EPIC arrays in a subgroup of COVID-19 patients previously characterized in a whole-genome methylation study by our research group [422]. One of the CpG locus (cg25481253, chr7:141973584–141973585, hg38), located in the coding region for the TAS2R38 receptor, showed a differential methylation level between asymptomatic and symptomatic patients, even more pronounced in those with the most severe symptoms (pneumonia, intubated with high flow oxygen) (Table SI).

The DNA extracted as described above was bisulfite converted using EZ DNA Methylation Gold Kit ™ (Zymo Research, Irvine, CA, USA) according to the manufacturer's instructions to bisulfite convert 1000 ng of each DNA sample. Briefly, DNA was incubated with the CT conversion reagent for 10 min at 98 °C followed by a 2.5 h incubation at 64 °C and a final storage step at 4 °C. After the bisulfite clean-up process each sample was collected in a single 1.5 mL Eppendorf tube by flushing the spin column using 10 µL of elution buffer, yielding a final concentration of 100 ng/µL for each sample. Bisulfite-converted DNA was diluted to a final concentration of 10ng/µL, aliquoted, and stored at -20 °C until further processing. The converted DNA was used to determine the *TAS2R38* gene methylation profiling status at the cg25481253 CpG locus.

To detect *TAS2R38* gene methylation, we designed a MethyLight assay that uses primers that hybridize to regions not influenced by methylation (not containing CpG loci) and a probe that hybridizes in the stretch of sequence containing the methylated form CpG site cg25481253. Specifically, a nested PCR approach was employed. The first standard PCR was performed in a conventional thermal cycler, and the second one with internal primers was a quantitative MethyLight assay carried out using the primers and probe reported in Table 1. The first-PCR mix solution was prepared to a final volume of 30 µL, containing 30 ng bisulfite-converted DNA, 1X PCR buffer, 50 mM $MgCl_2$, 10 mM of total dNTPs, 10 pmol of each primer, and 1 U Platinum™ *Taq* DNA Polymerase, high fidelity (Invitrogen™ Life Technologies, Carlsbad, CA, USA). The amplification reaction was performed with a touchdown method on Rotor-Gene Q (Qiagen, Venlo, Netherlands), with a denaturation step at 94 °C for 2 min and then the denaturation/annealing/extension cycles with annealing temperature decreasing 0.5 °C every cycle from 62 °C to 55 °C, for 12 cycles and then 20 cycles of 94 °C for 30 s, 55 °C for 30 s and 72 °C for 1 min. The initial PCR products were diluted 1000 times with ddH_2O, and 5 µL of this dilution was used as the DNA template for the qPCR.

Table 1. *TAS2R38* methylation assay.

Type	Seq (5'→3')	Tm (°C)
External_Primer Forward	TTTAATTTTTGGAAGTGGGTAAGTT	58
External_Primer Reverse	AATTTCCTACCAAAACTTTTTATAC	56
Internal_Primer Forward	ATTGTTGTTTAGTGTTTGTTTTTTT	54
Internal_Primer Reverse	ATTCATTTCAATCCTAAAATTTACA	54
Probe	6-FAM TATTAAGAAAACGAAGGTA	63.0

We carried out two qPCR reactions for each sample: one for the target assay and one for the bisulfite-dependent methylation-independent control (ALU-C4) used to normalize the quantity of the input DNA sample [416]. Each reaction was carried out in triplicate and included: 5 µL nested PCR product or 30 ng bisulfite-converted DNA, 1X TaqMan® Genotyping Master mix (Applied Biosystems, Foster City, CA, USA), 900 nM of each primer, and 250 nM of the probe in a final volume of 30 µL. The following temperature settings were used during the experiment on a Rotor-Gene Q (Qiagen, Venlo, Netherlands): 10 min at 95 °C, then 45 cycles of 95 °C for 15 s and 60 °C for 1 min. The methylation levels were expressed as Δ cycle threshold (Ct), which was determined as the difference between Ct of the target assay and Ct of the ALU-C4 control (a lower methylation level is indicated by a higher ΔCt and vice versa).

1.4. Statistical Analyses

The genotype distribution and haplotype frequencies of the *TAS2R38* SNPs were tested in the two groups and according to the severity of the disease by the Fisher method (Genepop software version 4.2; online software: http://genepop.curtin.edu.au/genepop_op3.html; Montpellier, France). Normality testing was done using the Kolmogorov-Smirnov test. Since the data didn't respect the normality test, the Kruskal-Wallis test was used to compare ΔCt values according to *TAS2R38* genotypes and according to the severity of the disease. Post-hoc comparisons were conducted with Dunn's multiple comparisons test. Statistical analyses were conducted using STATISTICA for WINDOWS (version 7; StatSoft Inc., Tulsa, OK, USA) and with GraphPad Prism 8 software (GraphPad Software, San Diego, CA, USA). * indicates $P < 0.05$, ** $P < 0.01$ and *** $P < 0.001$ according to the asterisk rating system.

2. Results

2.1. TAS2R38 polymorphism and condition concerning COVID-19

Table 2 shows the distribution of participants according to their *TAS2R38* genotype and condition concerning COVID-19. Nine participants in the first group and one in the second had rare haplotypes and were eliminated from subsequent analyses. The two groups did not differ statistically based on their genotype distribution ($\chi^2 = 0.359$; $P = 0.835$; Fisher's test) and haplotype frequencies ($\chi^2 = 0.025$; $P = 0.874$; Fisher's test), also considering the condition of participants concerning COVID-19 ($\chi2 < 3.76$; $P > 0.12$; Fisher's test). No differences related to the severity of the disease were found based on their genotype distribution (first group sample: $\chi2 = 0.910$; $P = 0.634$; second group: $\chi2 = 1.772$; $P = 0.412$; Fisher's test) and haplotype frequencies (first group: $\chi2 = 0.879$; $P = 0.644$; second group: $\chi2 = 1.946$; $P = 0.378$; Fisher's test).

Table 2. Number of participants of group 1 (at the time of infection) and group 2 (after the infection) according to *TAS2R38* genotype and condition concerning COVID-19.

TAS2R38 genotype	Condition of participants concerning COVID-19				
	Total *n* (%)	Severe *n* (%)	Mild-to-moderate *n* (%)	Asymptomatic *n* (%)	Post-COVID *n* (%)
Group 1					
PAV/PAV	8 (19.05)	0 -	6 (28.57)	1 (25.0)	1 (20.0)
PAV/AVI	22 (52.38)	9 (75.0)	9 (42.86)	2 (50.0)	2 (40.0)
AVI/AVI	12 (28.57)	3 (25.0)	6 (28.57)	1 (25.0)	2 (40.0)
Total	42	12	21	4	5
Group 2					
PAV/PAV	7 (21.87)	2 (33.33)	1 (8.33)	4 (28.57)	
PAV/AVI	14 (43.75)	3 (50.0)	5 (41.67)	6 (42.86)	
AVI/AVI	11 (34.38)	1 (16.67)	6 (50.0)	4 (28.57)	
Total	32	6	12	14	

2.2. Effect of SARS-CoV-2 on patterns of TAS2R38 DNAm during the infection

The analysis of the selected CpG locus of COVID-19 positive patients of the first group ($n = 44$), classified into severe ($n = 16$) and asymptomatic/mild-to-moderate ($n = 28$), and 7 post-COVID-19 patients is shown in Figure 1. The Kruskal-Wallis test showed that the ΔCt mean values were associated with the condition of participants concerning the disease ($H_{[2,51]} = 14.42$, $P = 0.0007$, Kruskal-Wallis test). We detected a statistically significant higher methylation level (ΔCt lower) in the severe group compared to other subgroups ($P = 0.0031$ vs. asymptomatic/mild-to-moderate and $P = 0.0047$ vs. post-COVID-19, Dunn's multiple comparison test). Of note, there is a tendency for a reduction in the mean methylation value in post-COVID-19 patients compared to the asymptomatic/mild-to-moderate subgroup ($P = 0.99$, Dunn's multiple comparison test).

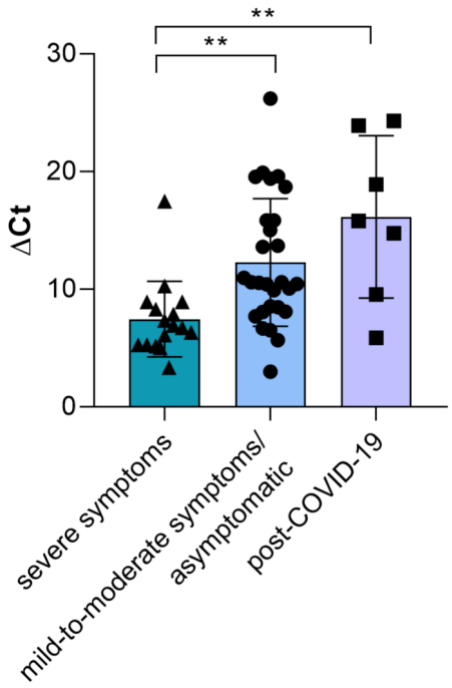

Figure1. *TAS2R38* DNAm in COVID-19 positive patients with different severity of the disease and post-COVID-19 participants. *n* = 51. Distribution of the ΔCt values and mean values ± SEM for the COVID-19 patients with severe COVID-19 (*n* = 16), mild-to-moderate COVID-19/asymptomatic (*n* = 28), and post-COVID-19 (*n* = 7) are reported. ** indicates a statistically significant difference (*P* ≤ 0.0031, Dunn's multiple comparisons test after the Kruskal-Wallis test).

2.3. Effect of SARS-CoV-2 on patterns of TAS2R38 DNAm after the infection

The distribution of the ΔCt values and mean values ± SEM, determined in the post-COVID-19 participants of the second group, who had contracted COVID-19 with severe symptoms, mild-to-moderate symptoms, and asymptomatic participants, is shown in Figure 2. As expected, according to the previous results, we did not observe any statistically significant difference ($H_{[2,33]} = 1.423$, $P = 0.4909$, Kruskal-Wallis test) among the samples divided according to the symptoms experienced during the time of infection. However, each sample group (severe symptoms, mild-to-moderate symptoms, and asymptomatic) is distributed in two subgroups with different ΔCt values.

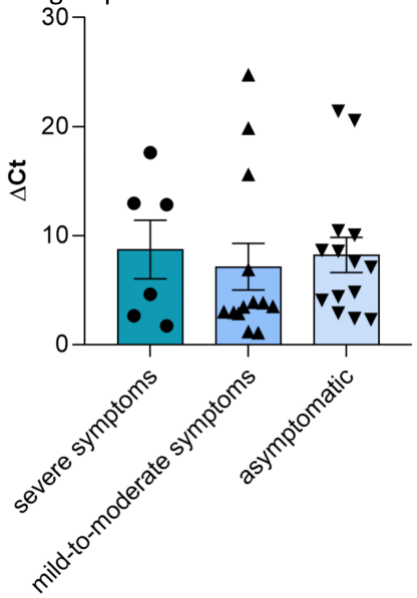

Figure2. *TAS2R38* DNAm in post-COVID-19 participants, who had previously contracted COVID-19 with different severity of the disease and then recovered. Distribution of the ΔCt values, and mean values ± SEM, for the participants who had had severe COVID-19 (*n* = 6), mild-to-moderate COVID-19 (*n* = 13), and had been asymptomatic (*n* = 14) are reported. *n* = 33.

2.4. TAS2R38 methylation analysis according to the TAS2R38 polymorphisms

Figure 3 shows the relationship between *TAS2R38* DNAm and *TAS2R38* SNP genotype of participants of the first group, during infection, and those of the second group, after the cessation of the exposure to the virus. The methylation analysis showed that there was no statistically significant difference in the first group of samples divided according to the SNP genotype i.e., those taking a snapshot of the methylation status at the time of the infection ($H_{[2,42]} = 3.578$, $P = 0.1671$, Kruskal-Wallis test) (Figure 4A). On the other hand, *TAS2R38* DNAm in post-COVID-19 participants of the second group, i.e., at the time when there was not no active disease, the ΔCt mean values were associated with the *TAS2R38* genotype of participants ($H_{[2,32]} = 8.514$, $P = 0.0142$, Kruskal-Wallis test) (Figure 4B). The ΔCt values were significantly higher for those who had the PAV/PAV genotype than in heterozygous ($P = 0.034$, Dunn's multiple comparison test), and AVI homozygous ($P = 0.019$, Dunn's multiple comparison test).

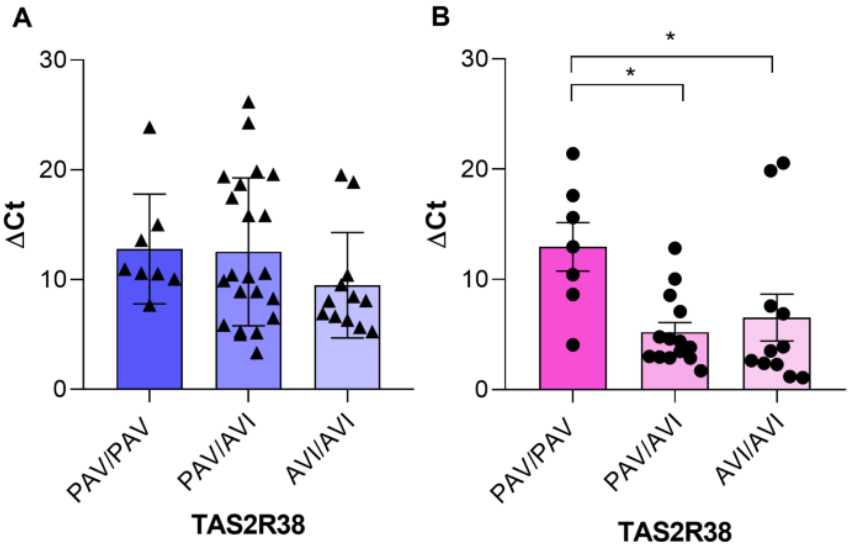

Figure3. TAS2R38 DNAm related to TAS2R38 genotype. (**A**) Distribution of the ΔCt values, and mean values ± SEM, for the PAV/PAV ($n = 8$), PAV/AVI ($n = 22$), and AVI/AVI ($n = 12$) participants of the first group at the time of the infection ($n = 42$); (**B**) Distribution of the ΔCt values, and mean values ± SEM, for the PAV/PAV ($n = 7$), PAV/AVI ($n = 14$), and AVI/AVI ($n = 11$) recovered participants of the second group ($n = 32$). * Indicate a significant difference ($P \leq 0.034$, Dunn's multiple comparison test after the Kruskal-Wallis test).

3. Discussion

TAS2R38 is the taste receptor most implicated in the innate immune response of the respiratory system [266, 326]. The polymorphisms in the *TAS2R38* gene, which affect taste sensitivity, also alter the immune responses to upper respiratory infections [326]. Homozygous patients for the PAV variant are less susceptible to respiratory infections than homozygous patients for the AVI variant, who have altered TAS2R38-dependent responses, and heterozygous patients. By detecting the bacterial quorum-sensing molecules, the TAS2R38 receptor activates an efficient immune response mediated by NO, which is shown to inhibit the replication of SARS-CoV [423]. Nevertheless, few studies have been conducted on the associations between TAS2R38 and COVID-19 severity and prognosis, and with inconsistent outcomes [328, 332, 424, 425].

Given that the efficient performance of a receptor depends on its expression, which is strongly associated with DNAm [317, 318], the main goal of the current study was to determine whether variations in *TAS2R38* DNAm patterns may shed light on the role of the TAS2R38 bitter taste receptor in COVID-19 infection and the severity of symptoms.

Our results show, for the first time, to our knowledge, that the cg25481253 methylation level, a CpG site located in the coding region of *TAS2R38*, is positively associated with COVID-19 severity during infection. Interestingly, the methylation pattern returns to a normal state after the infection, as evident from the data obtained from the post-COVID-19 participants in both groups, regardless of the biological matrix used. This is in line with the reversibility of DNA methylation after the cessation of exposure to an environmental trigger [426, 427] and could explain the restoration of taste shown in the post-COVID-19 condition, after a

period of ageusia during the infection [428]. Unfortunately, it was impossible to verify this hypothesis in our study. We were unable to collect taste function data in a sufficient number of patients. It would have been interesting to include an outward measure of receptor function to verify whether methylation changes affect the phenotypic expression of the receptor. Therefore, our results, suggesting a role of methylation changes at cg25481253 in regulating TAS2R38 expression, indicate a potential silencing effect of SARS-CoV-2 on TAS2R38 receptor expression that depends on disease severity. The levels of the *TAS2R38* DNAm were significantly higher in positive participants with severe symptoms compared to participants with mild-to-moderate symptoms or those who were asymptomatic and to those who recovered from the disease. From these results, it can be speculated that SARS-CoV-2 like other Coronaviruses [422, 429] can elude the host's innate immune responses by altering the DNA methylation pattern of genes involved in recognition and response against the pathogen. Interestingly, our results also showed that the methylation pattern returns to a normal state after recovery from the infection, regardless of the severity of the disease, suggesting that the silencing effect, depending on severity, disappears and the expression of the receptor returns to normal, restoring the patient's immune capacity.

Finally, we found that the levels of the *TAS2R38* DNAm were associated with the *TAS2R38* genotype of participants who were previously infected by SARS-CoV-2 and then recovered. Specifically, participants who had the PAV/PAV genotype showed lower DNAm levels, and therefore a potentially higher expression of the TAS2R38 receptor, compared to heterozygous and AVI homozygous. This result could be interpreted as linkage disequilibrium between the methylation profile and the SNP genotype, observable only when the methylation pattern is not altered by external factors such as viral infections. Unfortunately, we could not compare the ΔCt values of the post-COVID participants in relation to the *TAS2R38* genotype across the two groups because they resulted from a different biological matrix and only five were the post-COVID participants in the first group. It also seems to suggest that the receptor in the PAV form, is a genetic protective condition, not only because it has a higher affinity for the agonist, but also because it may be expressed more. Accordingly, one might speculate that, in case of infection, the PAV variant could activate a prompt and massive immune response, which is mediated by NO, could inhibit the replication of SARS-CoV. This could explain why very few PAV/PAV participants showed serious symptoms, none in the first group and only two in the second. On the other hand, the TAS2R38 in the AVI form would be at a genetic disadvantage, not only because it shows little or no affinity for the agonist, but also because it would be less expressed, further inhibiting its ability to activate the immune response.

Chapter 8

A Multi-Dimensional Study on Taste Deficits, α-Synuclein Genetics Profiling, and Supervised Learning for Diagnosis and Disease severity Stratification in Parkinson's Disease (PD)

1. Materials and Methods

1.1. Subjects

Ninety-nine PD patients and sixty HCs, closely matched for age (range: 50-90 years), sex, and ethnicity, were recruited in the area of Cagliari, Italy. PD patients were enrolled at the Parkinson Center of the Department of Neurology, Brotzu Hospital, Cagliari, Italy, while HCs at the University of Cagliari, Italy. The exclusion criteria consisted of major diseases (e.g., kidney disease and diabetes), food allergies, chronic rhinosinusitis, and medications that interfere with sensory functions. All PD patients were diagnosed according to Postuma criteria [430]. The age of onset, duration of illness (calculated as the difference between age and age of initial diagnosis), Hoehn and Yahr stage (moderate severity of PD, MSPD and high severity of PD, HSPD), Type of PD (Tremor-dominant, Akinetic-rigid, Mixed) and PD duration category (from 0 to 2 years, from 3 to 5 years, more the 5 years) were established. Unfortunately, for 2 PD patients, we could not have the Hoehn and Yahr stage and Type of PD, and for 1, the age of initial diagnosis. HCs were neurologically normal, and none had first-degree relatives with neurodegenerative diseases. After signing an informed consent, participants underwent a baseline medical screening to investigate their health status and anthropometric, demographic, and lifestyle factors, including smoking status and oral hygiene habits. The demographic and clinical features of the PD patients are shown in Table 1. Buccal swabs were collected and stored at −80°. Participants were asked not to drink, eat, or smoke for 1 hour before the taste measurements. Each participant received a verbal explanation of the study's purpose and methodology. The ethics committee of the University Hospital of Cagliari approved (prot. PG/2017/17817, verbal number 06, December 20, 2017) all procedures used in this investigation, which was carried out in compliance with the 1975 Declaration of Helsinki (updated in 1983).

Table 1. Demographic and clinical features of the patient' cohort.

Features	
Males/ Females *(n)*	60/39
Smokers/Non-smokers *(n)*	9/90
Age (y)	69.91 ± 0.95
Age of onset (y)	61.74± 1.15
Duration of illness (y)	8.14± 0.55
Hoehn and Yahr stage	2.64± 0.13
Moderate severity PD (n)	48
High severity PD (n)	49
Type of PD:	
Tremor-dominant (n)	28
Akinetic-rigid (n)	14
Mixed (n)	55
PD duration category	
from 0 to 2 years (n)	13
from 3 to 5 years (n)	27
more the 5 years (n)	58

Data are shown as mean values ± S.E.

1.2. Taste Measurements

The quality identification of stimulations with taste stimuli representative of four basic taste qualities (sweet, sour, salty, bitter) and of the astringency sensation was determined in PD patients and HCs. The measurements were performed by placing a taste strip of filter paper impregnated with taste solutions on the tongues of subjects. The "taste strips" used were the same as the validated "Taste Strip Test" (TST, Burghart Company, Wedel, Germany) [209, 210]. Since PD patients are subjects who have difficulty maintaining focus for long periods, to reduce the duration of taste measurements, only one stimulus for each quality was used in each subject. The choice of stimuli was based on the results of our previous work

in which an SL regression approach allowed us to automatically and accurately identify with high precision the different stimuli, which accurately predict the general taste status of HCs and patients with chemosensory loss [431]. Taste stimuli were presented in a semi-random order, with astringent stimuli presented last due to their persistence. Participants were instructed to rinse their mouths with spring water before each new test. Since gustatory perception is shaped by the context in which someone lives, the measurements did not include umami, for which, unlike the stimuli used, the European population shows a low familiarity [396].
The following concentrations were used: 0.4 g/mL sucrose, 0.3 g/mL citric acid, 0.016 g/mL sodium chloride, 0.006 g/mL quinine hydrochloride, and 0.2 g/mL tannin. All subjects had to identify the taste quality of each stimulus by choosing from a list of five possible answers (sweet, sour, salty, bitter, astringent) in a forced choice procedure [209]. The complete procedure required 10 minutes for each subject.

1.3. Molecular Analysis (SNCA Mutations)

Participants were genotyped for the following single-nucleotide polymorphisms (SNPs) of *α-synuclein* gene (*SNCA*): the *rs356219* (A/G), whose allele G is associated with an increase of α-synuclein [352, 432], the *rs181489* (C/T), whose allele T is associated with a higher risk of developing PD[433], the *rs2583988* (C/T), whose allele T is associated with higher risk of developing PD and cognitive deficits [434, 435], and the *rs356186* (A/G), whose allele A is associated with a lower risk of developing PD [433].
A buccal swab was taken from each participant by using a sterile cytobrush, and DNA was extracted using the salting-out method. The buccal swab samples were suspended in 500 µl lysis buffer (MLS Medisen Lysis Solution: 1M NaCl, 0.1 M Tris-HCl pH 8.0, 40 mM Disodium EDTA, and 0.2% SDS), and 5 µl 50 mg/ml proteinase K was added. The samples were incubated overnight at 56°C until the tissue was dissolved. Following lysis, a saturated Sodium Acetate solution (3 M, pH 8.0) was used to precipitate the proteins. Centrifugation at 8000 rpm for 10' removed the pellet. DNA was then precipitated by adding 100% isopropanol and isolated by centrifugation. After decanting the supernatant, 300 µl 70% ethanol was added, and the pellet was dissolved; the mixture was centrifuged at 10000 rpm for 10 min, and the supernatant was decanted gently. The pellet was air-dried under laminar air flow, and the dried pellet was resuspended in 50 µl nuclease-free water. The concentration and purity of the extracted DNA were assessed by measuring absorbance at 260 nm with a NanoDrop One/One Spectrophotometer (Thermo Fisher Scientific).
Molecular analyses were carried out using the TaqMan® SNP Genotyping Assay, following the manufacturer's guidelines (Applied Biosystems, Life Technologies, Milan, Italy). Reactions were performed in 96-well plates under fast thermal cycling conditions. Ten ng of DNA, nuclease-free water, 1X TaqMan® Genotyping Master Mix (code: 4371355), 1X TaqMan® Genotyping Assays (C_1020193_10, C_3208976_10, C_1658278_10, C_3208925_10) were included in each reaction.
The StepOne™ Real-Time PCR System was used for amplification and detection, and the Sequence Detection Software (Genotyping - Applied Biosystems, version 2.3; Life Technologies Italia, Monza, Italy) was used to determine genotypes through allelic discrimination. Replicates and positive and negative controls were included in every reaction. The low concentration and/or purity of the extracted DNA did not allow us to determine the genotype of some PD patients (2 for *rs356219*, 3 for *rs181489*, 5 for *rs2583988*, and 3 for *rs356186*) and HCs (2 for *rs356219*, 3 for *rs181489*, 3 for *rs2583988*, and 3 for *rs356186*).

1.4. Statistical Analysis

The distribution of PD patients and HCs who perceived no taste (under threshold), recognized the taste (correct identification), or described a different quality (incorrect identification) for each taste stimulus (sucrose, NaCl, citric acid, quinine, and tannic acid) was analyzed using Fisher's exact test.
The genotype distribution and allele frequency of the *rs356219*, *rs181489*, *rs2583988*, and *rs356186* SNPs of *SNCA* of the PD patients and HCs who correctly recognized the taste (PD-yes and HCs-yes) and those of PD patients and HCs who perceived no taste or described a different quality (PD-no and HCs-no) for each taste stimulus were compared using Fisher's exact test (Genepop software version 4.2; http://genepop.curtin.edu.au/genepop_op3.html). *P* values ≤ 0.05 were considered significant.

1.5. Supervised Learning

Two automatic binary classification tasks were carried out by using SL algorithms: the first to clarify the diagnostic significance of taste stimuli distinguishing between PD patients and HCs, and the second to make a prediction of the disease severity of PD patients and classify them into those who had a moderate severity of PD (MSPD; 1, 1.5, 2, 2.5 in the Hoehn and Yahr scale) and those who had high severity of PD (HSPD; 3, 3.5, 4, 5 in the Hoehn and Yahr scale). In both tasks, we used the same algorithms: Random Forest, Logistic Regression, K-Nearest Neighbors (KNN), Decision Tree, Gradient Boosting, and CatBoost Classifier. These models learned the relationships between input features and target classes during training, allowing them to predict the correct class for new data. The features for the first task included: Sucrose under threshold, Sucrose correct identification, Sucrose incorrect identification, NaCl under threshold, NaCl correct identification, NaCl incorrect identification, Citric acid under threshold, Citric acid correct identification, Citric acid incorrect identification, Quinine under threshold, Quinine correct identification, Quinine incorrect identification, Tannic acid under threshold, Tannic acid correct identification, Tannic acid incorrect identification, Total strips identified, Age, Male, Female, Smoker and Non-smoker. For the second task the following features were added: Type of PD (to which were assigned numerical categories: 0 = Tremor-dominant, 1 = Akinetic-rigid, 2 = Mixed), Years with PD (calculated as difference between age and age of initial diagnosis), PD duration category (to which were assigned numerical categories: 1 = from 0 to 2 years, 2 = from 3 to 5 years, 3 = more the 5 years), Age of initial diagnosis, and the three genotype of the *rs356219*, *rs181489*, *rs2583988* and *rs356186* SNPs of *SNCA*.

For both classification tasks, the One-Hot Encoding was applied to convert categorical variables into a numerical format [436], and the model performance was assessed using standard classification metrics, such as accuracy and macro-averaged F1-score [437]. The overall performance of the models was evaluated on both training and testing sets using the mentioned metrics, providing insights into their ability. Since in the first task, the training dataset showed a class imbalance (more PD patients than HCs), the class balancing was addressed using the Synthetic Minority Oversampling Technique (SMOTE) to generate synthetic samples for the minority class [379]. For training models, the datasets were randomly split into training and testing sets using an 80:20 ratio to avoid bias and ensure generalization. In the first task, the dataset consisted of 158 samples (98 patients and 60 HCs) and 19 features, resulting in 126 training samples and 32 testing samples. After SMOTE, the training set was balanced with 78 samples per class. In the second task, the dataset comprised 88 samples described by 34 features, randomly split into 70 samples for training and 18 for testing, with balanced class representation between the MSPD class and HSPD class.

The interpretation of the SL model predictions was performed by using the Shapley Additive exPlanations (SHAP), a game-theoretical method that links feature importance with feature effect [438]. It returns a SHAP summary plot that connects the significance of the features to their impacts.

2. Results

2.1. Determination of the Taste Perception of PD patients and Healthy Controls (HCs)

The distribution of PD patients and HCs who perceived no taste (under threshold),recognized the taste (correct identification), or described a different quality (incorrect identification) for each taste stimulus: sucrose, NaCl, citric acid, quinine, and tannic acid is shown in Figure 1. Fisher's exact test showed no differences between the two populations when subjects had to identify the sweet quality(p> 0.05) (Figure 1a): most subjects (89% of PD patients and 97% of HCs) correctly recognized the stimulus. The two populations showed different sensitivities when tasting the salty stimulus (χ^2 = 30.113, p< 0.0001) (Figure 1b); 11% of PD patients and 50% of HCs correctly identified salty stimulus, 50% of PD patients and 23% of HCs perceived no taste, and 39% of PD patients and 27% of HCs described a different taste quality. The two populations showed different sensitivities also when tasting the sour stimulus (χ^2 = 5.289, p = 0.021) (Figure 12c); 63% of PD patients and 80% of HCs correctly recognized the sour stimulus, no subjects of the two groups perceived any taste, and 37% of PD patients and 20% of HCs perceived a different quality. Fisher's exact test showed no differences between the two populations tasting the bitter taste stimulus (p > 0.005) (Figure 1d). Most of the subjects (68% of PD patients and 75% of HCs) correctly recognized the bitter

stimulus. Finally, the two populations showed different sensitivities when tasting the astringent stimulus (χ^2 = 3.917, p = 0.047) (Figure 1e); 60% of PD patients and 75% of HCs correctly identified the astringent stimulus, no subjects of the two groups reported any taste, and 40% of PD patients and 25% of HCs perceived a different quality.

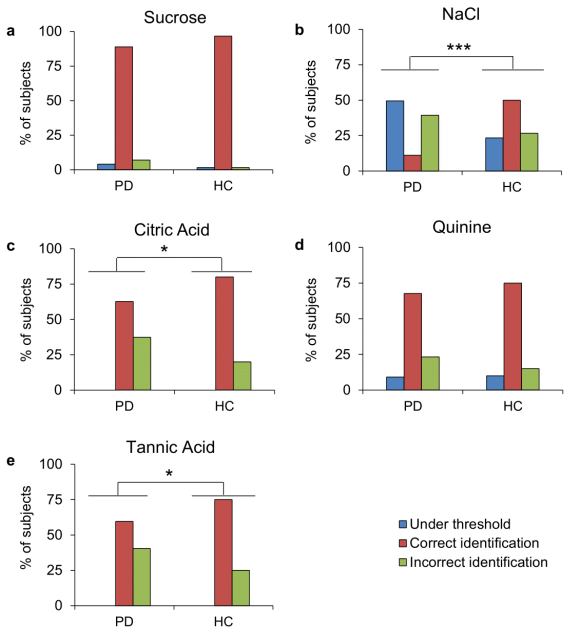

Figure 1. Distribution of PD patients and healthy controls (HCs) who perceived no taste (under threshold), recognized the taste (correct identification), or described a different quality (incorrect identification) for each taste stimulus: sucrose, NaCl, citric acid, quinine, and tannic acid. * Indicates significant difference between PD patients and HCs (χ 2 >3.917, p < 0.047; Fisher's exact test). PD patients (n = 99), HCs (n = 60).

2.2. Taste Stimuli Diagnostic Significance, by Supervised Learning

In the first automatic binary classification task carried out to clarify the diagnostic significance of taste stimuli distinguishing between PD patients and HCs, the metrics that evaluated the training and testing performance of the SL algorithms showed that the CatBoost algorithm achieved the best results (Table S1). Specifically, the CatBoost algorithm showed 91% training accuracy, 91% training macro-averaged F1-score, 84% testing accuracy, and 82% testing macro-averaged F1-score.

Table S1. Results of metrics for each classifier model in the first task.

Model	Training Accuracy	Training macro-averaged F1-score	Testing Accuracy	Testing macro-averaged F1-score
Random Forest	0.724	0.722	0.750	0.733
Logistic Regression	0.622	0.622	0.750	0.746
KNN	0.981	0.981	0.594	0.559
Decision Tree	0.763	0.758	0.781	0.752
Gradient Boosting	0.981	0.981	0.813	0.792
CatBoost	0.910	0.910	0.844	0.823

The SHAP algorithm allowed us to obtain an overview of the most important features and how they impact it to distinguish between PD patients and HCs (Figure 2). In the SHAP summary plot, the order of importance of the features is shown on the left-hand side of each Y-axis, going from the most significant at the top to the least significant at the bottom. Each point on the SHAP summary plot is a SHAP value that allows to understand the contribution of an input feature to that single prediction. In addition, SHAP values also indicate whether a feature has a favorable (red color) or unfavorable (blue color) influence on predictions. Specifically, the SHAP summary plot for the PD class highlights that the NaCl under threshold

and age were the first and second important features, with high values (red color) strongly associated with PD prediction (Figure 2a). Importantly, the Tannic acid incorrect identification resulted in the third position of importance, and high values (red color) pushed the model toward PD predictions. The male sex was the fourth important feature positively correlated with PD prediction. NaCl incorrect identification was the fifth important feature and strongly and positively correlated with PD prediction. The Total strips identified was the sixth feature, and low values (blue color) pushed the model towards PD predictions. The NaCl correct identification was the seventh important feature and correlated negatively with PD class. Eighth and ninth features were Citric acid incorrect identification and Quinine incorrect identification, both showing high values that pushed the model toward PD predictions. Notably, the smoking-related features showed an important impact on PD prediction: smoker and non-smoker status were positively and negatively correlated to PD class, respectively. Tannic acid correct identification, female sex, and Quinine correct identification had a moderate impact on the model, positively correlating with PD prediction, while Citric acid correct identification correlated negatively. Interestingly, Quinine under the threshold strongly and positively correlated with this class. The sucrose-related features (Correct identification, incorrect identification, and under threshold) showed a low impact, with different patterns.

The SHAP summary plot for the HC class revealed a different pattern of feature importance (Figure 2b). For this class, the NaCl under threshold was the most important for the model, and low estimated values (blue color) were strongly and positively correlated with the prediction of the HC class. Age was the second important feature, and the low and medium values (blue and violet colors) pushed the model to predict a subject as an HC, even though some outlier values are present. The NaCl correct identification was the third important feature, and high values (red color) were positively correlated with HC class. The male sex was the fourth important feature and was strongly and negatively correlated with HC prediction. The Tannic acid incorrect identification and the NaCl incorrect identification were the fifth and the sixth in order of importance, and low values (blue color) pushed the model prediction towards the HC class. The Total strips identified followed in order of importance, with high values (red color) positively correlated with an HC prediction, while female sex showed a negative correlation with HC class. The remaining features, including Tannic acid correct identification, Citric acid incorrect identification, Quinine correct identification, Quinine incorrect identification, Citric acid correct identification, Smoker, Quinine under threshold, Non-smoker, and the three features describing the sucrose sensitivity, showed progressively smaller impacts on the predictions of the model toward HC class. However, two SHAPE value outliers were present for Quinine under threshold and Sucrose correct identification.

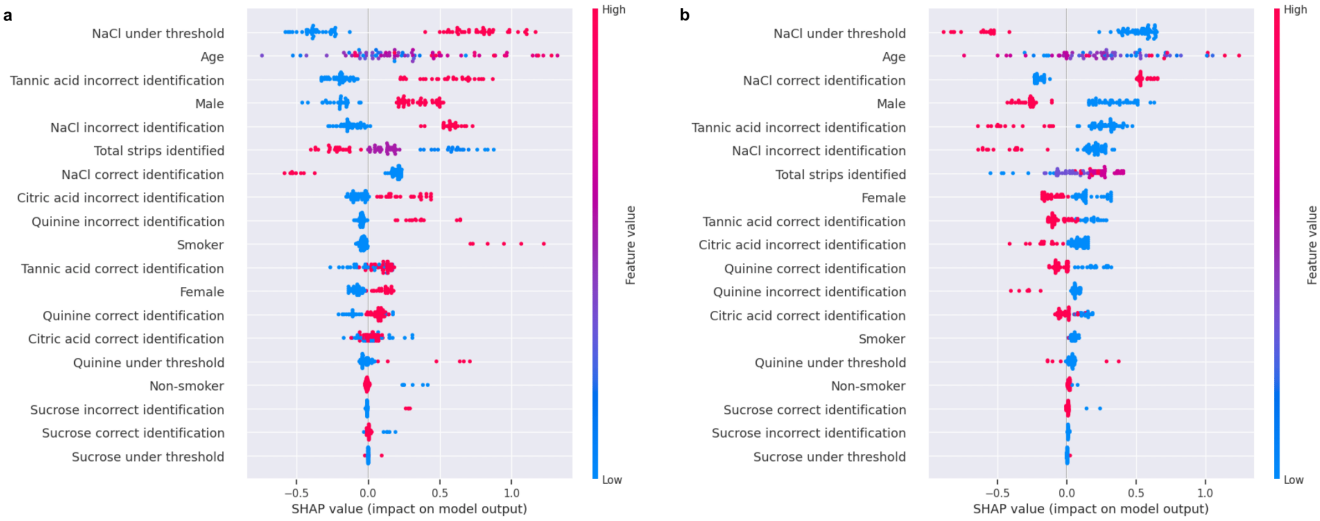

Figure 2. SHAP summary plots showing feature importance and their impact on the CatBoost classifier to make predictions of PD patients (a) or HCs (b). The descending order of importance of the features (from top to bottom) is shown on the left of each Y-axis; the impact on the model output (SHAP value) is shown on the X-axis. The position of the SHAP value on the X-axis shows whether the feature is associated with a higher or lower prediction score for the class. Each point in the plot is a SHAP value of a feature. The color of the line to the right of each graph represents the feature value: high value (red color), medium value (violet color), and low value (blue color).

2.3. Relationships between the PD patients and HCs' taste perception and SNCA mutations

Genotype distribution and allele frequencies of *SNCA* polymorphisms in PD patients and HCs are shown in Table S2. A significant difference was found between PD patients and HCs based on the genotype distribution and allele frequency of the *rs356186* SNP (χ^2> 7.389; p< 0.015). On the other hand, no differences were found between PD patients and HCs according to the genotype distribution and allele frequency of *rs356219, rs181489*, and *rs2583988*SNPs of *SNCA*(χ^2>1.557; p < 0.459, Fisher's method).

Table S2. Genotype distribution and allele frequencies of polymorphisms of SNCA in the PD patients and healthy controls (HCs).

	PD patients		HCs		*p*-value[a]
	n	%	n	%	
rs356219					
Genotype					
GG	19	19.59	7	12.07	0.279
AG	48	49.48	30	51.72	
AA	30	30.93	21	36.21	
Allele					
G	86	44.33	44	37.93	0.301
A	108	55.67	72	62.07	
rs181489					
Genotype					
TT	14	14.58	6	10.53	0.457
CT	45	46.88	26	45.61	
CC	37	38.54	25	43.86	
Allele					
T	73	38.02	38	33.33	0.468
C	119	61.98	76	66.67	
rs2583988					
Genotype					
TT	13	13.83	5	8.77	0.455
CT	40	42.55	25	43.86	
CC	41	43.62	27	47.37	
Allele					
T	66	35.11	35	30.70	0.459
C	122	64.89	79	69.30	
rs356186					
Genotype					
AA	3	3.13	5	8.77	0.025
AG	27	28.13	23	40.35	
GG	66	68.75	29	50.88	
Allele					
A	33	17.19	33	28.95	0.023
G	159	82.81	81	71.05	

[a] *p*-value derived from Fisher's method

Figure 3 shows the percentage of PD patients and HCs who correctly recognized the taste (PD-yes and HC-yes) and those of PD patients and HCs who perceived no taste or described a different quality (PD-no and HC-no) for each taste stimulus (sucrose, NaCl, citric acid, quinine, and tannic acid) according to the *rs356219*, *rs181489*, *rs2583988,*and *rs356186*SNPs of *SNCA*. When subjects tasted tannic acid, the molecular analysis at the *rs356219*, *rs181489*, *rs2583988*and *rs356186* SNPs of *SNCA* showed that the four groups differed statistically based on the genotype distributions (*rs356219*:χ^2= 10.794,*p* = 0.0045; *rs181489*:χ^2= 10.428,*p* = 0.0054;*rs2583988*: χ^2= 8.386,*p* = 0.015;*rs356186:*χ^2=7.280, *p*=0.026, Fisher's method) and allelic frequencies (*rs356219*: χ^2=10.331, *p* =0.0057; *rs181489*: χ^2=10.0627,*p*=0.0065; *rs2583988*: χ^2=8.855, *p*=0.0119; *rs356186*χ^2=7.681, *p*=0.021, Fisher's method) (Figure 3e). Pairwise comparisons discriminated PD-no and HC-no in the four SNPs (χ^2>7.080, *p*<0.028 and χ^2>6.017, *p*<0.049, Fisher's method), PD-yes and PD-no in the *rs356219*, *rs181489*, and *rs2583988* SNPs (χ^2>11.068, *p*<0.0039; χ^2>11.182, *p* <0.0037, Fisher's method), HC-yes and PD-no in the *rs356219* and*rs2583988*SNPs (χ^2>6.159, *p*<0.045; χ^2>6.044, *p*<0.048, Fisher's method), and PD-yes and HC-no in the *rs356186* SNP (χ^2=10.023, *p* <0.0066; χ^2=10.290, *p* <0.0058,Fisher's method).

Specifically, in the *rs356219* locus, PD-yes had a high frequency of subjects with a least one allele A (91 %), and a low frequency of genotypes GG (9%), whereas PD-no had a high frequency of subjects with a least one allele G (79%) and a low frequency of genotypes AA (21%). It is interesting to note that HC-yes and HC-no had a high frequency of subjects with at least one allele A (HC-yes: 88% and HC-no: 97%) and a low frequency of genotypes GG (HC-yes: 12% and HC-no: 13%).
In the *rs181489* locus, PD-yes had a high frequency of subjects with at least one allele C (93%), and a low frequency of genotypes TT (7%), whereas PD-no had a high frequency of subjects with a least one allele T (76%) and a low frequency of genotypes CC (23%). It is noteworthy that HC-yes and HC-no had a high frequency of subjects with at least one allele C (HC-yes: 91% and HC-no: 86%) and a low frequency of genotypes TT (HC-yes: 9 % and HC-no: 14%).
In the *rs2583988* locus, PD-yes had a high frequency of subjects with at least one allele T (87%), and a low frequency of genotypes CC (7%), PD-no had a high frequency of subjects with a least one allele T (76%) and a low frequency of genotypes CC (24%). In this locus, HC-yes and HC-no had a high frequency of subjects with at least one allele T (HC-yes: 91% and HC-no: 87%) and a low frequency of genotypes CC (HC-yes: 7% and HC-no: 13%).
In the *rs356186* locus, PD-yes and PD-no had a low frequency of subjects with at least one allele A (33% and 28%), and a high frequency of genotypes GG (67% and 72%), HC-no had a high frequency of subjects with a least one allele A (67%) and a low frequency of genotypes GG (33%) and HC-yes had a similar frequency of subjects with least one allele A and subjects with genotype GG (43 % and 57%).
The genotype distributions and allelic frequencies of the *rs356186* SNP also differed when subjects tasted NaCl ($\chi^2 = 8.193$, $p = 0.0166$; $\chi^2 = 9.659$, $p = 0.008$, Fisher's method). Pairwise comparison discriminated PD-no from PD-yes and HC-yes ($\chi^2>9.559$, $p<0.008$; $\chi^2>10.248$, $p<0.0059$, Fisher's method). PD-yes had a high frequency of heterozygous subjects (70%), a low frequency of genotypes GG (30%), and none had genotype AA, while PD-no had a high frequency of GG subjects (73%) and a low frequency of subjects with at least one allele A (27%). On the other hand, 56% of HC-yes and 43% of HC-no had at least one allele A, and 44% and 57% had genotypes GG.

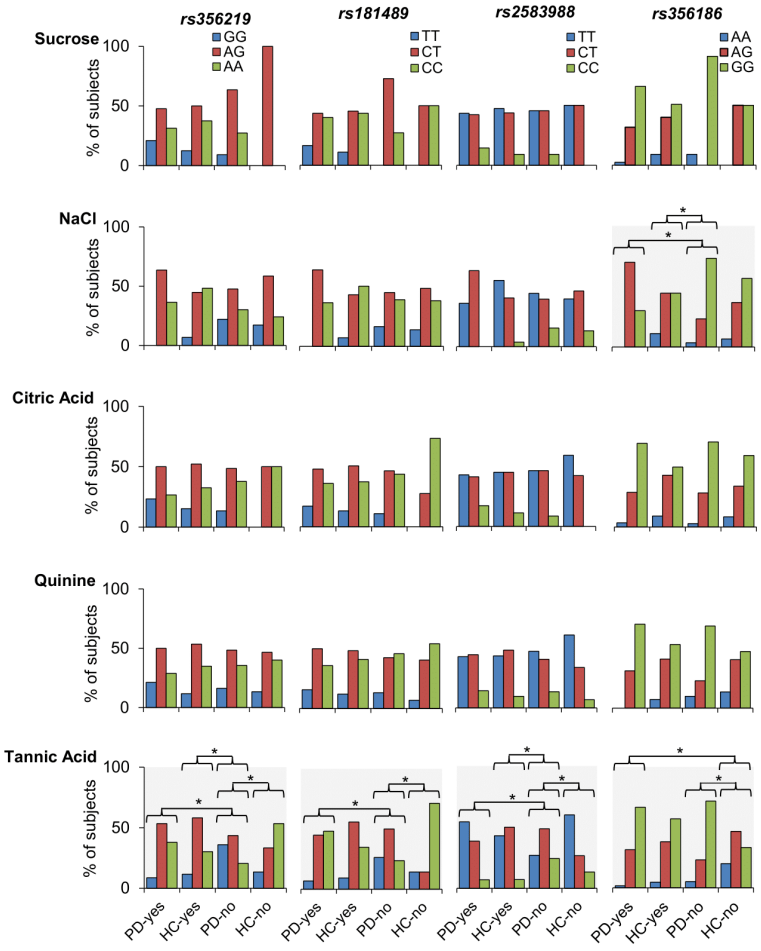

Figure 3. The percentage of PD patients and HCs who correctly recognized the taste (PD-yes and HC-yes) and those of PD patients and HCs who perceived no taste or described a different quality (PD-no and HC-no) for each taste stimulus (sucrose, NaCl, citric acid, quinine, and tannic acid) according to the rs356219, rs181489, rs2583988, and rs356186 SNPs of SNCA. The graphic area highlighted in grey indicates significant difference across the four group (PD-yes, HC-yes, PD-no and HC-no) based on their genotype distributions (rs356219: χ 2 = 10.704, p = 0.0045; rs181489: χ 2 =10.428, p = 0.0054; rs2583988: χ 2 = 8.386, p= 0.015; rs356186 χ 2 =7.280, p = 0.026, Fisher's method) and allelic frequencies (rs356219: χ 2 = 10.333, p = 0.0057; rs181489: χ 2 = 10.0627 p = 0.0065; rs2583988: χ 2 = 8.855, p = 0.012; rs356186: χ 2 = 7.681, p = 0.021, Fisher's method). * Indicates significant difference for population pair.

2.4. Classification of PD patients based on disease severity by Supervised Learning

In the second automatic binary classification task carried out to classify PD patients into those who had a moderate severity of PD (MSPD) and those who had high severity of PD (HSPD), the standard metrics to evaluate the training and testing performance of the SL algorithms showed that the CatBoost algorithm had the best performance, showing very high values of training accuracy (98%), training macro-averaged F1-score (98%), testing accuracy (94%), and testing macro-averaged F1-score (94) (Table S3).

Table S3. Results of metrics to evaluate each classifier model in the second task**.**

Model	Training Accuracy	Training macro-averaged F1-score	Testing Accuracy	Testing macro-averaged F1-score
Random Forest	0.757	0.756	0.833	0.833
Logistic Regression	0.686	0.685	0.722	0.721
KNN	1.000	1.000	0.778	0.778
Decision Tree	0.757	0.746	0.667	0.625
Gradient Boosting	0.743	0.735	0.667	0.625
CatBoost	0.986	0.986	0.944	0.944

The SHAP algorithm also provided comprehensive insights on the importance of features and their impact on the CatBoost model to classify PD patients into those who had moderate severity of PD (MSPD) and those who had high severity of PD (HSPD) (Figure 4). The analysis revealed distinct feature contribution patterns that differentiate the severity classes. The SHAP summary plot for the MSPD class highlights that the type of PD was the most important feature for the model, and low estimated values (blue), which represent the Tremor-dominant type, were strongly and positively correlated with the prediction of MSPD (Figure 4a). The Years with PD and the PD duration category were the second and third features in order of importance, and low and medium estimated values, which represent a shorter duration of PD (blue and violet, respectively) had a high impact on making the MSPD prediction. Age of initial diagnosis was the fourth significant feature, and low and medium estimated values (blue and violet, respectively) positively correlated with the MSPD class. The feature total strips identified was the fifth significant feature; however, in the plot, its impact on the model predictions was unclear. Among the genetic features, *SNCArs2583988*CC was the sixth most important feature, and positively correlated with the MSPD prediction. The Citric acid incorrect identification was the seventh important feature, and high values positively correlated with the target prediction. The *SNCArs356186*AA genotype was the eighth important feature and strongly correlated positively with the target prediction. Interestingly, the female sex had a negative impact to make a prediction of the MSPD prediction, contrary to the male, which had a positive impact on the target and were the ninth and tenth in order of importance, respectively. The *SNCA rs181489*CC was the eleventh feature and positively correlated with MSPD class. The *SNCA rs181489*CT, *SNCA rs2583988*CT, and *SNCA rs356186*GG that followed in importance order negatively correlated with MSPD class. On the contrary, the *SNCA rs2583988*TT positively correlated. The NaCl under threshold, Citric acid correct identification, NaCl incorrect identification, and Quinine correct identification features had a low impact on the model: the first one was favorable, while the other three were unfavorable.

The SHAP summary plot highlights the link between the importance of features and their impact on predicting the HSPD class, is shown in Figure 4b. Specifically, the plot shows that the Years with PD was the most important feature for the model, and high and medium estimated values (red and violet, respectively) were strongly and positively correlated with the prediction of the HSPD class. The type of PD was the second in order of importance, and high and medium estimated values (which represent the Akinetic-rigid and Mixed type) had a high impact on making an HSPD prediction. The PD duration category was the third significant feature, and high estimated values (red) positively correlated with the target. The age of initial diagnosis was the fourth significant feature, and high estimated values (red) positively correlated with the prediction of the HSPD class. The total strips identified was the fifth significant feature, and low and medium estimated values (blue and violet, respectively) positively correlated with the HSPD prediction. The Citric acid incorrect identification was the sixth most important feature, and low values estimated were positively correlated with the target or had a low impact. The *SNCA rs2583988*CC genotype was the seventh important feature and pushed the model forward to the other class. The sex features were the eighth and ninth in order of importance and impacted the model in making predictions, contrary to that for the MSPD. The female sex had a positive impact, while the male sex had a negative impact.

The *SNCA rs2583988*TT was the tenth feature and positively correlated with HSPD class. The low values of NaCl under threshold (the eleventh feature) pushed the model to the other class, while the high values of NaCl incorrect identification (the fifteenth feature) pushed the model to predict the HSPD class. The following features had a low impact: *SNCA rs181489*CT, *SNCA rs2583988*CT, *SNCA rs356186*GG, *SNCA rs356186*AG correlated positively with the target, while *SNCA rs356186*AA, *SNCA rs181489CC*, Citric acid correct identification, and Tannic acid correct identification correlated negatively.

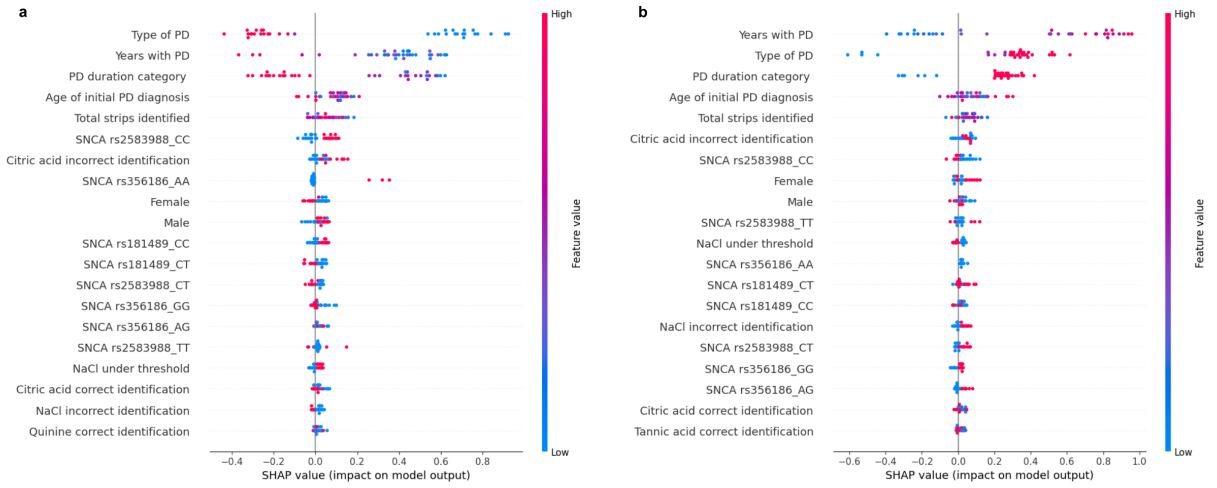

Figure 4. SHAP summary plots showing feature importance and their impact on the CatBoost classifier to make predictions of the disease severity of PD patients and classify them into those who had a moderate severity of PD (MSPD) (a) and those who had high severity of PD (HSPD) (b). The descending order of importance of the features (from top to bottom) is shown on the left of each Y-axis; the impact (SHAP value on the model output) is shown on the X-axis. The position of the SHAPE value on the X-axis shows whether the feature is associated with a higher or lower prediction score for the class. Each point in the plot is a SHAP value of a feature. The color of the line to the right of each graph represents the feature value: high value (red color), medium value (violet color), and low value (blue color).

3. Discussion

By integrating behavioral, demographic, computational, and genetic data, this study provides a multi-dimensional analysis of how taste perception is altered in PD, explores the underlying mechanisms, and offers a comprehensive view of how these alterations can be exploited both for diagnosis and disease severity purposes, by highlighting key sensory markers. Our study also provides novel findings on interactions between the taste deficits in PD and specific SNPs of the *SNCA* gene, already associated with PD predisposition[351, 439-441]. Our findings provide compelling evidence that taste impairments in PD are modality-specific, with saltiness and astringency most affected, and that genetic variations in the *SNCA* gene, which encodes alpha-synuclein, a key protein in PD pathology, modulate taste perception, contributing to the sensory phenotype of PD. These results support the hypothesis that modality-specific taste deficits in PD are not only functional but also genetically influenced, potentially offering a biomarker for early or prodromal PD. Specifically, the most significant taste deficit in PD was observed for salty taste (NaCl). Behavioral assessments revealed that PD patients showed different sensitivity to the salty stimulus compared to HCs. Only 11% of them correctly identified the stimulus with respect to 50% of HCs, and for half of PD patients, the NaCl stimulation was below threshold, while only 14% of HCs did not perceive any taste of NaCl. Astringency and sourness were also less accurately identified by PD patients, while sweet and bitter tastes showed no significant group differences. These findings suggest that PD-related taste deficits are selective, likely reflecting differential involvement of taste receptor pathways or central gustatory processing circuits. Impaired perception of astringency, a complex oral-sensory experience, may also indicate broader deficits in sensory integration.

In addition to behavioral measurements, we used SL models to confirm the involvement of taste impairments in PD and verify their possible diagnostic significance and distinguish between PD patients and HCs. The models learned the relationships between input features and target classes during training, allowing them to predict the correct class for new data. The training and testing performance of the SL models was evaluated using standard classification metrics, which provided insights into their ability to predict the two classes. The CatBoost algorithm achieved the best performance in classifying PD vs. HC based on taste and demographic features, with91% training accuracy, 91% training macro-averaged F1-score, 84% testing accuracy, and 82% testing macro-averaged F1-score.

The interpretation of the CatBoost classifier's results, performed using the SHAP algorithm, allowed us to establish a link between the importance of each feature and its impact on the prediction. The SHAP analysis revealed that, among the sensory features, the perception of any taste (under threshold) when subjects

taste salty, or the description of a different quality (incorrect identification), when they taste astringent stimulus (tannic acid), were the most influential features for PD classification. The NaCl under threshold feature was also important for the HC classification, but negatively correlated with HC target, whereas the NaCl correct identification was the third important feature with a positive correlation for the HC classification. These results indicate that our SL model classifies a subject as a PD patient if he/she perceived no taste for salty or described a different quality for the astringent stimulus, while it classifies as HC if he/she correctly identified the salty stimulus. The incorrect identification of sour stimulus was also positively correlated with the PD class, while sucrose-related features or bitter taste had little or no impact on the model prediction, consistent with behavioral findings. The total number of taste strips identified was inversely correlated to the PD classification, although it ranked sixth in importance, suggesting a general reduction in taste acuity in PD. These findings highlight the potential of taste testing as a non-invasive, biologically grounded tool for the diagnosis of PD and open new pathways for understanding the sensory dimensions of neurodegeneration. Age, sex, and smoking status also contributed significantly to PD prediction and were considered as variables that enhance the predictive power of the SL model. Age was a strong predictor of the PD classification, consistent with age-related PD risk [442]. Sex showed the already known pattern[443],with male sex associated with PD prediction. According to previous data [444], smoking status was positively associated with PD. Together, these results demonstrate the diagnostic potential of modality-specific taste disorders, especially when behavioral assessments are combined with analyses interpretable based on SL.

Genetic analysis of the *SNCA* SNPs, *rs356219*, *rs181489*, *rs2583988*, and *rs356186*, showed significant associations between genetic variations and the ability to perceive certain taste stimuli, particularly tannic acid and NaCl, in both PD patients and HCs. Specifically, when participants were exposed to tannic acid, the perception of astringency varied significantly across genotypes. Both genotype distributions and allele frequencies at all four *SNCA* loci differed significantly among the four groups (PD-yes, PD-no, HC-yes, HC-no). PD patients who failed to recognize astringency (PD-no) had distinct genotype and allele distributions compared to PD-yes and HCs, particularly at *rs356219*, *rs181489*, and *rs2583988*.PD-no also differed from HCs-no, suggesting that the inability to perceive astringency in PD may be genetically driven and not simply a result of general sensory decline. Specifically, at *rs356219*, PD-yes individuals had a high frequency of the A allele, while PD-no had a high frequency of the G allele, which has been associated with increased α-synuclein levels [352, 432]. This suggests that the A allele may be protective or associated with preserved astringency perception. At *rs181489*, a similar pattern emerged, with PD-yes enriched for the C allele and PD-no for the T allele, which has been associated with a higher risk of evolving PD [433]. At *rs2583988*, the T allele, which has been associated with a higher risk of developing PD [434, 435], was more common in PD-yes, while the CC genotype was more frequent in PD-no. Finally, at *rs356186*, both PD-yes and PD-no had high frequencies of the GG genotype, but HCs-no had a significantly higher frequency of the A allele, suggesting a potential protective role in non-PD individuals, in agreement with data showing a reduced risk of developing PD in A allele carriers [433]. These findings suggest that specific *SNCA* variants may influence the integrity of astringency perception pathways, potentially through effects on alpha-synuclein expression or aggregation in gustatory-related brain regions [352, 432, 445]. The *rs356186* SNP also showed a significant association with salt taste perception. PD-no individuals had a high frequency of the GG genotype and a low frequency of the A allele, while PD-yes individuals were predominantly heterozygous (AG) and lacked AA genotypes. In contrast, HCs-yes had a more balanced distribution, with more than 50% carrying at least one A allele and 44.44% having the GG genotype. These results suggest that the A allele at *rs356186* may be associated with preserved salt taste perception, while the GG genotype may predispose individuals to salt taste deficits, particularly in the context of PD.

The CatBoost classifier was also used to classify PD patients based on disease severity with very high accuracy values. In this second SL task, the SHAP software showed distinct patterns of feature importance and directionality for each severity class, reflecting the complex interplay between clinical, sensory, and genetic factors in PD progression. The SHAP analysis for the MSPD class highlighted features that were protective or indicative of less severe disease. PD Type was the most important, and low SHAP values, corresponding to the Tremor-dominant subtype, were strongly associated with the MSPD classification. This is consistent with the clinical literature suggesting that Tremor-dominant PD often progresses more

slowly and is associated with a more favorable prognosis [446-448]. Years with PD and PD Duration Category were the next most important features. Shorter disease duration (low and medium SHAP values) was positively associated with MSPD, indicating that earlier stages of the disease are more likely to be classified as moderate. Age of initial diagnosis also played a significant role. A younger age at diagnosis (blue and violet SHAP values) was associated with MSPD, suggesting that earlier onset may initially present with milder symptoms or slower progression. Among sensory features, the Total strips identified, an indicator for global taste acuity, was the fifth most important feature. Although its impact was less clear, higher taste acuity may reflect preserved sensory function and thus milder disease. The Citric acid incorrect identification was positively associated with MSPD, which may seem counterintuitive. However, this may indicate that mild sensory deficits are present even in moderate stages. Among genetic features, the *SNCArs2583988* CC genotype was positively associated with MSPD class, confirming its potential protective role [434, 435]. The *rs356186* AA and *rs181489* CC genotypes, already associated with a high risk of PD [433], also correlated positively with MSPD class, while heterozygous or alternative genotypes were negatively associated. Interestingly, the *rs2583988* TT genotype, typically associated with high risk, also showed a positive correlation with MSPD class, indicating a complex, possibly context-dependent genetic influence. It is noteworthy, male sex was positively associated with MSPD class, while female sex had a negative impact, suggesting potential sex-based differences in disease progression.

The SHAP summary plot for the HSPD class revealed a mirror image of the MSPD class profile, with features indicative of more advanced disease. Years with PD was the most important predictor. High SHAP values were strongly associated with HSPD class, reflecting the natural progression of PD over time. PD Type again played a major role. High and medium SHAP values, corresponding to Akinetic-Rigid and Mixed subtypes, were associated with HSPD class. These subtypes are known to be more disabling and progress more rapidly [449].PD Duration Category and Age at Diagnosis followed in terms of importance. Longer disease duration and older age at onset were both positively associated with HSPD class, consistent with clinical expectations[450]. Among sensory features, Total strips identified was inversely related to the HSPD class: lower taste acuity was associated with more severe disease, strengthening the link between sensory decline and PD progression. Citric acid incorrect identification had a lower impact, but still contributed positively to the HSPD classification, likely reflecting more widespread sensory dysfunction in advanced stages. NaCl incorrect identification was among the lower-ranked features, but still contributed positively to HSPD classification, suggesting that salt taste impairment may worsen with disease progression. Finally, among genetic features, the *rs2583988*CC genotype displaced the model from the HSPD class, while the *rs2583988*TT genotype was positively associated with HSPD class, confirming the non-protective role of the T allele. Other genotypes, such as *rs181489* CT, *rs2583988* CT, *rs356186* GG, and *rs356186* AG, although with low impact, were positively associated with HSPD class, while *rs356186* AA and *rs181489* CC were negatively associated, reinforcing the idea that specific *SNCA* variants modulate disease severity. In contrast to the MSPD class, female sex was positively associated with HSPD class, while male sex had a negative impact. This reversal may reflect sex-specific differences in disease progression or symptom burden. These SHAP-based insights underscore the multifactorial nature of PD severity, in which clinical history, sensory function, and genetic background interact to shape disease expression. The ability of the model to distinguish the MSPD class from the HSPD class suggests that SL may be a powerful tool for personalized disease monitoring, leveraging the integration of clinical, sensory, and genetic data into predictive models for PD staging and management.

Chapter 9
Conclusions and Future Directions

1. Key Findings

Taste perception represents one of the most fundamental sensory systems in humans, playing a central role in nutrition, food preference, and overall health. It not only influences dietary habits and metabolic balance but also contributes to quality of life and psychological well-being. Alterations in taste perception, such as hypogeusia or ageusia, are increasingly recognized as clinical indicators of systemic disorders, side effects of pharmacological treatments, or consequences of infectious diseases. Despite its importance, the physiological mechanisms underlying individual variability in taste perception remain only partially understood, as they arise from the complex interplay between genetic, epigenetic, and sensory factors.

Within this scientific context, the overall aim of my doctoral research was to clarify the determinants of human taste function through an integrative, multidisciplinary approach. By combining psychophysical, molecular, and computational methodologies, I worked on identifying predictive biological markers of taste perception and on developing innovative tools capable of improving diagnostic accuracy, scalability, and clinical applicability.

The first phase of my work focused on the genetic basis of bitter taste perception mediated by the *TAS2R38* receptor. I developed a supervised learning (SL) model capable of classifying *TAS2R38* genotypes (PAV/PAV, PAV/AVI, AVI/AVI) with high precision based only on biological and sensory data, eliminating the need for molecular genotyping. This model identified intensity ratings for low PROP concentrations and the medium taste (MT) category as the most discriminative parameters, demonstrating the feasibility of genotype prediction through psychophysical profiling. This advancement offers a cost-effective and scalable solution for large population-based studies investigating taste variability and nutrition.

To overcome the challenges and limitations associated with manual counting of FPs, I designed an Optimized U-Net deep learning model for their automatic identification on human tongue images. The optimized model significantly outperformed two classic U-Net architectures in terms of accuracy, stability, and robustness, enabling reliable large-scale and non-invasive assessments of FP density. By releasing the model as open-source software, this work also contributes to reproducibility and continuous improvement through collaborative development within the scientific community.

The second phase of my research explored taste function in health and disease through the implementation of a random forest regression model. By integrating sensory, clinical, and anthropometric parameters, this model provided an automated and objective means to distinguish between healthy individuals and patients with chemosensory loss. The analysis revealed that low concentrations of salt and high concentrations of sour stimuli characterized normal taste function, while high concentrations of bitter and astringent stimuli were most indicative of patients with chemosensory loss. These findings not only improve the understanding of the sensory mechanisms underlying taste loss but also introduce a novel computational framework for the rapid, reliable assessment of taste performance in clinical contexts, thus reducing the time and effort required by conventional psychophysical methods.

In the subsequent phase, I applied a CatBoost regression model to investigate the multidimensional nature of oral sensitivity, containing gustatory, olfactory, and trigeminal contributions. This approach revealed that trigeminal sensations, particularly astringency and spiciness, accounted for more than 60% of the variance in self-rated oral sensitivity. Notably, astringency played a predominant role in patients with chemosensory impairments compared to healthy controls, suggesting a differential weighting of trigeminal input in pathological conditions. These results offer practical implications for refining psychophysical protocols, allowing future assessments to be simplified and shortened from approximately 20 minutes to only 3 minutes per participant, without compromising diagnostic precision.

My research also clarifies the involvement of taste deficits in Parkinson's disease (PD), elucidating the mechanisms underlying them and clarifying their diagnostic significance. By integrating behavioural testing with machine learning and genetic profiling, we provided compelling evidence that such sensory alterations are influenced by both genetic and demographic factors. We found that taste impairments in PD are modality-specific, with saltiness and astringency most affected, and are modulated by the SNCA gene

variations. This study also offers a comprehensive view of how these alterations can be exploited both for diagnosis and disease severity purposes, by highlighting key sensory markers.
These findings open the way for personalized screening tools that could facilitate earlier intervention, preserve neuronal function, and reduce symptomatic burden, ultimately improving the quality of life for individuals at risk or affected by PD.
By using the molecular and epigenetic approaches, my work shows a significant relationship between *Gustin* gene methylation patterns, the expression of the two isoforms of Gustin protein, and the density of FPs. This evidence provides an epigenetic framework that may account for interindividual differences in taste sensitivity and could justify the conflicting data in the literature. Furthermore, the investigation of *TAS2R38* DNA methylation revealed that methylation levels at the *cg25481253* site were positively associated with the severity of COVID-19 during infection, potentially reflecting a regulatory mechanism influencing receptor expression and immune response. Although preliminary, this study offered novel insights into the epigenetic modulation of taste receptors and their possible role in systemic disease pathways.
Taken together, the studies conducted during my doctoral research illustrate how the integration of machine learning, molecular biology, and sensory science can substantially advance the understanding of human taste perception. The combination of psychophysical and computational approaches enabled the identification of key predictive features of taste function, while genetic and epigenetic analyses revealed novel biological pathways contributing to sensory variability and disease susceptibility. These findings establish a methodological and conceptual framework that links sensory physiology and artificial intelligence, opening the way for translational applications in clinical diagnostics, nutritional science, and personalized health.

2. Future Directions

The outcomes of this research lay the basics for several promising future investigations aimed at advancing the understanding of human taste perception through the integration of sensory, molecular, and computational approaches. Future studies should extend the application of the proposed machine learning models, both classification and regression, to larger and more diverse populations, to establish reliable and generalizable tools for assessing taste function and genotype-phenotype associations.
Building upon the evidence that alterations in saltiness and astringency perception represent early and selective markers of Parkinson's disease (PD), future research should prioritize longitudinal and multi-center studies to validate these sensory biomarkers across different disease stages and demographic groups. Integrating these behavioural, genetic, and computational markers into clinical practice could significantly enhance early diagnostic accuracy and support precision neurology approaches.
At the molecular level, longitudinal analyses of *Gustin* and *TAS2R38* methylation patterns are needed to elucidate their dynamic regulatory roles in taste sensitivity and disease susceptibility. Furthermore, the refinement and clinical translation of the Optimized U-Net model could provide an objective and non-invasive biomarker for taste-related morphology, enabling rapid assessment in both research and medical contexts.
Ultimately, combining these approaches into a unified, data-driven framework will deepen our comprehension of taste perception and its systemic implications, opening the way for the development of personalized strategies for diagnosis, nutrition, and health.

Chapter 10

References

1. Scott K. *Taste recognition: food for thought*. Neuron. 2005;**48**(3):455-64.
2. Donaldson LF, et al. *Taste and weight: is there a link?* Am. J. Clin. Nutr. 2009;**90**(3):800S-3S.
3. Chaudhari N, Roper SD. *The cell biology of taste*. J. Cell Biol. 2010;**190**(3):285-96.
4. Freeland WJaJ, D. H. *Strategies in herbivory by mammals: The role of plant secondary compounds.* The American Naturalist 1974;**108**:269-89.
5. Hladik CM, Simmen B. *Taste perception and feeding behavior in nonhuman primates and human populations*. Evolutionary Anthropology: Issues, News, and Reviews. 1996;**5**(2):58-71.
6. Reed DR, et al. *Diverse tastes: Genetics of sweet and bitter perception*. Physiol. Behav. 2006;**88**(3):215-26.
7. Kurihara K, Kashiwayanagi M. *Physiological studies on umami taste*. J Nutr. 2000;**130**(4S Suppl):931S-4S.
8. Bartoshuk LM, Beauchamp GK. *Chemical senses*. Annu Rev Psychol. 1994;**45**:419-49.
9. Lindemann B. *Receptors and transduction in taste*. Nature. 2001;**413**(6852):219-25.
10. Sugita M. *Taste perception and coding in the periphery*. Cell Mol Life Sci. 2006;**63**(17):2000-15.
11. Roper SD. *Signal transduction and information processing in mammalian taste buds*. Pflugers Arch. 2007;**454**(5):759-76.
12. Ebba S, et al. *The examination of fatty acid taste with edible strips*. Physiol. Behav. 2012;**106**(5):579-86.
13. Mattes RD. *Is there a fatty acid taste?* Annu. Rev. Nutr. 2009;**29**:305-27.
14. Mattes RD. Fat Taste in Humans: Is It a Primary? In: Montmayeur JP, le Coutre J, editors. Fat Detection: Taste, Texture, and Post Ingestive Effects. Frontiers in Neuroscience. CRC Press: Boca Raton (FL), USA2010. p. 167-93.
15. Pepino MY, et al. *The fatty acid translocase gene CD36 and lingual lipase influence oral sensitivity to fat in obese subjects*. J. Lipid Res. 2012;**53**(3):561-6.
16. Fukuwatari T, et al. *Role of gustation in the recognition of oleate and triolein in anosmic rats*. Physiol. Behav. 2003;**78**(4-5):579-83.
17. Smith JC, et al. *Orosensory factors in the ingestion of corn oil/sucrose mixtures by the rat*. Physiol. Behav. 2000;**69**(1-2):135-46.
18. Prescott J, et al. 6-n-Propylthiouracil tasting and the perception of nontaste oral sensations. In: Prescott J, Tepper BJ, editors. Genetic Variation in Taste Sensitivity. New York: Marcel Dekker; 2004. p. 89-104.
19. DeFazio RA, et al. *Separate populations of receptor cells and presynaptic cells in mouse taste buds*. J Neurosci. 2006;**26**(15):3971-80.
20. Finger TE, et al. *ATP signaling is crucial for communication from taste buds to gustatory nerves*. Science. 2005;**310**(5753):1495-9.
21. Miller IJ. Anatomy of peripheral taste system. In: Doty RL, editor. Handbook of Olfaction and Gustation. . Marcel Dekker, New York1995. p. 521-47.
22. Lawton DM, et al. *Localization of the glutamate-aspartate transporter, GLAST, in rat taste buds*. Eur J Neurosci. 2000;**12**(9):3163-71.
23. Bartel DL, et al. *Nucleoside triphosphate diphosphohydrolase-2 is the ecto-ATPase of type I cells in taste buds*. J Comp Neurol. 2006;**497**(1):1-12.
24. Pumplin DW, et al. *Light and dark cells of rat vallate taste buds are morphologically distinct cell types*. J Comp Neurol. 1997;**378**(3):389-410.
25. Dvoryanchikov G, et al. *Inward rectifier channel, ROMK, is localized to the apical tips of glial-like cells in mouse taste buds*. J Comp Neurol. 2009;**517**(1):1-14.
26. Adler E, et al. *A novel family of mammalian taste receptors*. Cell. 2000;**100**(6):693-702.
27. Romanov RA, et al. *Afferent neurotransmission mediated by hemichannels in mammalian taste cells*. EMBO J. 2007;**26**(3):657-67.
28. Zhang Y, et al. *Coding of sweet, bitter, and umami tastes: different receptor cells sharing similar signaling pathways*. Cell. 2003;**112**(3):293-301.
29. Nelson G, et al. *Mammalian sweet taste receptors*. Cell. 2001;**106**(3):381-90.

30. Tomchik SM, et al. *Breadth of tuning and taste coding in mammalian taste buds*. J. Neurosci. 2007;**27**(40):10840-8.
31. Roper SD. *Cell communication in taste buds*. Cell Mol Life Sci. 2006;**63**(13):1494-500.
32. Dvoryanchikov G, et al. *Biogenic amine synthesis and uptake in rodent taste buds*. J Comp Neurol. 2007;**505**(3):302-13.
33. Medler KF, et al. *Electrophysiological characterization of voltage-gated currents in defined taste cell types of mice*. J Neurosci. 2003;**23**(7):2608-17.
34. Gao N, et al. *Voltage-gated sodium channels in taste bud cells*. BMC Neurosci. 2009;**10**:20.
35. Kinnamon SC, Vandenbeuch A. *Receptors and transduction of umami taste stimuli*. Ann N Y Acad Sci. 2009;**1170**:55-9.
36. Vandenbeuch A, Kinnamon SC. *Why do taste cells generate action potentials?* J Biol. 2009;**8**(4):42.
37. Huang AL, et al. *The cells and logic for mammalian sour taste detection*. Nature. 2006;**442**(7105):934-8.
38. Huang YA, et al. *Presynaptic (Type III) cells in mouse taste buds sense sour (acid) taste*. J. Physiol. 2008;**586**(Pt 12):2903-12.
39. Chandrashekar J, et al. *The taste of carbonation*. Science. 2009;**326**(5951):443-5.
40. Farbman AI. *Fine Structure of the Taste Bud*. J Ultrastruct Res. 1965;**12**:328-50.
41. Kinnamon SC, Margolskee RF. *Mechanisms of taste transduction*. Curr Opin Neurobiol. 1996;**6**(4):506-13.
42. Drayna D. *Human taste genetics*. Annu. Rev. Genomics Hum. Genet. 2005;**6**:217-35.
43. Li X, et al. *Human receptors for sweet and umami taste*. Proc. Natl. Acad. Sci. U. S. A. 2002;**99**(7):4692-6.
44. Nelson G, et al. *An amino-acid taste receptor*. Nature. 2002;**416**(6877):199-202.
45. Zhao GQ, et al. *The receptors for mammalian sweet and umami taste*. Cell. 2003;**115**(3):255-66.
46. Chandrashekar J, et al. *T2Rs function as bitter taste receptors*. Cell. 2000;**100**(6):703-11.
47. Bufe B, et al. *The human TAS2R16 receptor mediates bitter taste in response to beta-glucopyranosides*. Nat Genet. 2002;**32**(3):397-401.
48. Kim UK, et al. *Positional cloning of the human quantitative trait locus underlying taste sensitivity to phenylthiocarbamide*. Science. 2003;**299**(5610):1221-5.
49. Meyerhof W, et al. *The molecular receptive ranges of human TAS2R bitter taste receptors*. Chem. Senses. 2010;**35**(2):157-70.
50. Caicedo A, Roper SD. *Taste receptor cells that discriminate between bitter stimuli*. Science. 2001;**291**(5508):1557-60.
51. Gaillard D, et al. *The gustatory pathway is involved in CD36-mediated orosensory perception of long-chain fatty acids in the mouse*. FASEB J. 2008;**22**(5):1458-68.
52. McLaughlin SK, et al. *Gustducin is a taste-cell-specific G protein closely related to the transducins*. Nature. 1992;**357**(6379):563-9.
53. Ming D, et al. *Blocking taste receptor activation of gustducin inhibits gustatory responses to bitter compounds*. Proc Natl Acad Sci U S A. 1999;**96**(17):9903-8.
54. Ruiz-Avila L, et al. *Coupling of bitter receptor to phosphodiesterase through transducin in taste receptor cells*. Nature. 1995;**376**(6535):80-5.
55. Wong GT, et al. *Transduction of bitter and sweet taste by gustducin*. Nature. 1996;**381**(6585):796-800.
56. Huang L, et al. *Ggamma13 colocalizes with gustducin in taste receptor cells and mediates IP3 responses to bitter denatonium*. Nat Neurosci. 1999;**2**(12):1055-62.
57. Avenet P, et al. *Transduction in taste receptor cells requires cAMP-dependent protein kinase*. Nature. 1988;**331**(6154):351-4.
58. Tonosaki K, Funakoshi M. *Cyclic nucleotides may mediate taste transduction*. Nature. 1988;**331**(6154):354-6.
59. Trubey KR, et al. *Tastants evoke cAMP signal in taste buds that is independent of calcium signaling*. Am J Physiol Cell Physiol. 2006;**291**(2):C237-44.
60. Bernhardt SJ, et al. *Changes in IP3 and cytosolic Ca2+ in response to sugars and non-sugar sweeteners in transduction of sweet taste in the rat*. J Physiol. 1996;**490 (Pt 2)**:325-36.

61. Clapp TR, et al. *Immunocytochemical evidence for co-expression of Type III IP3 receptor with signaling components of bitter taste transduction*. BMC Neurosci. 2001;**2**:6.
62. Hofmann T, et al. *TRPM5 is a voltage-modulated and Ca(2+)-activated monovalent selective cation channel*. Curr Biol. 2003;**13**(13):1153-8.
63. Perez CA, et al. *A transient receptor potential channel expressed in taste receptor cells*. Nat Neurosci. 2002;**5**(11):1169-76.
64. Ye Q, et al. *Effects of voltage perturbation of the lingual receptive field on chorda tympani responses to Na+ and K+ salts in the rat: implications for gustatory transduction*. J Gen Physiol. 1994;**104**(5):885-907.
65. Ishimaru Y, et al. *Transient receptor potential family members PKD1L3 and PKD2L1 form a candidate sour taste receptor*. Proc Natl Acad Sci U S A. 2006;**103**(33):12569-74.
66. LopezJimenez ND, et al. *Two members of the TRPP family of ion channels, Pkd1l3 and Pkd2l1, are co-expressed in a subset of taste receptor cells*. J Neurochem. 2006;**98**(1):68-77.
67. Lin W, et al. *Epithelial Na+ channel subunits in rat taste cells: localization and regulation by aldosterone*. J Comp Neurol. 1999;**405**(3):406-20.
68. Heck GL, et al. *Salt taste transduction occurs through an amiloride-sensitive sodium transport pathway*. Science. 1984;**223**(4634):403-5.
69. Chandrashekar J, et al. *The cells and peripheral representation of sodium taste in mice*. Nature. 2010;**464**(7286):297-301.
70. Desimone JA, et al. *The active ion transport properties of canine lingual epithelia in vitro. Implications for gustatory transduction*. J Gen Physiol. 1984;**83**(5):633-56.
71. Fish HS, et al. *The anatomy of the tongue of the domestic norway rat. I. The skin of the tongue; the various papillae; their number and distribution*. The Anatomical Record. 1944;**89**(4):429-40.
72. Oakley B. *On the specification of taste neurons in the rat tongue*. Brain Res. 1974;**75**(1):85-96.
73. Whiteside B. *Nerve overlap in the gustatory apparatus of the rat*. The Journal of Comparative Neurology. 1927;**44**(2):363-77.
74. Zalewski AA. *Role of nerve and epithelium in the regulation of alkaline phosphatase activity in gustatory papillae*. Exp Neurol. 1969;**23**(1):18-28.
75. Buck LM. Smell and taste: The chemical senses. Kandel ER, Schwartz, J. H. and Jessell, T. M. eds, editor2000.
76. Møller AR. Sensory Systems: Anatomy and Physiology. Academic Press, London, editors2003.
77. Scott TR, Plata-Salaman CR. *Taste in the monkey cortex*. Physiol Behav. 1999;**67**(4):489-511.
78. Penfield W, Faulk ME, Jr. *The insula; further observations on its function*. Brain. 1955;**78**(4):445-70.
79. Mombaerts P. *Genes and ligands for odorant, vomeronasal and taste receptors*. Nat Rev Neurosci. 2004;**5**(4):263-78.
80. Rolls ET. *Taste, olfactory, and food texture processing in the brain, and the control of food intake*. Physiol Behav. 2005;**85**(1):45-56.
81. Caterina MJ, et al. *The capsaicin receptor: a heat-activated ion channel in the pain pathway*. Nature. 1997;**389**(6653):816-24.
82. Everaerts W, et al. *The capsaicin receptor TRPV1 is a crucial mediator of the noxious effects of mustard oil*. Curr Biol. 2011;**21**(4):316-21.
83. Bautista DM, et al. *Pungent products from garlic activate the sensory ion channel TRPA1*. Proc Natl Acad Sci U S A. 2005;**102**(34):12248-52.
84. Roper SD. *TRPs in taste and chemesthesis*. Handb Exp Pharmacol. 2014;**223**:827-71.
85. Lee CB, Lawless HT. *Time-course of astringent materials.* Chemical Senses. 1991;**16** 225-38.
86. Jöbstl E, et al. *Molecular model for astringency produced by polyphenol/protein interactions*. Biomacromolecules. 2004;**5**(3):942-9.
87. Charlton AJ, et al. *Polyphenol/peptide binding and precipitation*. J Agric Food Chem. 2002;**50**(6):1593-601.
88. Siebert KJ, Chassy AW. *An alternate mechanism for the astringent sensation of acids*. Food Quality and Preference. 2004;**15**(1):13-8.

89. Siebert KJ, et al. *Nature of Polyphenol–Protein Interactions*. J. Agric. Food Chem. 1996;**44**(1):80-5.
90. Tepper BJ. *Nutritional implications of genetic taste variation: the role of PROP sensitivity and other taste phenotypes*. Annu. Rev. Nutr. 2008;**28**:367-88.
91. Soranzo N, et al. *Positive selection on a high-sensitivity allele of the human bitter-taste receptor TAS2R16*. Curr Biol. 2005;**15**(14):1257-65.
92. Del Río JA, et al. *Changes of polymethoxylated flavones levels during development of Citrus aurantium (cv. Sevillano) fruits*. Planta medica. 1998;**64**(06):575-6.
93. Drewnowski A, Gomez-Carneros C. *Bitter taste, phytonutrients, and the consumer: a review*. Am J Clin Nutr. 2000;**72**(6):1424-35.
94. D'Archivio M, et al. *Polyphenols, dietary sources and bioavailability*. Ann Ist Super Sanita. 2007;**43**(4):348-61.
95. Kalmus H. *Improvements in the classification of the taster genotypes*. Ann. Hum. Genet. 1958;**22**(3):222-30.
96. Fox AL. *The relationship between chemical constitution and taste*. Proc. Natl. Acad. Sci. USA. 1932;**18**(1):115-20.
97. Harris H, Kalmus H. *Chemical specificity in genetical differences of taste sensitivity*. Annals of eugenics. 1949;**15**(1):32-45.
98. Fahey JW, et al. *The chemical diversity and distribution of glucosinolates and isothiocyanates among plants*. Phytochemistry. 2001;**56**(1):5-51.
99. Delange F. *The role of iodine in brain development*. Proceedings of the Nutrition Society. 2000;**59**(1):75-9.
100. Liang F. *Sustentacular Cell Enwrapment of Olfactory Receptor Neuronal Dendrites: An Update*. Genes (Basel). 2020;**11**(5).
101. Cuschieri A, Bannister LH. *The development of the olfactory mucosa in the mouse: electron microscopy*. J Anat. 1975;**119**(Pt 3):471-98.
102. Dear TN, et al. *Molecular cloning of putative odorant-binding and odorant-metabolizing proteins*. Biochemistry. 1991;**30**(43):10376-82.
103. Guo SW, Reed DR. *The genetics of phenylthiocarbamide perception*. Ann. Hum. Biol. 2001;**28**(2):111-42.
104. Wooding S, et al. *Natural Selection and Molecular Evolution in PTC, a Bitter-Taste Receptor Gene*. Am. J. Hum. Genet. 2004;**74**(4):637-46.
105. Blakeslee AF, Fox AL. *Our different taste worlds: P. t. c. as a demonstration of genetic differences in taste*. J. Hered. 1932;**23**(3):97-107.
106. Tepper BJ, et al. *Variation in the bitter-taste receptor gene TAS2R38, and adiposity in a genetically isolated population in Southern Italy*. Obesity (Silver Spring). 2008;**16**(10):2289-95.
107. Prodi DA, et al. *Bitter taste study in a Sardinian genetic isolate supports the association of phenylthiocarbamide sensitivity to the TAS2R38 bitter receptor gene*. Chem. Senses. 2004;**29**(8):697-702.
108. Bartoshuk LM. *The biological basis of food perception and acceptance.* Food Qual. Prefer. 1993;**4**:21-32.
109. Bartoshuk LM, et al. *PTC/PROP tasting: anatomy, psychophysics, and sex effects*. Physiol. Behav. 1994;**56**(6):1165-71.
110. Tepper BJ, et al. *Variation in the bitter-taste receptor gene TAS2R38, and adiposity in a genetically isolated population in Southern Italy*. Obesity. 2008;**16**(10):2289-95.
111. Hayes JE, Duffy VB. *Revisiting sugar-fat mixtures: sweetness and creaminess vary with phenotypic markers of oral sensation*. Chem. Senses. 2007;**32**(3):225-36.
112. Tepper BJ, Nurse RJ. *PROP taster status is related to fat perception and preference*. Ann. N. Y. Acad. Sci. 1998;**855**:802-4.
113. Bartoshuk LM, et al. *PROP (6-n-propylthiouracil) supertasters and the saltiness of NaCl*. Ann. N. Y. Acad. Sci. 1998;**855**:793-6.
114. Duffy VB, et al. *Bitter Receptor Gene (TAS2R38), 6-n-Propylthiouracil (PROP) Bitterness and Alcohol Intake*. Alcohol. Clin. Exp. Res. 2004;**28**(11):1629-37.

115. Hayes JE, et al. *Supertasting and PROP bitterness depends on more than the TAS2R38 gene*. Chem. Senses. 2008;**33**(3):255-65.
116. Bajec MR, Pickering GJ. *Thermal taste, PROP responsiveness, and perception of oral sensations*. Physiol. Behav. . 2008;**95**(4):581-90.
117. Tepper BJ, et al. *Development of brief methods to classify individuals by PROP taster status*. Physiol. Behav. 2001;**73**(4):571-7.
118. Yeomans MR, et al. *Acquired hedonic and sensory characteristics of odours: Influence of sweet liker and propylthiouracil taster status*. Q J Exp Psychol A. 2009;**62**(8):1648-64.
119. Duffy VB, Bartoshuk LM. *Food acceptance and genetic variation in taste*. J. Am. Diet Assoc. 2000;**100**(6):647-55.
120. Bufe B, et al. *The molecular basis of individual differences in phenylthiocarbamide and propylthiouracil bitterness perception*. Curr. Biol. 2005;**15**(4):322-7.
121. Olson JM, et al. *Alternative genetic models for the inheritance of the phenylthiocarbamide taste deficiency*. Genetic Epidemiology. 1989;**6**(3):423-34.
122. Drayna D, et al. *Genetic analysis of a complex trait in the Utah Genetic Reference Project: a major locus for PTC taste ability on chromosome 7q and a secondary locus on chromosome 16p*. Hum. Genet. 2003;**112**(5-6):567-72.
123. Reed DR, et al. *The perception of quinine taste intensity is associated with common genetic variants in a bitter receptor cluster on chromosome 12*. Human Molecular Genetics. 2010;**19**(21):4278-85.
124. Tepper BJ, Nurse RJ. *Fat perception is related to PROP taster status*. Physiol. Behav. 1997;**61**(6):949-54.
125. Yackinous C, Guinard JX. *Relation between PROP taster status and fat perception, touch, and olfaction*. Physiol. Behav. 2001;**72**(3):427-37.
126. Essick G, et al. *Lingual tactile acuity, taste perception, and the density and diameter of fungiform papillae in female subjects*. Physiol. Behav. 2003;**80**(2-3):289-302.
127. Padiglia A, et al. *Sensitivity to 6-n-propylthiouracil is associated with gustin (carbonic anhydrase VI) gene polymorphism, salivary zinc, and body mass index in humans*. Am. J. Clin. Nutr. 2010;**92**(3):539-45.
128. Gent J, Bartoshuk L. *Sweetness of sucrose, neohesperidin dihydrochalcone, and saccharin is related to genetic ability to taste the bitter substance 6-n-propylthiouracil.* Chem. Senses. 1983;**7**:265-72.
129. Bartoshuk LM. *Bitter taste of saccharin related to the genetic ability to taste the bitter substance 6-n-propylthiouracil*. Science. 1979;**205**(4409):934-5.
130. Bartoshuk LM, et al. *Taste and aging*. J. Gerontol. 1986;**41**(1):51-7.
131. Bartoshuk LM, et al. *Bitterness of KCl and benzoate: related to genetic status for sensitivity to PTC/PROP*. Chem. Senses. 1988;**13**(4):517-28.
132. Bartoshuk L, et al. *PROP supertasters and the perception of sweetness and bitterness*. Chem. Senses. 1992;**17**:594.
133. Yeomans MR, et al. *Human hedonic responses to sweetness: role of taste genetics and anatomy*. Physiol. Behav. 2007;**91**(2-3):264-73.
134. Prescott J, Swain-Campbell N. *Responses to repeated oral irritation by capsaicin, cinnamaldehyde and ethanol in PROP tasters and non-tasters*. Chem. Senses. 2000;**25**(3):239-46.
135. Keller KL, et al. *Genetic taste sensitivity to 6-n-propylthiouracil influences food preference and reported intake in preschool children*. Appetite. 2002;**38**(1):3-12.
136. Forrai G, Bánkövi G. *Taste perception for phenylthiocarbamide and food choice--a Hungarian twin study*. Acta Physiol. Hung. 1984;**64**(1):33-40.
137. Goldstein GL, et al. *Adiposity in middle-aged women is associated with genetic taste blindness to 6-n-propylthiouracil*. Obes. Res. 2005;**13**(6):1017-23.
138. Tepper BJ. *Does genetic taste sensitivity to PROP influence food preferences and body weight?* Appetite. 1999;**32**(3):422.
139. Tepper BJ, Ullrich NV. *Influence of genetic taste sensitivity to 6-n-propylthiouracil (PROP), dietary restraint and disinhibition on body mass index in middle-aged women*. Physiol. Behav. 2002;**75**(3):305-12.

140. Love-Gregory L, et al. *Common CD36 SNPs reduce protein expression and may contribute to a protective atherogenic profile*. Hum. Mol. Genet. 2011;**20**(1):193-201.
141. Mrizak I, et al. *The A allele of cluster of differentiation 36 (CD36) SNP 1761667 associates with decreased lipid taste perception in obese Tunisian women*. Br. J. Nutr. 2015;**113**(8):1330-7.
142. Melis M, et al. *Associations between orosensory perception of oleic acid, the common single nucleotide polymorphisms (rs1761667 and rs1527483) in the CD36 gene, and 6-n-propylthiouracil (PROP) tasting*. Nutrients. 2015;**7**(3):2068-84.
143. Burgess B, et al. *Effects of CD36 Genotype on Oral Perception of Oleic Acid Supplemented Safflower Oil Emulsions in Two Ethnic Groups: A Preliminary Study*. J. Food Sci. 2018;**83**(5):1373-80.
144. Keller KL, et al. *Common variants in the CD36 gene are associated with oral fat perception, fat preferences, and obesity in African Americans*. Obesity. 2012;**20**(5):1066-73.
145. Tomassini Barbarossa I, et al. *Variant in a common odorant-binding protein gene is associated with bitter sensitivity in people*. Behav. Brain Res. 2017;**329**:200-4.
146. Mattes RD. 6-n-Propylthiouracil taster status: dietary modifier, marker or misleader? In: Prescott J, Tepper BJ, editors. Genetic Variation in Taste Sensitivity. New York: Marcel Dekker; 2004. p. 229-50.
147. Drewnowski A, et al. *Genetic Sensitivity to 6-n-Propylthiouracil Has No Influence on Dietary Patterns, Body Mass Indexes, or Plasma Lipid Profiles of Women*. J. Am. Diet. Assoc. 2007;**107**(8):1340-8.
148. Kaminski LC, et al. *Young women's food preferences and taste responsiveness to 6-n-propylthiouracil (PROP)*. Physiol. Behav. 2000;**68**(5):691-7.
149. Timpson NJ, et al. *TAS2R38 (phenylthiocarbamide) haplotypes, coronary heart disease traits, and eating behavior in the British Women's Heart and Health Study*. Am. J. Clin. Nutr. 2005;**81**(5):1005-11.
150. Yackinous CA, Guinard JX. *Relation between PROP (6-n-propylthiouracil) taster status, taste anatomy and dietary intake measures for young men and women*. Appetite. 2002;**38**(3):201-9.
151. Rodrigues L, et al. *Salivary proteome and glucose levels are related with sweet taste sensitivity in young adults*. Food. Nutr. Res. 2017;**61**(1):1389208.
152. Stolle T, et al. *Salivary proteome patterns affecting human salt taste sensitivity*. J. Agric. Food Chem. 2017;**65**(42):9275-86.
153. Scinska-Bienkowska A, et al. *Glutamate concentration in whole saliva and taste responses to monosodium glutamate in humans*. Nutr. Neurosci. 2006;**9**(1-2):25-31.
154. Méjean C, et al. *Salivary composition is associated with liking and usual nutrient intake*. PloS one. 2015;**10**(9):e0137473.
155. Morzel M, et al. *Salivary protein profiles are linked to bitter taste acceptance in infants*. Eur. J. Pediatr. 2014;**173**(5):575-82.
156. Neyraud E, et al. *Proteomic analysis of human whole and parotid salivas following stimulation by different tastes*. J. Proteome Res. 2006;**5**(9):2474-80.
157. Quintana M, et al. *Short-term modification of human salivary proteome induced by two bitter tastants, urea and quinine*. Chemosens. Percept. 2009;**2**(3):133-42.
158. Cabras T, et al. *Responsiveness to 6-n-propylthiouracil (PROP) is associated with salivary levels of two specific basic proline-rich proteins in humans*. PLoS One. 2012;**7**(2):e30962.
159. Melis M, et al. *Marked increase in PROP taste responsiveness following oral supplementation with selected salivary proteins or their related free amino acids*. PLoS One. 2013;**8**(3):e59810.
160. Melis M, et al. *Dose-Dependent Effects of L-Arginine on PROP Bitterness Intensity and Latency and Characteristics of the Chemical Interaction between PROP and L-Arginine*. PLoS One. 2015;**10**(6):e0131104.
161. Melis M, et al. *Effect of chemical interaction between oleic acid and L-Arginine on oral perception, as a function of polymorphisms of CD36 and OBPIIa and genetic ability to taste 6-n-propylthiouracil*. PLoS One. 2018;**13**(3):e0194953.
162. Melis M, Tomassini Barbarossa I. *Taste Perception of Sweet, Sour, Salty, Bitter, and Umami and Changes Due to l-Arginine Supplementation, as a Function of Genetic Ability to Taste 6-n-Propylthiouracil*. Nutrients. 2017;**9**(6):541-58.
163. Melis M, et al. *Sensory perception of and salivary protein response to astringency as a function of the 6-n-propylthioural (PROP) bitter-taste phenotype*. Physiol. Behav. 2017;**173**:163-73.

164. Williamson MP. *The structure and function of proline-rich regions in proteins*. Biochem. J. 1994;**297 (Pt 2)**:249-60.
165. Yan Q, Bennick A. *Identification of histatins as tannin-binding proteins in human saliva*. Biochem. J. 1995;**311**(1):341-7.
166. Bennick A. *Interaction of plant polyphenols with salivary proteins*. Crit. Rev. Oral Biol. Med. 2002;**13**(2):184-96.
167. Ployon S, et al. *Mechanisms of astringency: Structural alteration of the oral mucosal pellicle by dietary tannins and protective effect of bPRPs*. Food Chemistry. 2018;**253**:79-87.
168. Frenkel ES, Ribbeck K. *Salivary mucins protect surfaces from colonization by cariogenic bacteria*. Appl Environ Microbiol. 2015;**81**(1):332-8.
169. Nayak A, Carpenter GH. *A physiological model of tea-induced astringency*. Physiol Behav. 2008;**95**(3):290-4.
170. Horne J, Hayes, J., Lawless, H.T. *Turbidity as a measure of salivary protein reactions with astringent substances.* Chem Senses. 2002;**27**:653-9.
171. Naish M, et al. *Sensory astringency of 5-O-caffeoylquinic acid, tannic acid and grape-seed tannin by a time-intensity procedure*. 1993;**61**(1):57-64.
172. Valentová H, et al. *Time–intensity studies of astringent taste*. Food Chemistry. 2002;**78**(1):29-37.
173. Bajec MR, Pickering GJ. *Astringency: mechanisms and perception*. Crit Rev Food Sci Nutr. 2008;**48**(9):858-75.
174. Brandão E, et al. *In Vivo Interactions between Procyanidins and Human Saliva Proteins: Effect of Repeated Exposures to Procyanidins Solution*. Journal of Agricultural and Food Chemistry. 2014;**62**(39):9562-8.
175. Peleg H, et al. *Bitterness and astringency of flavan-3-ol monomers, dimers and trimers*. 1999;**79**(8):1123-8.
176. Hufnagel JC, Hofmann T. *Orosensory-directed identification of astringent mouthfeel and bitter-tasting compounds in red wine*. J Agric Food Chem. 2008;**56**(4):1376-86.
177. Kershaw JC, Running CA. *Dose–response functions and methodological insights for sensory tests with astringent stimuli*. 2019;**34**(1):e12480.
178. Fleming EE, et al. *Check-All-That-Apply (CATA), Sorting, and Polarized Sensory Positioning (PSP) with Astringent Stimuli*. Food Qual Prefer. 2015;**45**:41-9.
179. Zhao L, et al. *A paper screening test to assess genetic taste sensitivity to 6-n-propylthiouracil*. Physiol. Behav. 2003;**78**(4-5):625-33.
180. Genick UK, et al. *Sensitivity of Genome-Wide-Association Signals to Phenotyping Strategy: The PROP-TAS2R38 Taste Association as a Benchmark*. Plos One. 2011;**6**(11).
181. Barbarossa IT, et al. *The gustin (CA6) gene polymorphism, rs2274333 (A/G), is associated with fungiform papilla density, whereas PROP bitterness is mostly due to TAS2R38 in an ethnically-mixed population*. Physiol. Behav. 2015;**138**:6-12.
182. Prutkin J, et al. *Genetic variation and inferences about perceived taste intensity in mice and men*. Physiol Behav. 2000;**69**(1-2):161-73.
183. Hayes JE, et al. *Explaining variability in sodium intake through oral sensory phenotype, salt sensation and liking*. Physiol Behav. 2010;**100**(4):369-80.
184. Kirkmeyer SV, Tepper BJ. *Understanding creaminess perception of dairy products using free-choice profiling and genetic responsivity to 6-n-propylthiouracil*. Chem. Senses. 2003;**28**(6):527-36.
185. Calò C, et al. *Polymorphisms in TAS2R38 and the taste bud trophic factor, gustin gene co-operate in modulating PROP taste phenotype*. Physiol. Behav. 2011;**104**(5):1065-71.
186. Drewnowski A, et al. *Genetic sensitivity to 6-n-propylthiouracil (PROP) and hedonic responses to bitter and sweet tastes*. Chem Senses. 1997;**22**(1):27-37.
187. Goldstein GL, et al. *Influence of PROP taster status and maternal variables on energy intake and body weight of pre-adolescents*. Physiol. Behav. 2007;**90**(5):809-17.
188. Zhao L, Tepper BF. *Perception and acceptance of selected high-intensity sweeteners and blends in model soft drinks by propylthiouracil (PROP) non-tasters and super-tasters.* Food Quality & Preference. 2006:(in press).

189. Robino A, et al. *A Population-Based Approach to Study the Impact of PROP Perception on Food Liking in Populations along the Silk Road*. PLoS One. 2014;**9**(3):e91716.
190. Robino A, et al. *Understanding the role of personality and alexithymia in food preferences and PROP taste perception*. Physiol. Behav. 2016;**157**:72-8.
191. Burgess B, et al. *Changes in liking for sweet and fatty foods following weight loss in women are related to prop phenotype but not to diet*. Obesity (Silver Spring). 2016;**24**(9):1867-73.
192. Kirkmeyer SV, Tepper BJ. *Consumer reactions to creaminess and genetic sensitivity to 6-n-propylthiouracil: A multidimensional study*. Food Qual. Prefer. 2005;**16**(6):545-56.
193. Shafaie Y, et al. *Consumption of a high-fat soup preload leads to differences in short-term energy and fat intake between PROP non-taster and super-taster women*. Appetite. 2015;**89**:196-202.
194. Shafaie Y, et al. *Energy intake and diet selection during buffet consumption in women classified by the 6-n-propylthiouracil bitter taste phenotype*. Am. J. Clin. Nutr. 2013;**98**(6):1583-91.
195. Burgess B, et al. *PROP Nontaster Women Lose More Weight Following a Low-Carbohydrate Versus a Low-Fat Diet in a Randomized Controlled Trial*. Obesity (Silver Spring). 2017;**25**(10):1682-90.
196. Ahijevych K, et al. *Relationships of PROP Taste Phenotype, Taste Receptor Genotype, and Oral Nicotine Replacement Use*. Nicotine Tob. Res. 2015;**17**(9):1149-55.
197. Choi SE. *Racial differences between African Americans and Asian Americans in the effect of 6-n-propylthiouracil taste intensity and food liking on body mass index*. J. Acad. Nutr. Diet. 2014;**114**(6):938-44.
198. Oter B, et al. *The relation between 6-n-propylthiouracil sensitivity and caries activity in schoolchildren*. Caries Res. 2011;**45**(6):556-60.
199. Deshaware S, Singhal R. *Genetic variation in bitter taste receptor gene TAS2R38, PROP taster status and their association with body mass index and food preferences in Indian population*. Gene. 2017.
200. Macht M, Mueller J. *Increased negative emotional responses in PROP supertasters*. Physiol. Behav. 2007;**90**(2-3):466-72.
201. Green BG, et al. *Derivation and evaluation of a semantic scale of oral sensation magnitude with apparent ratio properties*. Chem. Senses. 1993;**18**(6):683-702.
202. Bartoshuk LM, et al. *Valid across-group comparisons with labeled scales: the gLMS versus magnitude matching*. Physiol Behav. 2004;**82**(1):109-14.
203. Melis M, et al. *The gustin (CA6) gene polymorphism, rs2274333 (A/G), as a mechanistic link between PROP tasting and fungiform taste papilla density and maintenance*. Plos One. 2013;**8**(9):e74151.
204. Oftedal KN, Tepper BJ. *Influence of the PROP bitter taste phenotype and eating attitudes on energy intake and weight status in pre-adolescents: a 6-year follow-up study*. Physiol Behav. 2013;**118**:103-11.
205. Boxer EE, Garneau NL. *Rare haplotypes of the gene TAS2R38 confer bitter taste sensitivity in humans*. SpringerPlus. 2015;**4**:505.
206. Bembich S, et al. *Individual differences in prefrontal cortex activity during perception of bitter taste using fNIRS methodology*. Chem Senses. 2010;**35**(9):801-12.
207. Sollai G, et al. *First objective evaluation of taste sensitivity to 6-n-propylthiouracil (PROP), a paradigm gustatory stimulus in humans*. Sci. Rep. 2017;**7**:40353.
208. Pani D, et al. *An automated system for the objective evaluation of human gustatory sensitivity using tongue biopotential recordings*. PLoS ONE. 2017;**12**(8):e0177246.
209. Landis BN, et al. *"Taste Strips" - a rapid, lateralized, gustatory bedside identification test based on impregnated filter papers*. J. Neurol. 2009;**256**(2):242-8.
210. Mueller C, et al. *Quantitative assessment of gustatory function in a clinical context using impregnated "taste strips"*. Rhinol. 2003;**41**(1):2-6.
211. Kobal G, et al. *"Sniffin' sticks": screening of olfactory performance*. Rhinology. 1996;**34**(4):222-6.
212. Heckmann JG, et al. *Taste disorders in acute stroke: a prospective observational study on taste disorders in 102 stroke patients*. Stroke. 2005;**36**(8):1690-4.
213. Just T, et al. *Confocal microscopy of the Peripheral Gustatory System: Comparison between Healthy Subjects and Patients Suffering from Taste Disorders during Radiochemotherapy*. 2005;**115**(12):2178-82.

214. Kamel UF. *Hypogeusia as a complication of uvulopalatopharyngoplasty and use of taste strips as a practical tool for quantifying hypogeusia*. Acta Otolaryngol. 2004;**124**(10):1235-6.
215. Landis BN, et al. *Gustatory function in chronic inflammatory middle ear diseases*. Laryngoscope. 2005;**115**(6):1124-7.
216. Landis BN, et al. *Gustatory function after microlaryngoscopy*. Acta Otolaryngol. 2007;**127**(10):1086-90.
217. Lang CJ, et al. *Taste in dementing diseases and parkinsonism*. J Neurol Sci. 2006;**248**(1-2):177-84.
218. Mueller CA, et al. *Gustatory function after tonsillectomy*. Arch Otolaryngol Head Neck Surg. 2007;**133**(7):668-71.
219. Nordin S, et al. *Substance and tongue-region specific loss in basic taste-quality identification in elderly adults*. Eur Arch Otorhinolaryngol. 2007;**264**(3):285-9.
220. Melis M, et al. *Associations between Orosensory Perception of Oleic Acid, the Common Single Nucleotide Polymorphisms (rs1761667 and rs1527483) in the CD36 Gene, and 6-n-Propylthiouracil (PROP) Tasting*. 2015;**7**(3):2068-84.
221. Miller IJ, Reedy FE. *Variations in human taste bud density and taste intensity perception*. Physiol. Behav. 1990;**47**(6):1213-9.
222. Mistretta CM, Bradley RM. *The fungiform papilla is a complex, multimodal, oral sensory organ*. Curr. Opin. Physiol. 2021;**20**:165-73.
223. Shahbake M, et al. *Rapid quantitative assessment of fungiform papillae density in the human tongue*. Brain Res. 2005;**1052**(2):196-201.
224. Nuessle TM, et al. *Denver Papillae Protocol for Objective Analysis of Fungiform Papillae*. JoVE. 2015(100):e52860.
225. Feeney EL, Hayes JE. *Exploring associations between taste perception, oral anatomy and polymorphisms in the carbonic anhydrase (gustin) gene CA6*. Physiol. Behav. 2014;**128**:148-54.
226. Piochi M, et al. *Associations between human fungiform papillae and responsiveness to oral stimuli: effects of individual variability, population characteristics, and methods for papillae quantification*. Chemical Senses. 2018;**43**(5):313-27.
227. Cattaneo C, et al. *Comparison of manual and machine learning image processing approaches to determine fungiform papillae on the tongue*. Scientific Reports. 2020;**10**(1):18694.
228. Eldeghaidy S, et al. *An automated method to detect and quantify fungiform papillae in the human tongue: Validation and relationship to phenotypical differences in taste perception*. Physiol Behav. 2018;**184**:226-34.
229. Sanyal S, et al. *TongueSim: Development of an Automated Method for Rapid Assessment of Fungiform Papillae Density for Taste Research*. Chem. Senses. 2016;**41**(4):357-65.
230. Dias AG, et al. *Variation in the TAS1R2 Gene, Sweet Taste Perception and Intake of Sugars*. J Nutrigenet Nutrigenomics. 2015;**8**(2):81-90.
231. Fushan AA, et al. *Allelic polymorphism within the TAS1R3 promoter is associated with human taste sensitivity to sucrose*. Curr. Biol. 2009;**19**(15):1288-93.
232. Chamoun E, et al. *Single nucleotide polymorphisms in sweet, fat, umami, salt, bitter and sour taste receptor genes are associated with gustatory function and taste preferences in young adults*. Nutr Res. 2021;**85**:40-6.
233. B AR, et al. *Association Between TAS1R2 Gene Polymorphism (rs12033832) and Sweet Taste Perception Amongst Malay Obese and Non- obese Subjects*. Malaysian Journal of Medicine and Health Sciences. 2020;**16**:2636-9346.
234. Melis M, et al. *Associations between Sweet Taste Sensitivity and Polymorphisms (SNPs) in the TAS1R2 and TAS1R3 Genes, Gender, PROP Taster Status, and Density of Fungiform Papillae in a Genetically Homogeneous Sardinian Cohort*. Nutrients. 2022;**14**(22).
235. Stewart JE, et al. *Oral sensitivity to fatty acids, food consumption and BMI in human subjects*. Br. J. Nutr. 2010;**104**(1):145-52.
236. Mattes RD. *Oral detection of short-, medium-, and long-chain free fatty acids in humans*. Chem Senses. 2009;**34**(2):145-50.
237. LeCun Y, et al. *Deep learning*. Nature. 2015;**521**(7553):436-44.

238. Litjens G, et al. *A survey on deep learning in medical image analysis*. Med Image Anal. 2017;**42**:60-88.
239. Ronneberger O, et al., editors. U-Net: Convolutional Networks for Biomedical Image Segmentation2015; Cham: Springer International Publishing.
240. Antonello P, et al. *Tracking unlabeled cancer cells imaged with low resolution in wide migration chambers via U-NET class-1 probability (pseudofluorescence)*. J. Biol. Eng. 2023;**17**(1):5.
241. Welge-Lüssen A, et al. *A study about the frequency of taste disorders*. J. Neurol. 2011;**258**(3):386-92.
242. Doty RL. *Age-related deficits in taste and smell*. Otolaryngol. Clin. North Am. 2018;**51**(4):815-25.
243. Mojet J, et al. *Taste perception with age: generic or specific losses in threshold sensitivity to the five basic tastes?* Chem. Senses. 2001;**26**(7):845-60.
244. Mojet J, et al. *Taste perception with age: generic or specific losses in supra-threshold intensities of five taste qualities?* Chem Senses. 2003;**28**(5):397-413.
245. Doty RL, et al. *Influences of age, tongue region, and chorda tympani nerve sectioning on signal detection measures of lingual taste sensitivity*. Physiol Behav. 2016;**155**:202-7.
246. Schiffman SS. *Taste and smell losses in normal aging and disease*. JAMA. 1997;**278**(16):1357-62.
247. Boesveldt S, et al. *Gustatory and olfactory dysfunction in older adults: a national probability study*. Rhinology. 2011;**49**(3):324-30.
248. Chen B, et al. *Symptoms of Depression in Patients with Chemosensory Disorders*. ORL J. Otorhinolaryngol. Relat. Spec. 2021;**83**(3):135-43.
249. Croy I, et al. *Learning about the Functions of the Olfactory System from People without a Sense of Smell*. Plos One. 2012;**7**(3):e33365.
250. Walliczek-Dworschak U, et al. *Differences in the Density of Fungiform Papillae and Composition of Saliva in Patients With Taste Disorders Compared to Healthy Controls*. Chem Senses. 2017;**42**(8):699-708.
251. Deems DA, et al. *Smell and taste disorders, a study of 750 patients from the University of Pennsylvania Smell and Taste Center*. Arch. Otolaryngol. Head Neck Surg. 1991;**117**(5):519-28.
252. Tepper BJ, et al. *Genetic sensitivity to the bitter taste of 6-n-propylthiouracil (PROP) and its association with physiological mechanisms controlling body mass index (BMI)*. Nutrients. 2014;**6**(9):3363-81.
253. Skrandies W, Zschieschang R. *Olfactory and gustatory functions and its relation to body weight*. Physiol Behav. 2015;**142**:1-4.
254. Park DC, et al. *Differences in taste detection thresholds between normal-weight and obese young adults*. Acta Oto-Laryngologica. 2015;**135**(5):478-83.
255. Overberg J, et al. *Differences in taste sensitivity between obese and non-obese children and adolescents*. Arch. Dis. Child. 2012;**97**(12):1048-52.
256. Pasquet P, et al. *Taste perception in massively obese and in non-obese adolescents*. Int J Pediatr Obes. 2007;**2**(4):242-8.
257. Kumari BG, Kumar ZN. *Evaluation of sweet taste sensitivity in type-II Diabetes Mellitus patients*. IJCBR. 2020:10-2.
258. Anderson GH. *Sugars, sweetness, and food intake*. Am J Clin Nutr. 1995;**62**(1 Suppl):195S-201S; discussion S-2S.
259. Simchen U, et al. *Odour and taste sensitivity is associated with body weight and extent of misreporting of body weight*. Eur J Clin Nutr. 2006;**60**(6):698-705.
260. Melis M, et al. *Changes of Taste, Smell and Eating Behavior in Patients Undergoing Bariatric Surgery: Associations with PROP Phenotypes and Polymorphisms in the Odorant-Binding Protein OBPIIa and CD36 Receptor Genes*. Nutrients. 2021;**13**(1).
261. Dinehart ME, et al. *Bitter taste markers explain variability in vegetable sweetness, bitterness, and intake*. Physiol. Behav. 2006;**87**(2):304-13.
262. Yousaf NY, et al. *Time Course of Salivary Protein Responses to Cranberry-Derived Polyphenol Exposure as a Function of PROP Taster Status*. Nutrients. 2020;**12**(9):2878.
263. Yousaf NY, Tepper BJ. *The Effects of Cranberry Polyphenol Extract (CPE) Supplementation on Astringency and Flavor Perception as a Function of PROP Taster Status and Other Individual Factors*. International Journal of Environmental Research and Public Health. 2022;**19**(19):11995.

264. Whissell-Buechy D. *Effects of age and sex on taste sensitivity to phenylthiocarbamide (PTC) in the Berkeley Guidance sample*. Chem. Senses. 1990;**15**(1):39-57.
265. Melis M, et al. *TAS2R38 bitter taste receptor and attainment of exceptional longevity*. Sci. Rep. 2019;**9**(1):18047.
266. Lee RJ, Cohen NA. *Role of the bitter taste receptor T2R38 in upper respiratory infection and chronic rhinosinusitis*. Curr. Opin. Allergy Clin. Immunol. 2015;**15**(1):14-20.
267. Cossu G, et al. *6-n-propylthiouracil taste disruption and TAS2R38 nontasting form in Parkinson's disease*. Mov. Disord. 2018;**33**(8):1331-9.
268. Lumeng JC, et al. *Ability to taste 6-n-propylthiouracil and BMI in low-income preschool-aged children*. Obesity. 2008;**16**(7):1522-8.
269. Miras AD, le Roux CW. *Bariatric surgery and taste: novel mechanisms of weight loss*. Curr. Opin. Gastroenterol. 2010;**26**(2):140-5.
270. Stice E, et al. *Relation between obesity and blunted striatal response to food is moderated by TaqIA A1 allele*. Science. 2008;**322**(5900):449-52.
271. Stice E, et al. *Relation of reward from food intake and anticipated food intake to obesity: a functional magnetic resonance imaging study*. J. Abnorm. Psychol. 2008;**117**(4):924-35.
272. Vignini A, et al. *General Decrease of Taste Sensitivity Is Related to Increase of BMI: A Simple Method to Monitor Eating Behavior*. Dis. Markers. 2019;**2019**:2978026.
273. Pepino MY, et al. *Obese women have lower monosodium glutamate taste sensitivity and prefer higher concentrations than do normal-weight women*. Obesity (Silver Spring). 2010;**18**(5):959-65.
274. Stewart JE, et al. *Oral sensitivity to oleic acid is associated with fat intake and body mass index*. Clin. Nutr. 2011;**30**(6):838-44.
275. Drewnowski A, et al. *Food preferences in human obesity: carbohydrates versus fats*. Appetite. 1992;**18**(3):207-21.
276. Macdiarmid JI, et al. *The sugar-fat relationship revisited: differences in consumption between men and women of varying BMI*. Int J Obes Relat Metab Disord. 1998;**22**(11):1053-61.
277. Rissanen A, et al. *Acquired preference especially for dietary fat and obesity: a study of weight-discordant monozygotic twin pairs*. Int J Obes Relat Metab Disord. 2002;**26**(7):973-7.
278. Bartoshuk LM, et al. *Psychophysics of sweet and fat perception in obesity: problems, solutions and new perspectives*. Philos Trans R Soc Lond B Biol Sci. 2006;**361**(1471):1137-48.
279. Malik VS, et al. *Global obesity: trends, risk factors and policy implications*. Nature Reviews Endocrinology. 2013;**9**(1):13-27.
280. Drewnowski A, et al. *Obesity and flavor perception: multidimensional scaling of soft drinks*. Appetite. 1982;**3**(4):361-8.
281. Tichansky DS, et al. *Taste change after laparoscopic Roux-en-Y gastric bypass and laparoscopic adjustable gastric banding*. Surg Obes Relat Dis. 2006;**2**(4):440-4.
282. Graham L, et al. *Taste, smell and appetite change after Roux-en-Y gastric bypass surgery*. Obes Surg. 2014;**24**(9):1463-8.
283. Makaronidis JM, et al. *Reported appetite, taste and smell changes following Roux-en-Y gastric bypass and sleeve gastrectomy: Effect of gender, type 2 diabetes and relationship to post-operative weight loss*. Appetite. 2016;**107**:93-105.
284. Ochner CN, et al. *Selective reduction in neural responses to high calorie foods following gastric bypass surgery*. Ann Surg. 2011;**253**(3):502-7.
285. Miras AD, et al. *Gastric bypass surgery for obesity decreases the reward value of a sweet-fat stimulus as assessed in a progressive ratio task*. Am J Clin Nutr. 2012;**96**(3):467-73.
286. Thirlby RC, et al. *Effect of Roux-en-Y gastric bypass on satiety and food likes: the role of genetics*. J Gastrointest Surg. 2006;**10**(2):270-7.
287. le Roux CW, et al. *Gastric bypass reduces fat intake and preference*. Am J Physiol Regul Integr Comp Physiol. 2011;**301**(4):R1057-66.
288. Coluzzi I, et al. *Food Intake and Changes in Eating Behavior After Laparoscopic Sleeve Gastrectomy*. Obes Surg. 2016;**26**(9):2059-67.
289. Pepino MY, et al. *Changes in taste perception and eating behavior after bariatric surgery-induced weight loss in women*. Obesity (Silver Spring). 2014;**22**(5):E13-20.

290. Ammon BS, et al. *Short-term pilot study of the effect of sleeve gastrectomy on food preference*. Obes Surg. 2015;**25**(6):1094-7.
291. Burge JC, et al. *Changes in patients' taste acuity after Roux-en-Y gastric bypass for clinically severe obesity*. J Am Diet Assoc. 1995;**95**(6):666-70.
292. Zerrweck C, et al. *Taste and Olfactory Changes Following Laparoscopic Gastric Bypass and Sleeve Gastrectomy*. Obes Surg. 2016;**26**(6):1296-302.
293. Scruggs DM, et al. *Taste Acuity of the Morbidly Obese before and after Gastric Bypass Surgery*. Obes Surg. 1994;**4**(1):24-8.
294. Bueter M, et al. *Alterations of sucrose preference after Roux-en-Y gastric bypass*. Physiol Behav. 2011;**104**(5):709-21.
295. Nance K, et al. *Effects of Sleeve Gastrectomy vs. Roux-en-Y Gastric Bypass on Eating Behavior and Sweet Taste Perception in Subjects with Obesity*. Nutrients. 2017;**10**(1).
296. Holinski F, et al. *Olfactory and Gustatory Function After Bariatric Surgery*. Obes Surg. 2015;**25**(12):2314-20.
297. Altun H, et al. *Improved Gustatory Sensitivity in Morbidly Obese Patients After Laparoscopic Sleeve Gastrectomy*. Ann Otol Rhinol Laryngol. 2016;**125**(7):536-40.
298. Tiomny E, et al. *Serum zinc and taste acuity in Tel-Aviv patients with inflammatory bowel disease*. Am. J. Gastroenterol. 1982;**77**(2):101-4.
299. Penny WJ, et al. *Relationship between trace elements, sugar consumption, and taste in Crohn's disease*. Gut. 1983;**24**(4):288-92.
300. Solomons NW, et al. *Zinc deficiency in Crohn's disease*. Digestion. 1977;**16**(1-2):87-95.
301. Schutz T, et al. *Sugar intake, taste changes and dental health in Crohn's disease*. Dig. Dis. 2003;**21**(3):252-7.
302. Kasper H, Sommer H. *Taste thresholds in patients with Crohn's disease*. J. Hum. Nutr. 1980;**34**(6):455-6.
303. Steinbach S, et al. *Smell and taste in inflammatory bowel disease*. PLoS One. 2013;**8**(9):e73454.
304. McClain C, et al. *Zinc deficiency: a complication of Crohn's disease*. Gastroenterology. 1980;**78**(2):272-9.
305. Martini GA, Brandes JW. *Increased consumption of refined carbohydrates in patients with Crohn's disease*. Klin. Wochenschr. 1976;**54**(8):367-71.
306. Huart C, et al. *Chemosensory pathways: from periphery to cortex*. B-ent. 2009;**5 Suppl 13**:3-9.
307. Auvray M, Spence C. *The multisensory perception of flavor*. Conscious. Cogn. 2008;**17**(3):1016-31.
308. Kershaw JC, Mattes RD. *Nutrition and taste and smell dysfunction*. World J. Otorhinolaryngol. Head Neck Surg. 2018;**4**(1):3-10.
309. Melis M, et al. *Taste Changes in Patients with Inflammatory Bowel Disease: Associations with PROP Phenotypes and polymorphisms in the salivary protein, Gustin and CD36 Receptor Genes*. Nutrients. 2020;**12**(2).
310. Fark T, et al. *Characteristics of taste disorders*. Eur. Arch. Otorhinolaryngol. 2013;**270**(6):1855-60.
311. Melis M, et al. *Molecular and Genetic Factors Involved in Olfactory and Gustatory Deficits and Associations with Microbiota in Parkinson's Disease*. Int. J. Mol. Sci. 2021;**22**(8).
312. Ghias K, et al. *The impact of treatment-induced dysgeusia on the nutritional status of cancer patients*. Clin. Nutr. Open Sci. 2023;**50**:57-76.
313. Merkonidis C, et al. *Characteristics of chemosensory disorders--results from a survey*. Eur. Arch. Otorhinolaryngol. 2015;**272**(6):1403-16.
314. Risso D, et al. *Alteration, Reduction and Taste Loss: Main Causes and Potential Implications on Dietary Habits*. Nutrients. 2020;**12**(11).
315. Soter A, et al. *Accuracy of self-report in detecting taste dysfunction*. Laryngoscope. 2008;**118**(4):611-7.
316. Lu P, et al. *Extraoral bitter taste receptors in health and disease*. J. Gen. Physiol. 2017;**149**(2):181-97.
317. Weber M, Schübeler D. *Genomic patterns of DNA methylation: targets and function of an epigenetic mark*. Curr Opin Cell Biol. 2007;**19**(3):273-80.

318. Dhar GA, et al. *DNA methylation and regulation of gene expression: Guardian of our health*. Nucleus (Calcutta). 2021;**64**(3):259-70.
319. Jeziorska DM, et al. *DNA methylation of intragenic CpG islands depends on their transcriptional activity during differentiation and disease*. Proc Natl Acad Sci U S A. 2017;**114**(36):E7526-e35.
320. Moore K, et al. *Epigenome-wide association study for Parkinson's disease*. Neuromolecular Med. 2014;**16**(4):845-55.
321. Chuang Y-H, et al. *Parkinson's disease is associated with DNA methylation levels in human blood and saliva*. Genome medicine. 2017;**9**(1):1-12.
322. Masliah E, et al. *Distinctive patterns of DNA methylation associated with Parkinson disease: identification of concordant epigenetic changes in brain and peripheral blood leukocytes*. Epigenetics. 2013;**8**(10):1030-8.
323. Jin Z, Liu Y. *DNA methylation in human diseases*. Genes Dis. 2018;**5**(1):1-8.
324. Kulis M, Esteller M. *DNA methylation and cancer*. Adv Genet. 2010;**70**:27-56.
325. Melis M, et al. *Gene Methylation Affects Salivary Levels of the Taste Buds' Trophic Factor, Gustin Protein*. Nutrients. 2024;**16**(9).
326. Lee RJ, et al. *T2R38 taste receptor polymorphisms underlie susceptibility to upper respiratory infection*. J. Clin. Invest. 2012;**122**(11):4145-59.
327. Viswanathan VK. *Sensing bacteria, without bitterness?* Gut Microbes. 2013;**4**(2):91-3.
328. Kumar SA, Cheng W. *A hypothesis: Bitter taste receptors as a therapeutic target for the clinical symptoms of SARS-CoV-2*. Pharmazie. 2021;**76**(2):43-54.
329. Aab A, et al. *Search for patterns by combining cosmic-ray energy and arrival directions at the Pierre Auger Observatory*. Eur Phys J C Part Fields. 2015;**75**(6):269.
330. Åkerström S, et al. *Nitric Oxide Inhibits the Replication Cycle of Severe Acute Respiratory Syndrome Coronavirus*. J. Virol. 2005;**79**(3):1966-9.
331. Doyle ME, et al. *Human Type II Taste Cells Express Angiotensin-Converting Enzyme 2 and Are Infected by Severe Acute Respiratory Syndrome Coronavirus 2 (SARS-CoV-2)*. Am. J. Pathol. 2021;**191**(9):1511-9.
332. Parsa S, et al. *COVID-19 as a worldwide selective event and bitter taste receptor polymorphisms: An ecological correlational study*. Int. J. Biol. Macromol. 2021;**177**:204-10.
333. Cersosimo MG, Benarroch EE. *Pathological correlates of gastrointestinal dysfunction in Parkinson's disease*. Neurobiol Dis. 2012;**46**(3):559-64.
334. Cersosimo MG, et al. *Dry mouth: an overlooked autonomic symptom of Parkinson's disease*. J Parkinsons Dis. 2011;**1**(2):169-73.
335. Proulx M, et al. *Salivary production in Parkinson's disease*. Mov Disord. 2005;**20**(2):204-7.
336. Olcay BO, et al. *Using chemosensory-induced EEG signals to identify patients with de novo Parkinson's disease*. Biomed. Signal Process. Control. 2024;**87**(Part B):105438.
337. Ou Z, et al. *Global Trends in the Incidence, Prevalence, and Years Lived With Disability of Parkinson's Disease in 204 Countries/Territories From 1990 to 2019*. Front. Public Health. . 2021;**Volume 9 - 2021**.
338. Kalia LV, Lang AE. *Parkinson's disease*. Lancet. 2015;**386**(9996):896-912.
339. Nijakowski K, et al. *Salivary Biomarkers for Parkinson's Disease: A Systematic Review with Meta-Analysis*. Cells. 2024;**13**(4).
340. Alia S, et al. *Chemosensory Impairments and Their Impact on Nutrition in Parkinson's Disease: A Narrative Literature Review*. Nutrients. 2025;**17**(4):671.
341. Zhu Q, et al. *Taste impairment in patients with Parkinsonism*. J. Neurol. 2025;**272**(3):238.
342. Jagota P, et al. *Umami and Other Taste Perceptions in Patients With Parkinson's Disease*. J Mov Disord. 2022;**15**(2):115-23.
343. Cecchini MP, et al. *Taste in Parkinson's disease*. J Neurol. 2015;**262**(4):806-13.
344. Nigam M, et al. *Sweet or Bland Dreams? Taste Loss in Isolated REM-Sleep Behavior Disorder and Parkinson's Disease*. Mov Disord. 2021;**36**(10):2431-5.
345. Shah M, et al. *Abnormality of taste and smell in Parkinson's disease*. Parkinsonism Relat. Disord. 2009;**15**(3):232-7.
346. Melis M, et al. *Taste disorders are partly genetically determined: Role of the TAS2R38 gene, a pilot study*. Laryngoscope. 2019.

347. Behrens M, Meyerhof W. Oral and extraoral bitter taste receptors. In: Meyerhof W. BU, Joost HG. , editor. Sensory and Metabolic Control of Energy Balance. Results and Problems in Cell Differentiation. 52. 2010/09/25 ed. Berlin, Heidelberg: Springer; 2011. p. 87-99.
348. Cecati M, et al. *TAS1R3 and TAS2R38 Polymorphisms Affect Sweet Taste Perception: An Observational Study on Healthy and Obese Subjects*. Nutrients. 2022;**14**(9):1711.
349. Oppo V, et al. *"Smelling and Tasting" Parkinson's Disease: Using Senses to Improve the Knowledge of the Disease*. Front. Aging Neurosci. 2020;**12**:43.
350. Angius F, et al. *Combined measure of salivary alpha-synuclein species as diagnostic biomarker for Parkinson's disease*. J. Neurol. 2023;**270**(11):5613-21.
351. Han W, et al. *Alpha-synuclein (SNCA) polymorphisms and susceptibility to Parkinson's disease: a meta-analysis*. Am J Med Genet B Neuropsychiatr Genet. 2015;**168b**(2):123-34.
352. Mohammadi R, et al. *Common SNCA Genetic Variants and Parkinson's Disease Risk: A Systematic Review and Meta-Analysis*. Int. J. Mol. Sci. 2025;**26**(13):6001.
353. Lee RJ, Cohen NA. *The emerging role of the bitter taste receptor T2R38 in upper respiratory infection and chronic rhinosinusitis*. Am. J. Rhinol. Allergy. 2013;**27**(4):283-6.
354. Adappa ND, et al. *Correlation of T2R38 taste phenotype and in vitro biofilm formation from nonpolypoid chronic rhinosinusitis patients*. Int. Forum Allergy Rhinol. 2016;**6**(8):783-91.
355. Adappa ND, et al. *T2R38 genotype is correlated with sinonasal quality of life in homozygous DeltaF508 cystic fibrosis patients*. Int. Forum Allergy Rhinol. 2016;**6**(4):356-61.
356. Adappa ND, et al. *The bitter taste receptor T2R38 is an independent risk factor for chronic rhinosinusitis requiring sinus surgery*. Int. Forum Allergy Rhinol. 2014;**4**(1):3-7.
357. Workman AD, Cohen NA. *Bitter taste receptors in innate immunity: T2R38 and chronic rhinosinusitis*. J. Rhinol.-Otol. 2017;**5**:12-8.
358. Carrai M, et al. *Association between TAS2R38 gene polymorphisms and colorectal cancer risk: a case-control study in two independent populations of Caucasian origin*. PLoS One. 2011;**6**(6):e20464.
359. Choi JH, et al. *Genetic Variation in the TAS2R38 Bitter Taste Receptor and Gastric Cancer Risk in Koreans*. Sci. Rep. 2016;**6**:26904.
360. Ibtehaz N, Rahman MS. *MultiResUNet : Rethinking the U-Net architecture for multimodal biomedical image segmentation*. Neural Netw. 2020;**121**:74-87.
361. Cabini RF, et al. *CompositIA: an open-source automated quantification tool for body composition scores from thoraco-abdominal CT scans*. Eur Radiol Exp. 2025;**9**(1):12.
362. Tepper BJ, et al. *Factors Influencing the Phenotypic Characterization of the Oral Marker, PROP*. Nutrients. 2017;**9**(12):1275.
363. Tepper BJ, et al. *Greater energy intake from a buffet meal in lean, young women is associated with the 6-n-propylthiouracil (PROP) non-taster phenotype*. Appetite. 2011;**56**(1):104-10.
364. Enoch MA, et al. *Does a reduced sensitivity to bitter taste increase the risk of becoming nicotine addicted?* Addict. Behav. 2001;**26**(3):399-404.
365. Mangold JE, et al. *Bitter taste receptor gene polymorphisms are an important factor in the development of nicotine dependence in African Americans*. J. Med. Genet. 2008;**45**(9):578-82.
366. Risso DS, et al. *Genetic Variation in the TAS2R38 Bitter Taste Receptor and Smoking Behaviors*. PLoS One. 2016;**11**(10):e0164157.
367. Glanville EV, Kaplan AR. *Taste Perception and the Menstrual Cycle*. Nature. 1965;**205**(4974):930-1.
368. Mueller CA, et al. *Clinical test of gustatory function including umami taste*. Annals of Otology, Rhinology and Laryngology. 2011;**120**(6):358-62.
369. Sollai G, et al. *Human Tongue Electrophysiological Response to Oleic Acid and Its Associations with PROP Taster Status and the CD36 Polymorphism (rs1761667)*. Nutrients. 2019;**11**(2).
370. Melis M, et al. *Electrophysiological Responses from the Human Tongue to the Six Taste Qualities and Their Relationships with PROP Taster Status*. Nutrients. 2020;**12**(7).
371. Naciri LC, et al. *Automated Classification of 6-n-Propylthiouracil Taster Status with Machine Learning*. Nutrients. 2022;**14**(2).
372. Bishop CM. Pattern Recognition and Machine Learning: Springer-Verlag; 2006.
373. Breiman L, et al., editors. Classification and Regression Trees1983.
374. Breiman L. *Random Forests*. Machine Learning. 2001;**1**.

375. Goldberger J, et al. *Neighbourhood components analysis*. Advances in neural information processing systems. 2004;**17**.
376. Prokhorenkova L, et al. *CatBoost: unbiased boosting with categorical features*. 2018;**31**.
377. Jiang J, et al. *Boosting tree-assisted multitask deep learning for small scientific datasets*. 2020;**60**(3):1235-44.
378. Friedman JHJCs, analysis d. *Stochastic gradient boosting*. 2002;**38**(4):367-78.
379. Barua S, et al. A Novel Synthetic Minority Oversampling Technique for Imbalanced Data Set Learning. Neural Information Processing. ICONIP 2011. Lecture Notes in Computer Science. Lu B, Zhang L, Kwok J, editors: Springer, Berlin, Heidelberg; 2011.
380. Browne MWJJomp. *Cross-validation methods*. 2000;**44**(1):108-32.
381. Wu J, et al. *Hyperparameter optimization for machine learning models based on Bayesian optimization*. 2019;**17**(1):26-40.
382. Zahedi L, et al. *Search Algorithms for Automated Hyper-Parameter Tuning.* . arXiv Prepr. . 2021;**arXiv:2104.14677**.
383. Lundberg SM, Lee S-I. *A Unified Approach to Interpreting Model Predictions*. Nips'17. 2017:4768–77.
384. Adappa ND, et al. *TAS2R38 genotype predicts surgical outcome in nonpolypoid chronic rhinosinusitis*. Int. Forum Allergy Rhinol. 2016;**6**(1):25-33.
385. Vascellari S, et al. *Genetic variants of TAS2R38 bitter taste receptor associate with distinct gut microbiota traits in Parkinson's disease: A pilot study*. Int. J. Biol. Macromol. 2020;**165**(Pt A):665-74.
386. Mennella J, et al. *Age modifies the genotype-phenotype relationship for the bitter receptor TAS2R38*. BMC Genetics. 2010;**11**(1):60.
387. Whissell-Buechy D, Wills C. *Male and female correlations for taster (P.T.C.) phenotypes and rate of adolescent development*. Ann. Hum. Biol. 1989;**16**(2):131-46.
388. Prescott J, et al. *Responses of PROP taster groups to variations in sensory qualities within foods and beverages*. Physiol. Behav. 2004;**82**(2-3):459-69.
389. Dan C, Armin S. *Multiple testing of local maxima for detection of peaks in random fields*. Ann. Stat. 2017;**45**(2):529-56.
390. Tsai C-A, Chang Y-J. *Efficient Selection of Gaussian Kernel SVM Parameters for Imbalanced Data*. Genes. 2023;**14**(3):583.
391. Refaeilzadeh P, et al. Cross-Validation. In: Liu L, ÖZsu MT, editors. Encyclopedia of Database Systems. Boston, MA: Springer US; 2009. p. 532-8.
392. Willmott CJ, Matsuura K. *Advantages of the mean absolute error (MAE) over the root mean square error (RMSE) in assessing average model performance*. Clim. Res. 2005;**30**(1):79-82.
393. Gourdeau D, et al. *On the proper use of structural similarity for the robust evaluation of medical image synthesis models*. Medical Physics. 2022;**49**(4):2462-74.
394. Topp CW, et al. *The WHO-5 Well-Being Index: a systematic review of the literature*. Psychother. Psychosom. 2015;**84**(3):167-76.
395. World Health Organization. Regional Office for E. Wellbeing measures in primary health care/the DepCare Project: report on a WHO meeting: Stockholm, Sweden, 12–13 February 1998. Copenhagen: World Health Organization. Regional Office for Europe; 1998 1998. Contract No.: WHO/EURO:1998-4234-43993-62027.
396. Maria Paola C, et al. *A cross-cultural survey of umami familiarity in European countries*. Food Qual Prefer. 2019;**74**:172-8.
397. Sidey-Gibbons JAM, Sidey-Gibbons CJ. *Machine learning in medicine: a practical introduction*. BMC Med. Res. Methodol. 2019;**19**(1):64.
398. Yousef M, et al. Application of Biological Domain Knowledge Based Feature Selection on Gene Expression Data. Entropy [Internet]. 2021; 23(1).
399. Yu L, Liu H. Feature Selection for High-Dimensional Data: A Fast Correlation-Based Filter Solution2003. 856-63 p.
400. Czerwinska U. Interpretability of Machine Learning Models: How Can One Explain Machine Learning Models? Applied Data Science in Tourism: Interdisciplinary Approaches, Methodologies, and Applications: Springer; 2022. p. 275-303.

401. Naciri L, et al. *Automated identification of the genetic variants of TAS2R38 bitter taste receptor with supervised learning*. Comput. Struct. Biotechnol. J. 2023;**21**:1054-65.
402. Lundberg SM, et al. *From local explanations to global understanding with explainable AI for trees*. Nat. Mach. Intell. 2020;**2**(1):56-67.
403. Lundberg SM, et al. *Explainable machine-learning predictions for the prevention of hypoxaemia during surgery*. Nat. Biomed. Eng. 2018;**2**(10):749-60.
404. Doty RL, De Fonte TP. *Relationship of Phenylthiocarbamide (PTC) Taster Status to Olfactory and Gustatory Function in Patients with Chemosensory Disturbances*. Chem. Senses. 2016;**41**(8):685-96.
405. Cavazzana A, et al. *Detection thresholds for quinine, PTC, and PROP measured using taste strips*. Eur Arch Otorhinolaryngol. 2019;**276**(3):753-9.
406. Peng M, et al. *Systematic review of olfactory shifts related to obesity*. Obes. Rev. 2019;**20**(2):325-38.
407. Fernández-Aranda F, et al. *Smell-taste dysfunctions in extreme weight/eating conditions: analysis of hormonal and psychological interactions*. Endocrine. 2016;**51**(2):256-67.
408. Fernandez-Garcia JC, et al. *An increase in visceral fat is associated with a decrease in the taste and olfactory capacity*. PLoS One. 2017;**12**(2):e0171204.
409. Gorovic N, et al. *Genetic variation in the hTAS2R38 taste receptor and brassica vegetable intake*. Scand. J. Clin. Lab. Invest. 2011;**71**(4):274-9.
410. Feeney E, et al. *Genetic variation in taste perception: does it have a role in healthy eating?* Proc. Nutr. Soc. 2011;**70**(1):135-43.
411. Baranowski T, et al. *6-n-propylthiouracil taster status not related to reported cruciferous vegetable intake among ethnically diverse children*. Nutr. Res. 2011;**31**(8):594-600.
412. Mennella JA, et al. *Genetic and environmental determinants of bitter perception and sweet preferences*. Pediatrics. 2005;**115**(2):e216-22.
413. O'Brien SA, et al. *Bitter taste perception and dietary intake patterns in irish children*. J. Nutrigenet. Nutrigenomics. 2013;**6**(1):43-58.
414. Carta G, et al. *Participants with Normal Weight or with Obesity Show Different Relationships of 6-n-Propylthiouracil (PROP) Taster Status with BMI and Plasma Endocannabinoids*. Sci. Rep. 2017;**7**(1):1361.
415. Green BG, et al. *Evaluating the 'Labeled Magnitude Scale' for measuring sensations of taste and smell.* Chem. Senses. 1996;**21**(3):323-34.
416. Campan M, et al. *MethyLight and Digital MethyLight*. Methods Mol Biol. 2018;**1708**:497-513.
417. Anastasiadi D, et al. *Consistent inverse correlation between DNA methylation of the first intron and gene expression across tissues and species*. Epigenet. Chromatin. 2018;**11**(1):37.
418. Brenet F, et al. *DNA Methylation of the First Exon Is Tightly Linked to Transcriptional Silencing*. Plos One. 2011;**6**(1):e14524.
419. Sakamoto A, et al. *DNA Methylation in the Exon 1 Region and Complex Regulation of Twist1 Expression in Gastric Cancer Cells*. Plos One. 2015;**10**(12):e0145630.
420. Tian S, et al. *Characteristics of COVID-19 infection in Beijing*. J Infect. 2020;**80**(4):401-6.
421. Tuzim K, Korolczuk A. *An update on extra-oral bitter taste receptors*. Journal of Translational Medicine. 2021;**19**(1):440.
422. Loi E, et al. *HLA-C dysregulation as a possible mechanism of immune evasion in SARS-CoV-2 and other RNA-virus infections*. Front Immunol. 2022;**13**:1011829.
423. Akerström S, et al. *Dual effect of nitric oxide on SARS-CoV replication: viral RNA production and palmitoylation of the S protein are affected*. Virology. 2009;**395**(1):1-9.
424. Barham HP, et al. *Does phenotypic expression of bitter taste receptor T2R38 show association with COVID-19 severity?* Int. Forum. Allergy Rhinol. 2020;**10**(11):1255-7.
425. Risso D, et al. *Distribution of TAS2R38 bitter taste receptor phenotype and haplotypes among COVID-19 patients*. Sci. Rep. 2022;**12**(1):7381.
426. Ma Y, et al. *DNMT1-mediated Foxp3 gene promoter hypermethylation involved in immune dysfunction caused by arsenic in human lymphocytes*. Toxicol. Res. 2020;**9**(4):519-29.
427. Kang KA, et al. *Epigenetic changes induced by oxidative stress in colorectal cancer cells: methylation of tumor suppressor RUNX3*. Tumor Biology. 2012;**33**(2):403-12.

428. Hannum ME, et al. *Taste loss as a distinct symptom of COVID-19: a systematic review and meta-analysis*. Chem. Senses. 2023;**48**.
429. Menachery VD, et al. *MERS-CoV and H5N1 influenza virus antagonize antigen presentation by altering the epigenetic landscape*. PNAS. 2018;**115**(5):E1012-E21.
430. Gibb WR, Lees AJ. *The relevance of the Lewy body to the pathogenesis of idiopathic Parkinson's disease*. J Neurol Neurosurg Psychiatry. 1988;**51**(6):745-52.
431. Naciri LC, et al. *A Supervised Learning Regression Method for the Analysis of the Taste Functions of Healthy Controls and Patients with Chemosensory Loss*. Biomedicines. 2023;**11**(8).
432. Hou B, et al. *Association of rs356219 and rs3822086 polymorphisms with the risk of Parkinson's disease: A meta-analysis*. Neurosci Lett. 2019;**709**:134380.
433. Zhang Y, et al. *A Comprehensive Analysis of the Association Between SNCA Polymorphisms and the Risk of Parkinson's Disease*. Front. Mol. Neurosci. . 2018;**Volume 11 - 2018**.
434. Winkler S, et al. *α-Synuclein and Parkinson disease susceptibility*. Neurol. 2007;**69**(18):1745-50.
435. Campêlo CLC, et al. *Variants in SNCA Gene Are Associated with Parkinson's Disease Risk and Cognitive Symptoms in a Brazilian Sample*. Front. Aging Neurosci. . 2017;**Volume 9 - 2017**.
436. Samuels J. One-Hot Encoding and Two-Hot Encoding: An Introduction2024.
437. Opitz J. *A Closer Look at Classification Evaluation Metrics and a Critical Reflection of Common Evaluation Practice*. Trans. Assoc. Comput. Linguist. 2024;**12**:820-36.
438. Lundberg SM, Lee S-I. A unified approach to interpreting model predictions. Proceedings of the 31st International Conference on Neural Information Processing Systems; Long Beach, California, USA: Curran Associates Inc.; 2017. p. 4768–77.
439. Tobin JE, et al. *Haplotypes and gene expression implicate the MAPT region for Parkinson disease*. Neurol. 2008;**71**(1):28-34.
440. Zabetian CP, et al. *Association analysis of MAPT H1 haplotype and subhaplotypes in Parkinson's disease*. Ann. Neurol. 2007;**62**(2):137-44.
441. Refenes N, et al. *Role of the H1 haplotype of microtubule-associated protein tau (MAPT) gene in Greek patients with Parkinson's disease*. BMC neurology. 2009;**9**(1):1-8.
442. Lee A, Gilbert RM. *Epidemiology of Parkinson Disease*. Neurol Clin. 2016;**34**(4):955-65.
443. Gillies GE, et al. *Sex differences in Parkinson's disease*. Front Neuroendocrinol. 2014;**35**(3):370-84.
444. Mappin-Kasirer B, et al. *Tobacco smoking and the risk of Parkinson disease: A 65-year follow-up of 30,000 male British doctors*. Neurol. 2020;**94**(20):e2132-e8.
445. Fathy YY, et al. *Differential insular cortex subregional vulnerability to α-synuclein pathology in Parkinson's disease and dementia with Lewy bodies*. Neuropathol Appl Neurobiol. 2019;**45**(3):262-77.
446. Hoehn MM, Yahr MD. *Parkinsonism: onset, progression and mortality*. Neurol. 1967;**17**(5):427-42.
447. Reinoso G, et al. *Clinical evolution of Parkinson's disease and prognostic factors affecting motor progression: 9-year follow-up study*. Eur J Neurol. 2015;**22**(3):457-63.
448. Rajput AH, et al. *Baseline motor findings and Parkinson disease prognostic subtypes*. Neurol. 2017;**89**(2):138-43.
449. Rajput AH, et al. *Course in Parkinson disease subtypes: A 39-year clinicopathologic study*. Neurol. 2009;**73**(3):206-12.
450. Pagano G, et al. *Age at onset and Parkinson disease phenotype*. Neurol. 2016;**86**(15):1400-7.